Universitat Politècnica de València
Departamento de Máquinas y Motores Térmicos

EXPERIMENTAL ANALYSIS OF THERMAL MANAGEMENT INFLUENCE ON PERFORMANCE AND EMISSIONS IN DIESEL ENGINES AT LOW AMBIENT TEMPERATURE

Doctoral Thesis
Presented by:
Ausias Moratal Martínez
Directed by:
Prof. Jose Manuel Luján Martínez

Valencia, July 26, 2018

Abstract. Automotive world-wide pollutant emissions regulations are getting more stringent everyday. New testing procedures are pushing the automotive industry towards researching new technologies to accomplish the emissions targets. In the mid-term future is expected that low ambient temperature emissions testing will become mandatory for any engine model type approval. Low ignition temperature greatly influences on combustion rate leading to emissions increase and eventually to misfiring events. In these conditions, high emissions of unburned hydrocarbon (HC) and carbon monoxide (CO) are released along with fuel consumption penalties. In addition, nitrogen oxides (NOx) emissions may rise under cold conditions owing to the disabling of Exhaust Gas Recirculation (EGR) systems at cold conditions.

In this thesis the effect of low ambient temperature in a High Speed Direct Injection (HSDI) Light Duty (LD) engine is analysed. Tests were performed in New European Driving Cycles (NEDC) and Worldwide harmonized Light vehicles Tests (WLTC). Direct influence of low temperature on engine emissions was addressed by engine out pollutants sampling. The effect on aftertreatment systems was also evaluated by the CO and HC oxidation efficiency. The results of this survey indicated a general detriment of pollutant emissions and brake thermal efficiency at low ambient temperatures. The effect of low temperature varied depending on the engine load test conditions. NEDC comes up as the worst scenario for low temperature testing with an increase of 270% in HC, 250% in NOx, 125% in CO and 20% in Brake Specific Fuel Consumption (BSFC). Running at higher engine loads and transient conditions, as it's performed in WLTC tests, showed a lower effect of ambient temperature with an increase of 150% in HC and 250% in NOx. In contrast to NEDC, CO emissions were reduced in 20% and no engine efficiency penalty was spotted. In addition to the pollutant emission formation increase, the aftertreatment analysis showed a significant reduction of the Diesel Oxidative Catalyst (DOC) efficiency in both NEDC and WLTC.

This work is aimed to analyse and compare two different thermal management approaches for engine enhancement running at low ambient temperature. The first approach relied on coolant management aimed to avoid overcooling when running at cold conditions. On one hand, low flow and 0 flow engine coolant strategies were performed while Water Charge Air Cooled (WCAC) coolant is recirculated. On the other hand, WCAC 0 flow was applied for avoiding overcooling at low ambient temperatures. The other layout was based on an exhaust gas heat recovery system (EGHR). WCAC coolant was directed to an exhaust tail pipe heat exchanger for waste heat recovery. Recovered heat was released in the WCAC for speeding up the intake air temperature increase. The first part of the thermal management results is focused on the analysis by thermal layout. Comparison of both thermal management is discussed in the conclusions section of that chapter. By enabling an EGHR system, HC emissions were reduced during low load driving phases in comparison with the other of layouts.

EGHR energy analysis was also conducted, focusing on energy efficiency and phase change recovery analysis. The role that latent enthalpy plays on waste heat recovery was addressed by measuring the water vapour concentration in the exhaust stream at both EGHR heat exchanger inlet and outlet. Water vapour condensation represented the 25% of the total recovered energy.

Resumen. La regulación mundial de emisiones contaminantes en el sector de la automoción esta siendo cada día mas estricta. Los implantación de nuevos procedimientos está presionando la industria hacia la búsqueda de nuevas tecnologías que cumplan los objetivos de reducción de emisiones contaminantes. En el medio plazo se espera que las pruebas de emisiones a baja temperatura ambiente sean obligatorias en el proceso de homologación. La combustión a bajas temperaturas influye de forma importante en la velocidad de la reacción conllevando un aumento de las emisiones y finalmente al apagado de llama. Bajo estas condiciones, se produce un aumento de las emisiones de hidrocarburos (HC) y monóxido de carbono (CO) así como un aumento del consumo de combustible. Además, en condiciones de baja temperatura ambiente las emisiones de óxidos de nitrógeno (NOx) pueden aumentar debido a la desactivación de los sistemas de recirculación de gases de escape.

En la presente tesis, se ha analizado el efecto de la baja temperatura ambiente en un motor diesel HSDI. Los ensayos fueron realizados en ciclos de conducción NEDC y WLTC. La influencia directa de las bajas temperaturas en las emisiones se analizó por medio de las medida bruta de contaminates, aguas arriba de los sistemas de postratamiento. El funcionamiento de los sistemas de postratamiento tambien fue evaluado a bajas temperaturas mediante la eficiencia de la oxidación catalítica de HC y CO. Los resultados de este estudio mostraron un deterioro general de las emisiones y del rendimiento efectivo a bajas temperaturas. El efecto de las bajas temperaturas varió dependiendo de condiciones de carga. El ciclo NEDC se consolida como el peor escenario de conducción, para la realización de pruebas a baja temperatura, con un incremento del 270% en HC, 250% en NOx, 125% en CO y 20% en consumo específico. El mayor grado de carga junto con el carácter más transitorio del ciclo WLTC mostraron un efecto menor de las bajas temperaturas ambiente con un aumento del 150% en HC y 250% en NOx. A diferencia del ciclo NEDC, las emisiones de CO se redujeron en un 20% y no se detectó un aumento del consumo de combustible. Además del aumento de la formación de contaminates, el análisis del catalizador de oxidación mostró un reducción de la eficiencia en ambos ciclos de conducción NEDC y WLTC.

El presente trabajo tiene por objetivo analizar y comparar dos sistemas de gestión térmica para la mejora del funcionamiento de MCIA a bajas temperaturas. El primer sistema estaba basado en la gestión del flujo de refrigerante para evitar subenfriamiento en condiciones de funcionamiento en frío. Por un lado, se propusieron estrategias de bajo y nulo flujo en el circuito de refrigerante motor. Por otro lado, se realizaron ensayos con 0 flujo en el circuito de refrigerante del WCAC para evitar el subenfriamiento del aire de admisión durante puntos de baja carga en condiciones de funcioanmineto en frío. El otro sistema incluía la recuperación de energía térmica del escape (EGHR). El refrigerante del WCAC se empleó como fluido de recuperación conectandose con un intercambiador de escape para la absorción de energía térmica residual. La energía recuperada era entregada en el WCAC al aire para acelerar el aumento de la temperatura de admisión. La primera parte de los resultados de la gestión térmica están centrados en el análisis individual de los distintos sistemas de gestión. En las conclusiones se comparan todos los sistemas propuestas explicando las diferencias entre ellos. Mediante el uso del EGHR las emisiones de HC fueron reducidas, durante los puntos de baja carga, en comparación con el resto de estrategias

térmicas planteadas.
El análisis energético del EGHR se centró en la eficiencia y en el estudio la recuperación por cambio de fase. El papel que la entalpía de cambio de fase juega en la recuperación de calor residual fué estudiado por medio de la medición de concentración de vapor de agua en el gas de escape en la entrada y salida del intercambiador del EGHR. La condensación del vapor de agua de escape representó el 25% de toda la energía recuperada.

Resum. La regulació mundial d'emissions contaminants en el sector de l'automoció està sent cada vegada més estricta. La implantació de nous procediments està pressionant la indústria cap a la cerca de noves tecnologies que complisquen els objectius de reducció d'emissions contaminants. En el mig termini s'espera que les proves d'emissions a baixa temperatura ambient siguen obligatòries en el procés d'homologació. La combustió a baixes temperatures influeix de forma important en la velocitat de la reacció comportant un augment de les emissions i finalment a l'apagat de flama. Sota aquestes condicions, es produeix un augment de les emissions d'hidrocarburs (HC) i monòxid de carboni (CO) així com un augment del consum de combustible. A més, en condicions de baixa temperatura ambiente les emissions d'òxids de nitrogen (NOx) poden augmentar a causa de la desactivació dels sistemes de recirculació de gasos d'escapament.

En la present tesi, s'ha analitzat l'efecte de la baixa temperatura ambiente en un motor dièsel HSDI. Els assajos van ser realitzats en cicles de conducció NEDC i WLTC. La influència directa de les baixes temperatures en les emissions es va analitzar per mitjà de la mesura bruta de contaminants, aigües a dalt dels sistemes de postractament. El funcionament dels sistemes de postractament també va ser avaluat a baixes temperatures mitjançant l'eficiència de la oxidació catalítica de HC i CO. Els resultats d'aquest estudi van mostrar una deterioració general de les emissions i del rendiment efectiu a baixes temperatures. L'efecte de les baixes temperatures variava depenent de les condicions de càrrega. El cicle NEDC es consolida com el pitjor escenari de conducció, per a la realització de proves a baixa temperatura, amb un increment del 270% en HC, 250% en NOx, 125% en CO i 20% en consum específic. El major grau de càrrega juntament amb el caràcter més transitori del cicle WLTC van mostrar un efecte menor de les baixes temperatures ambient amb un augment del 150% en HC i 250% en NOx. A diferència del cicle NEDC, les emissions de CO es van reduir en un 20% i no es va detectar un augment del consum de combustible. A més de l'augment de la formació de contaminants, l'anàlisi del catalitzador d' oxidació va mostrar una reducció de l'eficiència en tots dos cicles de conducció NEDC i WLTC.

El present treball té per objectiu analitzar i comparar dos sistemes de gestió tèrmica per a la millora del funcionament dels MCIA a baixes temperatures. El primer sistema estava basat en la gestió del flux de refrigerant per a evitar subrefredament en condicions de funcionament en fred. D'una banda, es van proposar estratègies de baix i nul flux en el circuit de refrigerant motor. D'altra banda, es van realitzar assajos amb 0 flux en el circuit de refrigerant del WCAC per a evitar el subrefredament de l'aire d'admissió durant punts de baixa càrrega en condicions de funcionament en fred. L'altre sistema incloïa la recuperació d'energia tèrmica de l'escapament (EGHR). El refrigerant del WCAC es va emprar com fluït de recuperació connectant-se amb un bescanviador d'escapament per a l'absorció d'energia tèrmica residual. L'energia recuperada era lliurada en el WCAC a l'aire per a accelerar l'augment de la temperatura d'admissió. La primera part dels resultats de la gestió tèrmica estan centrats en l'anàlisi individual dels diferents sistemes de gestió. En les conclusions es comparen tots els sistemes proposats explicant les diferències entre ells. Mitjançant l'ús del EGHR les emissions de HC van ser reduïdes, durant els punts de baixa càrrega, en comparació de la resta d'estratègies tèrmiques plantejades.

L'anàlisi energètic del EGHR es va centrar en l'eficiència i en l'estudi de la recuperació

per canvi de fase. El paper que l'entalpia de canvi de fase juga en la recuperació de calor residual va ser estudiat per mitjà del mesurament de concentració de vapor d'aigua en el gas d'escapament en l'entrada i eixida del bescanviador del EGHR. La condensació del vapor d'aigua de l'escapamanet va representar el 25% de tota l'energia recuperada.

Table of Contents

Index of Figures

Index of Tables

Nomenclature

Initials and acronyms

AFR	Air to Fuel Ratio
AIM	Air Intake Module
BTE	Brake Thermal Efficiency
BSFC	Brake Specific Fuel Consumption
CAD	Crank Angle Degrees or deg aTDC
CI	Compression Ignition
cp	Specific heat capacity
CO	Carbon monoxide
CO_2	Carbon dioxide
DOC	Diesel Oxidation Catalyzer
DPF	Diesel Particulate Filter
EGR	Exhaust Gas Recirculation
EGHR	Exhaust Gas Heat Recovery
EPA	Environmental Protection Agency
EUDC	Extra Urban Driving Cycle
FTIR	Fourier Transform Infrared
FTP	Federal Test Procedure
GEMS	Global Environment Monitoring System
GRPE	Working Party on Pollution and Energy
HC	Hydrocarbon
HD	Heavy-duty
HRR	Heat release rate
IARC	International Agency for Research on Cancer
ICE	Internal Combustion Engine

IMEP	Indicated Mean Effective Pressure
IVC	Intake Valve Closing
LHV	Low Heat Value
LNT	Lean NOx Trap
MPD	MagentoPneumatic Detector
PMD	ParaMagnetic Detection
PEMS	Portable Emissions Measurement Systems
PLC	Programmable Logic Controller
PM	Particle Matter
PN	Particle Number
n	Engine speed
N	Torque
NEDC	New European Driving Cycle
NIST	National Institute of Standards and Technology
NOx	Nitroden oxides
OECD	Organisation for Economic Co-operation and Development
PN	Particles Number
RDE	Real Driving Emissions
RH	Rejected Heat power
ROS	Reacting Oxygen Species
Rx	Emission ratio
SCR	Selective Catalytic Reduction
SEPA	Swedish Environmental Protection Agency
SI	Spark ignition
SOI	Start Of Injection
TSP	Total Suspended Particle
UDC	Urban Driving Cycle
UNECE	United Nations Economic Commission for Europe
UNEP	United Nations Environment Programme
TDC	Top Dead Center
WCAC	Water Charge Air Cooler
WHO	Wolrd Health Organization
WLTC	World-wide harmonized Light duty Test Cycle

Chapter 1

Objectives and methodology

Contents

1.1 Introduction

The first four-stroke internal combustion engine (ICE) was created by Nicolaus Otto circa 1876 [1]. However, it was not until 1908 when Ford sold the Model T as the first mass-produced vehicle. This was the first model designed to be affordable for the average costumer. The first year of production, the number of cars produced were just over 10000 but 10 years later the car production exceeded the million units already [2]. This trend continued over the years increasing the car production and sales until today. The number of cars has increased drastically over the last 30 years and it is expected that by 2040 the number of cars on the road will be nearly doubled, especially in developing countries like China or India [3]. This growth directly affects the worldwide pollution, therefore the emission levels of the vehicles is a topic that has been extensively discussed in recent years.
As emissions regulations get more stringent, new technologies are developed to reduce the amount of emitted pollutants such hydrocarbons (HC), carbon monoxide (CO), nitrogen oxides (NOx) and particle matter (PM). Current European regulations include engine performance tests at low ambient temperatures in diesel engines. It's expected that future regulations will also consider emissions analysis at subzero ambient temperature.

1.2 Objective

The main objective of this thesis is to analyse the effect of two different thermal management systems on pollutant emissions reduction in diesel engines running at low ambient temperature. In addition Break Thermal Efficiency (BTE) is also analysed by means of the fuel consumption.
To achieve the major aim of this thesis other goals needed to be accomplished previously:

- Low ambient temperature engine out pollutant emissions were studied in a Euro 6 serial engine.
- The performance of the Diesel Oxidation Catalyst (DOC) running at low ambient temperatures was analysed.

The aim of the aforementioned goals is to analyse the current state of technology in diesel engines when running at low ambient temperature. Once the characterization of engine out emissions and DOC performance was

done, the thermal management systems were tested. Two different thermal management approaches were developed:

- Two systems, based on coolant flow management, were proposed. On one hand, the engine coolant flow was regulated for avoiding cylinder overcooling during cold conditions. On the other hand, 0 flow strategies were applied at the the Water Charge Air Cooler (WCAC) coolant for avoiding intake air overcooling.
- An Exhaust Gas Heat Recovery (EGHR) system was used to recover waste enthalpy from the exhaust gases. The recovered energy was used to heat up the intake air flow during low temperature operation.

1.3 Methodology

An general literature review of engine pollutant emissions is presented in Chapter 2. An historic road emissions regulation review is included at Section 2.3. An additional specific literature review is included in each chapter. Theoretical tools and experimental description of test facilities are presented in Chapter 3. Tested engines in this thesis and facilities description are presented at Section 3.2 and Section 3.3 respectively. The different thermal management layouts are depicted in Section 3.4. The data analysis procedure in Section 3.6.1 describes how pollutant mass emissions are calculated, the analysis of the repeatability of the tests, the experimental uncertainty of the outcomes and the propagation of error.
An experimental approach methodology was established in this work. All tests were carried out in transient conditions of driving cycles in a climatic engine bench. Pollutant emissions were sampled at the DOC upstream to analyse how ambient temperature influences on pollutants formation. Results of this study are shown in Chapter 4. DOC efficiency was analysed in Chapter 5 by means of the dwell time, oxygen and pollutant concentration measurement. Thermal management results are discussed in Chapter 6, where a comparison of all systems is carried out. Nevertheless, before studying the different thermal systems, the EGR strategy was recalibrated for running at low ambient temperature. In Section 6.2 the baseline EGR calibration is described. Finally, in Chapter 7 the main conclusions of this work are summarized and the future works related to this thesis that may be considered in the short and mid term are described.

Bibliography

[1] C. R. Ferguson and A. T. Kirkpatrick. *Internal combustion engines: applied thermosciences*. John Wiley & Sons, 2015.

[2] A. Altshuler, M. Anderson, D. Roos, J. P. Womack, and D. Jones. *The future of the automobile: the report of MIT's international automobile program*. MIT press, 1986.

[3] F. Birol et al. "World energy outlook 2010". *International Energy Agency* 1.3 (2010).

Chapter 2

Introduction

Contents

2.1 Air pollution

According to United Nations (UN) definition, pollutant is any substance that is present in concentrations that may harm organisms (humans, plants and animals) or exceed an environmental quality standard. The term is frequently used synonymously with contaminant. Two kind of pollutants have to be addressed regarding their global and local effect in the atmosphere. Global air pollution regards the world wide atmosphere damage by altering the whole chemical composition. CO_2 is estimated to be responsible for 64% of man-made global warming. Other greenhouse gases are released in much smaller amounts but still contribute significantly to the overall warming effect, as they are much more potent heat-trapping gases than CO_2. This is the case with methane (CH_4), which is responsible for 17% of man-made global warming, and with nitrous oxide (N2O), which accounts for 6% of the effect [4]. Regarding the major emitted pollutant, increase of CO_2 concentration is leading a global temperature rise in a process that is common named as global warming. CO_2 concentration rise is changing the earth energy balance in what is known as greenhouse effect. Input earth radiation is mainly limited to the visible range wavelength, while earth emission is radiated at the infrared (IR) band. As CO_2 rotational and vibration energy absorption is produced at the near and mid-IR range, radiated energy from the earth to the space reduces, driving to an earth heatsurplus that eventually drives to a world climate change [5], [6] and [7]. On the other hand, local air pollution refers to those pollutants that alterate the chemical composition in limited areas dangering the health of animals and human beings. Local pollution can be produced either directly by the presence of combustion products, what is known as primary pollution, or by transformation of the released products into new toxic compounds, what is named as secondary pollution. Harmful effect of primary local pollution is caused by direct exposure to products such as carbon monoxide (CO), nitrogen oxides (NOx), hydrocarbons (HC), sulfure oxides (SOx) and particle matter among other. Secondary pollution is caused by combination of some of the primary chemical compounds. For example, photochemical smog is produced by the reaction of NOx and HC in presence of sunlight which leaves airborne particles and ground level ozone formation [8] and [9].

Concerning global warming contribution by CO_2 emissions, automotive sector is responsible of 14% of the total anthropogenic CO_2. In Fig. 2.1 carbon dioxide emissions distribution by sector is shown. Details about the sources included in these estimates can be found in [10]. Agriculture and forestry,

heat and electricity production and industry are the main areas of emissions with a contribution of 24%, 25% and 21% respectively.

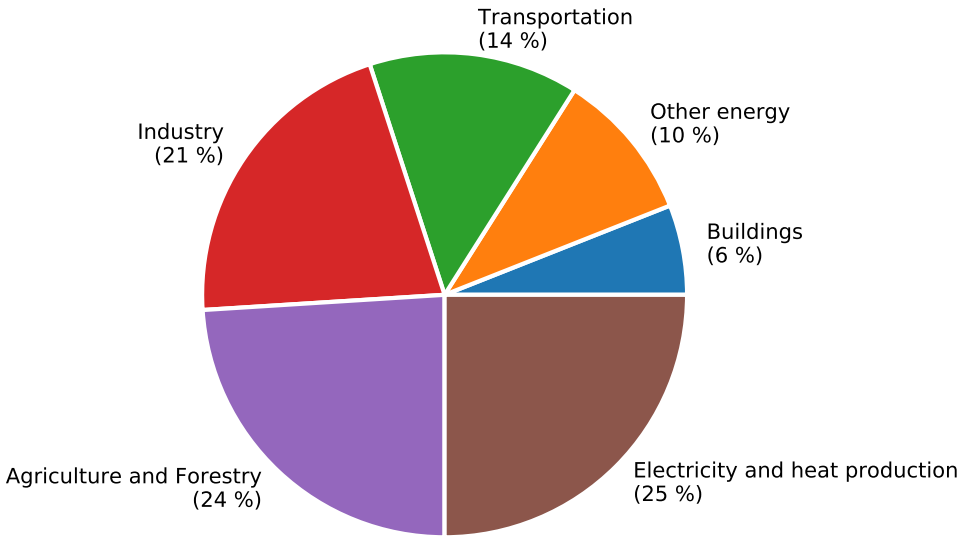

Figure 2.1: Distribution of CO_2 emissions by sector Fig. 2.1

In Fig. 2.2 CO_2 concentration measurements are displayed from 1958 until 2018 [11]. Measurements are monthly done by NOAA at Mauna Loa Observatory in Hawaii. Since 1958 to 2018, atmospheric CO_2 concentration has risen in 30 % reaching the current value of 409 ppm.

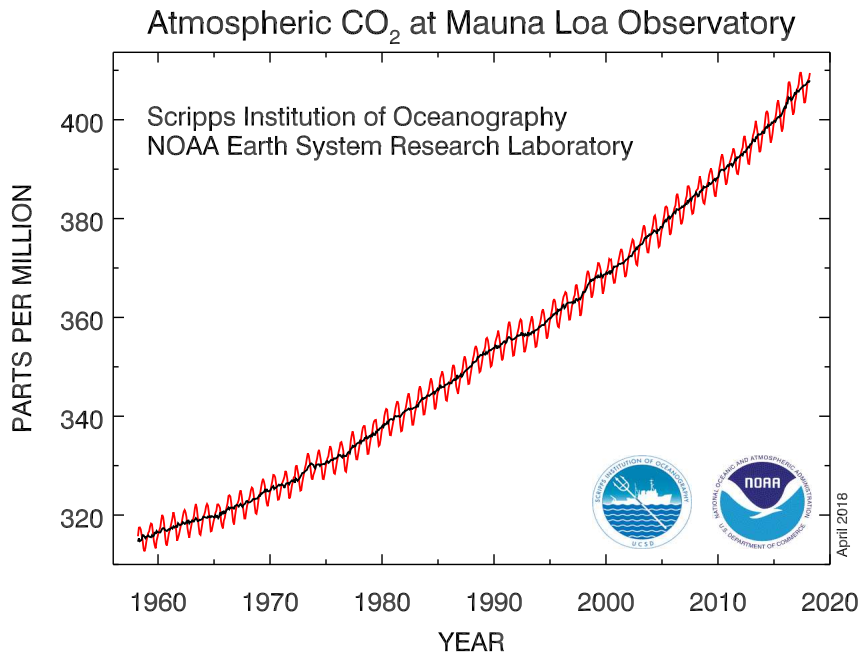

Figure 2.2: CO_2, depicted in red curve, is measured in dry conditions. Measurements were started at the Scripps Institution of Oceanography in March of 1958. NOAA started the CO_2 measurements in May of 1974, and they have run in parallel with those made by Scripps since then [12]. The black curve represents the seasonally corrected data.

The effect of CO_2 rising over the world temperature is depicted in Fig. 2.3. Average temperature variation by area is compared to a reference time period. Generally the period 1951-1980 is used as temperature reference [13]. Temperature variation have been averaged for the 2000-2017 period. Comparing both periods of time, the average world temperature has increased in 0.6^{o}C. The highest temperature increase areas are located in land regions of the north hemisphere. Higher temperature increase is experienced in the north hemisphere compared to the south because of the larger areas of land. As water heat capacity is higher than ground, water temperature increase is lower. In addition the broad area of ice and snow at the Antarctica continent increases the reflected fraction of solar irradiance named as albedo [14].

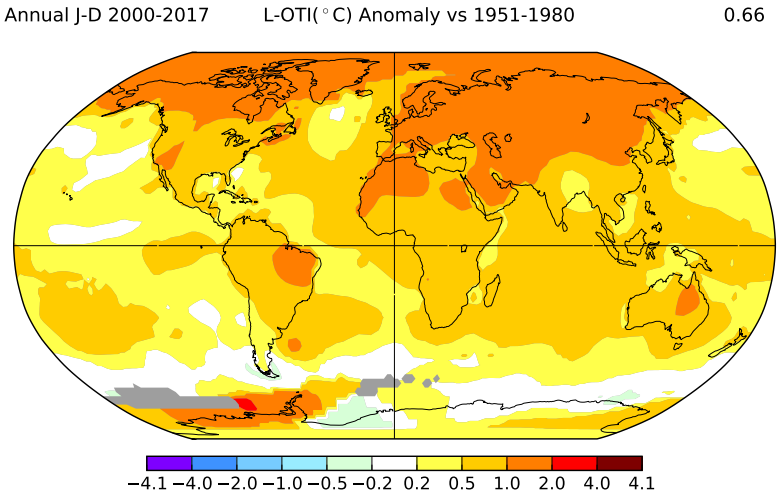

Figure 2.3: World surface temperature anomaly [15] and [16]. Sampling period of time 2000-2017. Reference period of time: 1951-1980. Temperatures data sources: land: GISS, Ocean: ERSST-v5. Robinson map projection. Areas in gray correspond to missing data

In order to control greenhouse emissions of the automotive sector, in all major countries (USA, Europe, China, Japan) of the world, tough emissions targets were being set to reduce the vehicle traffic's contribution of CO_2. These are derived from the 2015 global climate conference target to limit the maximum temperature increase of the earth to 2 degrees Celsius until 2100 [17]. In order to achieve these stringent targets the automotive industry will face a major change in its drivetrain. It will move from combustion to electrical engines. The technical realization of these engines will most likely be battery and fuel cell driven propulsion systems. In order to achieve that transition a major effort will be required in 4 industrial areas, i.e. growing electrical charging infrastructure, lowering battery cost, increasing the battery-electric vehicle ranges and developing new environmental friendly hydrogen production methods [18]. The road emissions make roughly 50% of the transport sector,

mainly in diesel and gasoline engines, resulting in 7% of the global CO_2 emissions. Several countries around the world are planning CO_2 reduction targets. Regarding EU, regulation policies proposal starts with the target of 95 g/km and 147 g/km for passenger cars and light commercial vehicles respectively before the year 2021 tested by the NEDC procedure. From 2021 the emission targets will be based on the new emissions test procedure, the Worldwide Harmonised Light Vehicle Test Procedure (WLTP). For 2025, targets for cars and vans will be 15% lower than in 2021 and for 2030 will have to be 30% lower than in 2021 [19].
In order to get the fleet average on CO_2 emissions down, the electrification of the drivetrain of future vehicles is a necessity. At the moment there are 5 different variants of powertrain electrification: Hybrid electric vehicles (HEV), plug-in hybrids (PHEV), range extender vehicles (EREV), battery electric vehicles (BEV) and fuel cell electric vehicles (FCEV). In spite of the future expansion of electrical vehicles the obstacles found in battery development technology makes unavoidable the existence of thermal engines. Main drawbacks encountered in BEV are related to energy density, limited by battery capacity, and the availability of materials world supply needed for batteries manufacturing [20]. As a result, much research is aimed towards addressing the limitations placed on performance by the weight, bulk and storage capacity of batteries [21]. The expected mid term future is a mixed transportation system, where engine technology will be spread depending on the autonomy requirements of transport.
Regarding local emission, urban traffic is generally addressed as the main source of pollution in urban areas. Mage et al. [22] indicates that motor traffic is a major source of air pollution in megacities. In half of them it is the single most important source. Since 1950, the global vehicle fleet has grown tenfold, and is estimated to double again within the next 20–30 years. Much of the expected growth in vehicle numbers is likely to occur in developing countries and in eastern Europe. As cities expand, more people will drive more vehicles over greater distances and for longer time. Emissions of air pollutants by motor traffic depends on different factors such as traffic density, driving habits or ratio of automobiles to trucks. In contrast to the trend in the industrialised countries of decreasing emissions of air pollutants, emissions are presently increasing in some cities of non-industrialised countries. Dispersion and dilution of air pollutants are strongly influenced by meteorological conditions, especially by wind direction, wind speed, turbulence, and atmospheric stability. Topographical siting and urban structures like street canyons, for example, have a great effect on these meteorological parameters. Chemical reactions also depend on ambient

weather conditions because they are influenced by short-wave radiation, air temperature and humidity [23]. In most of the industrialised world urban air pollution is now monitored routinely. Since 1974 World Health Organization (WHO) and the United Nations Environment Programme (UNEP) have, within the Global Environment Monitoring System (GEMS), collaborated on a project to monitor urban air quality, the so-called GEMS/AIR [23]. Concentrations of air pollutants by country are also reported yearly by the OECD at [24]. Megacities often contain high concentrations of ozone (O_3), sulphur dioxide (SO_2), nitric oxide (NO) and nitrogen dioxide (NO_2), the sum of which is known as nitrogen oxides (NOx); carbon monoxide (CO), hydrocarbons (HC) and particulate matter (PM). PM is often reported as mass concentration in the total suspended particulates (TSP), PM_{10}, and $PM_{2.5}$(particles with aerodynamic diameters of less than 40, 10, and 2.5 μm, respectively). The major PM chemical components are sulphate (SO_4), nitrate (NO_3), ammonium (NH_4) and organic carbon (OC), element carbon and soil (a weighted sum of mineral elements) [25]. High TSP and SO_2 concentrations are reported mostly in Asian cities. Gurjar et al. [26] carried out a study of health risks in megacities based on terms of mortality and morbidity (hospital admissions) due to air pollution focusing on SO_2, NO_2 and total suspended particles. Results suggested that some megacities like Los Angeles, New York, Osaka Kobe, Sao Paulo and Tokyo have low mortality from these pollutants. In contrast, the approximate numbers of cases is highest in cities characterized by a very high concentration of total TSP like Karachi, Dhaka and Beijing among others. According to the WHO, exposure to air pollutants can affect human health in various ways, leading to increased mortality and morbidity. Today, air pollution is the largest environmental risk factor in the world. High number of air pollutants are associated with significant excess mortality or morbidity, including NOx, ozone, carbon monoxide and sulphur dioxides and $PM_{2.5}$. Those pollutants have been most closely studied and are commonly used as proxy indicator of exposure to air pollution more generally. Evidence from epidemiological and toxicological studies on the effects of transport-related air pollution on health has increased substantially, although it is only a fraction of the total evidence on the effects of urban air pollution on health. A review of this evidence can be found at the WHO report of the Regional Office for Europe [27]. Based on the proven genotoxicity of its constituents, diesel exhaust has been judged as mutagenic and carcinogenic to humans by the World Health Organization. In June 2012, the International Agency for Research on Cancer (IARC) classified diesel engine exhaust gas as a group 1 carcinogen to humans [28], predominantly based upon epidemiological studies [29],[30] supported by a large number of experimental studies [31],[32].

These studies indicated that transport-related air pollution affects a number of health outcomes, including mortality, non-allergic respiratory morbidity, allergic illness and symptoms (such as asthma), cardiovascular morbidity, cancer, birth outcomes and male fertility. Transport-related air pollution increases the risk of death, particularly from cardiopulmonary causes, and of non-allergic respiratory symptoms and disease. Experimental research indicates that the effects are linked to changes in the formation of reactive oxygen species (ROS), changes in antioxidant defence, and increased non-allergic inflammation. While laboratory studies indicate that transport-related air pollution may increase the risk of developing an allergy and can exacerbate symptoms, particularly in susceptible subgroups, the evidence from population studies that supports this conclusion is inconsistent. Though only a few studies have been conducted, a significant increase in the risk of heart attack (myocardial infarction) following exposure to transport-related air pollution has been reported. Other studies and the experimental evidence indicate changes in autonomic nervous system regulation and increased inflammatory responses, as a result of exposure. A few studies suggest an increased incidence of lung cancer in people exposed to transport-related air pollution for a long time. An elevated incidence of cancer in children with high or prolonged exposure to air pollution cannot be excluded, though the supporting evidence is less consistent than that for adults.
In this section a summary of health studies of transport related air pollution is shown in population and experimental studies by pollutant and health impact. According to the WHO handbook [27], 4 different degrees of evidence are considered:

- Strong evidence: demonstrated by studies that are interpreted as showing a dose-related increase of pathologies.
- Some evidence: demonstrated by studies that are interpreted as showing a related increased incidence. The strength of the response is less than that required for clear evidence.
- Equivocal: demonstrated by studies that are interpreted as showing a marginal increase.
- No evidence: demonstrated by studies that are interpreted as showing no related increased incidence.

A substantial part of current knowledge about the health effects of transport-related air pollution comes from cross-sectional or cohort studies, in which exposure to indicators of transport-related air pollution were measured,

modelled or assessed by questionnaire, or indirect indicators of transport-related air pollution (such as distance to nearest street or traffic count) were used. Because long-term epidemiological studies were often started for reasons other than assessing the effects of air pollution or its transport-related portion, they are not designed optimally for contrasts in exposure and for end-point and confounder information. Some studies were designed to achieve a contrast in exposure to transport-related air pollution. It's therefore likely that differences in health between study subjects can be attributed to differences in this exposure. Although such studies address the issue of the role of road traffic better than time-series and panel studies, they have other limitations.

Health outcome	Population studies		Experimental studies	
	Pollutant	Evidence	Pollutant	Evidence
Mortality	Black smoke	Some	-	-
	Ozone	Some		
	PM2.5	Some		
Respiratory diseases (non-allergic)	Black smoke	Some	CAPs	Strong
	Ozone	Some	Ozone	Strong
	Nitrogen dioxide	Some	Nitrogen dioxide	Strong
	VOCs	Some	Diesel	Strong
Respiratory diseases (allergic)	Ozone	Some	PM	Strong
	Nitrogen dioxide	Some	CAPs	Some
	VOCs	Some	Diesel	Strong
			Nitrogen dioxide	Some
Cardiovascular diseases	Black smoke	Some	CAPs	Some
Cancer	Nitrogen dioxide	Some	VOCs	Some
	Diesel exhaust gas	Some	Diesel exhaust gas	Some
Reproductive outcomes	Nitrogen dioxide	Equivocal	Diesel exhaust gas	Some
	Carbon monoxide	Equivocal		
	Sulfur dioxide	Equivocal		
	PM	Equivocal		

Table 2.2: Health outcomes by pollutant in population and experimental studies. CAPs are a set of air pollutants that cause smog and acid rain. VOC are volatile organic compounds.

2.2 Pollutants formation

Despite CO_2 and H_2O are the main combustion products, several and harmful chemical species are formed during a combustion process. Around 80% (in volume) of the composition of diesel and gasoline fuels are saturated hydrocarbons. In Eq. (2.1) typical reaction process of an alkane is depicted. Depending on combustion conditions such as air to fuel ratio, temperature, pressure and oxygen concentration some of the pollutants may be increased and others reduced.

$$C_xH_{2x+2} + O_2 \longrightarrow H_2O + CO_2 + CO + CH_4 + \sum HxCy + NOx + C \tag{2.1}$$

Owing to the stratified combustion of direct injection diesel engines, pollutant emissions, mainly NOx and PM, are high in comparison to homogeneous combustion of spark ignition engines [33].

2.2.1 Nitrogen oxides

Most of emitted NOx by combustion sources is NO, and only a small fraction (typically 5% or less) appears as NO_2. A detailed analysis of the NO formation in combustion process can be found at [34]. NO is formed by three independent mechanisms: thermal NO, owing to the fixation of molecular nitrogen by oxygen atoms produced at high temperatures, prompt NO, driven by the attack of hydrocarbon free radicals on molecular nitrogen producing NO precursors and intermediate N_2O mechanism. The kinetics involved in these NO formation mechanisms are generally rate limiting. Concentrations of NO measured in hot combustion gases are typically orders of magnitude less than equilibrium concentrations at hot gas temperatures. Conversely, NO levels are effectively frozen as the combustion gases are cooled, resulting in flue gas concentrations which are much greater than equilibrium concentrations at low temperatures.
Thermal mechanism was proposed by Zeldovich in 1944. NO is caused by the oxidation of N_2 in presence of oxygen.

$$N_2 + O_2 \longleftrightarrow 2\,NO \tag{2.2}$$

The oxidation requires high levels of energy due to the triple bond of the nitrogen molecule. In Eq. (2.3) the two reaction steps are shown.

$$\begin{aligned} N_2 + O &\longleftrightarrow NO + N \\ N + O_2 &\longleftrightarrow NO + O \end{aligned} \tag{2.3}$$

The first step is rate-limiting and has a very high activation energy (75 kcal/mol). This high activation energy implies that high temperatures are required for significant NO formation, hence the designation "thermal NO". The Zeldovich mechanism is frequently extended to more accurately description of thermal NO formation under fuel-rich conditions and near stoichiometric conditions by including a third reaction step. This added reaction was proposed by Lavoie et al. [35]. Nitrogen atoms from the first step of Eq. (2.3) are oxidized in presence of OH free radicals.

$$\mathrm{N + OH \longleftrightarrow NO + H} \tag{2.4}$$

Nevertheless, it was observed that at the flame boundaries, in enriched fuel conditions, NO concentrations were higher than the thermal NO predictions. Fenimore [36] proposed a mechanism based on the role that hydrocarbons play on the formation of nitrogen radicals. The mechanism is a three steps reaction where eventually, nitrogen radicals are converted to NO by means of the Eq. (2.4). This mechanism is known as prompt-NO.

$$\begin{aligned} \mathrm{CH + 2\,N} &\longleftrightarrow \mathrm{HCN + N} \\ \mathrm{C + 2\,N} &\longleftrightarrow \mathrm{CN + N} \\ \mathrm{CH_2 + N_2} &\longleftrightarrow \mathrm{HCN + NH} \\ \mathrm{CH_2 + N_2} &\longleftrightarrow \mathrm{H_2 + CN + N} \end{aligned} \tag{2.5}$$

Finally, the intermediate N_2O mechanism is important in low temperature combustion, where temperature is lower than 1500 K, and in high air to fuel ratio conditions, where relative Air to Fuel Ratio (AFR) is higher than 1.25 [37]. Lavoie et al. [35] proposed the following mechanism that involves three N_2O reactions:

$$\begin{aligned} \mathrm{N_2O + O} &\longleftrightarrow \mathrm{NO + NO} \\ \mathrm{N_2O + O} &\longleftrightarrow \mathrm{N_2 + O_2} \\ \mathrm{N_2O + H} &\longleftrightarrow \mathrm{N_2 + OH} \end{aligned} \tag{2.6}$$

2.2.2 Hydrocarbons

Emissions of HC are mainly produced by incomplete combustion of hydrocarbon fuel. Essential components of unburned hydrocarbons are aromatics (benzene, toluene, ethyl benzene), olefins (e.g.propane, ethylene), acetylene and paraffins (e.g. methane). Unburned hydrocarbons will remain only in those areas where the flame does not propagate such as gaps close to the cylinder head gasket, piston top land, piston rings and spark plugs. HC

emissions are also formed due to the quench effect, misfire as well as due to the detachment of lubricating film [38].
Regarding diesel engines, since the air—fuel mixture is not an homogeneous mixture, extremely high excess-air ratios are present in certain zones during the diesel combustion process. The higher the air/fuel ratio, the lower is the local temperature. This means that chemical reactions proceed fairly slowly or may even 'freeze-up', thus leading to increased HC emissions. Concerning spark ignition engines, HC is significantly present in fuel-rich combustion products, and in high-temperature burned gases. HC emissions are very sensitive to the air-fuel ratio.

2.2.3 Carbon monoxide

CO is an intermediate compound in the hydrocarbon oxidation. CO emissions are highly dependent on air to fuel ratio. At enriched fuel conditions, CO emissions rise [37]. Maximum CO is generated when an engine runs rich, such as when starting or accelerating under load. Even when the intake air-fuel mixture is stoichiometric or lean, some CO will be generated. Poor mixing, local rich regions, and incomplete combustion will create some CO. All the reasons mentioned before for HC formation also apply for CO. But that does not mean that if HC increases CO emissions also rise, because the amount of dissociated CO_2 can decrease owing to lower combustion temperature, reducing the total CO emissions [39].

2.3 Road emissions regulation

Regarding the health risk that road pollutant emissions entail to population, several emissions regulations have been enforced by governments over time. The first worldwide road emission regulation was promoted by the state of California, USA. Congress passed the landmark Clean Air Act in 1970 and gave the newly-formed EPA the legal authority to regulate pollution from cars and other forms of transportation. EPA and the State of California have led the national effort to reduce vehicle pollution by adopting increasingly stringent standards [40]. In 1992, EPA established standards setting emission limits for CO at cold temperatures for the first time. Vehicle exhaust emissions are inherently rather variable, and so the best way to ensure that an emission test is reproducible is to perform it under standardised laboratory conditions. The procedures for the collection and analysis of the pollutants are specified

in detail in the legislation [41]. Light-duty vehicles are tested using a power-absorbing chassis dynamometer, whereas heavy-duty engines are operated on a test bed. A driving cycle is therefore a fixed schedule of vehicle operation which allows an emission test to be conducted under reproducible conditions [42]. Driving cycles are usually defined in terms of vehicle speed and gear selection as a function of time. A trained driver is employed to follow the driving cycle on the chassis dynamometer, and a 'driver's aid' is provided to ensure that the driven cycle is as close as possible, within stated tolerances, to the defined cycle. Emission levels are dependent upon many parameters, including vehicle-related factors such as model, size, fuel type, technology level and mileage, and operational factors such as speed, acceleration, gear selection and road gradient. Not surprisingly, therefore, different driving cycles have been developed for different types of vehicle such as cars, vans, trucks, buses and motorcycles. It is also useful to note that driving cycles may be used for a variety of purposes other than emissions measurement, such as testing engine or drive train durability, and may be used on a test track rather than in the laboratory. Depending on the character of speed and engine load changes, cycles can be broadly divided into 'steady state' cycles and 'transient' cycles. US Federal and California regulation defines four different driving cycles to test engine emissions:

- The city driving cycle (also known as FTP-75).
  - 1874 s. of duration.
  - 17.77 km length.
  - 32.2 km/h of average speed.
  - 91.2 km/h of maximum speed.
- The highway driving cycle (also known as Highway Fuel Economy Test).
  - 765 s. of duration.
  - 16.5 km length.
  - 77.7 km/h of average speed.
  - 96.4 km/h of maximum speed.
- SC03 air conditioning driving cycle.
  - 598 s. of duration.
  - 5.76 km length.
  - 34.9 km/h of average speed.

  - 88 km/h of maximum speed.

- US06 high speed/high load cycle.
  - 596 s. of duration.
  - 12.86 km length.
  - 77.2 km/h of average speed.
  - 129 km/h of maximum speed.

The European Union, in comparison, started to regulate vehicle emissions a bit later. The initial drivers for legislation in 1970 were objectives related to vehicle safety and a coherent internal market rather than environmental objectives. Responses to the oil crisis of the 70s tended to focus on the introduction of fuel taxes of varying intensity at Member State level in order to reduce consumption pressures, rather than the adoption of efficiency standards. It was not until 1992 that legislation (the "Euro 1" requirements) was passed to set limits for nitrogen oxides emissions (NOx) and tackle acidification and other air quality issues. In effect, tighter limits meant that three-way catalytic converters were eventually required in new petrol cars from the early 1990. A broaden study comparing emissions standards between US and EU was carried out in 2016 by the policy department A: Economic and Scientific Policy [43]. In terms of the level of emission limits relating to air quality, EU emission limits are on average less stringent than those in the US. Within the US, however, two sets of emission limits apply depending on the State concerned, with stricter limits applying in California and a dozen US states which have chosen to follow Californian standards. When it comes to the control of greenhouse gas emissions, it is the EU that has stricter standards (in addition to generally higher fuel taxes in EU Member States than in the US). Regarding European test driving cycles, in 1970 the ECE-15, also known as UDC, was launched. The cycle represented the typical driving pattern of European cities, and is characterized by low engine load, low exhaust gas temperature, and low vehicle speed. In 1990, the Extra-Urban Driving Cycle (EUDC) was introduced [44]. The combination of the ECE-15 and the EUDC leaded to the MVEG-A test cycle, which is composed by four ECE-15 repetitions and one EUDC at the end of the cycle. In 2000, cold start emissions measurement were included in the driving test leading to the New European Driving Cycle (NEDC) [45], also known as MVEG-B. Previous MVEG-A procedure allowed an initial idling period where emissions weren't sampled for the first 40 s. Nowadays, NEDC procedure has been replaced by the Worldwide harmonized Light vehicles Test Cycle (WLTC).

The WLTC differs from the NEDC in the intense transient conditions of the driving pattern. Driving features by cycle are:

- ECE-15:
  - 195 s. of duration.
  - 1 km length.
  - 25.93 km/h of average speed.
  - 50 km/h of maximum speed.
- NEDC:
  - 1180 s. of duration.
  - 10.9 km length.
  - 43.1 km/h of average speed.
  - 120 km/h of maximum speed.
- WLTC:
  - 1800 s. of duration.
  - 23.25 km length.
  - 53.76 km/h of average speed.
  - 131.3 km/h of maximum speed.

In addition to the driving cycles procedures, European regulation includes on road pollutant emission measurement, by means of Portable Emissions Measurement Systems (PEMS), known as Real Driving Emissions testing. Under this type approval, vehicles are not tested on rolling test bed but in real outdoors routes. A wide range of engine loads, vehicle speeds and ambient temperature and pressure differences have to be meet by a real driving route. Currently, there is a conformity factor between the driving cycle emissions and the RDE that carmakers have to comply. This factor will be more stringent with time.
As engine technology improves, pollutant reduction is accomplished. Stringent future pollutant regulations are expected in the mid term future. Fig. 2.4 depicts the EU emissions regulation timeline since 2013 to 2023. In september 2017 the WLTC procedure replaced the NEDC. Nevertheless, CO_2 targets that car manufacturers have to meet are still based on the old NEDC test. For checking the compliance of new vehicles the WLTP-CO_2 values will be translated back to NEDC-equivalent values to monitor compliance against

the CO_2 targets set by the European Union. By correlation analysis, the European Commission determine how the values for new cars measured on the WLTP cycle will be translated back to NEDC equivalent values for monitoring against the EU CO_2 targets [46]. These correlated NEDC values will either be calculated using a correlation simulation tool or based on the results of physical NEDC tests. By 2020 CO_2 compliance will be based on WLTC procedures. In addition to driving cycles test procedure, EU commission approved the application of Real Driving Emissions testing type approval since 2017.

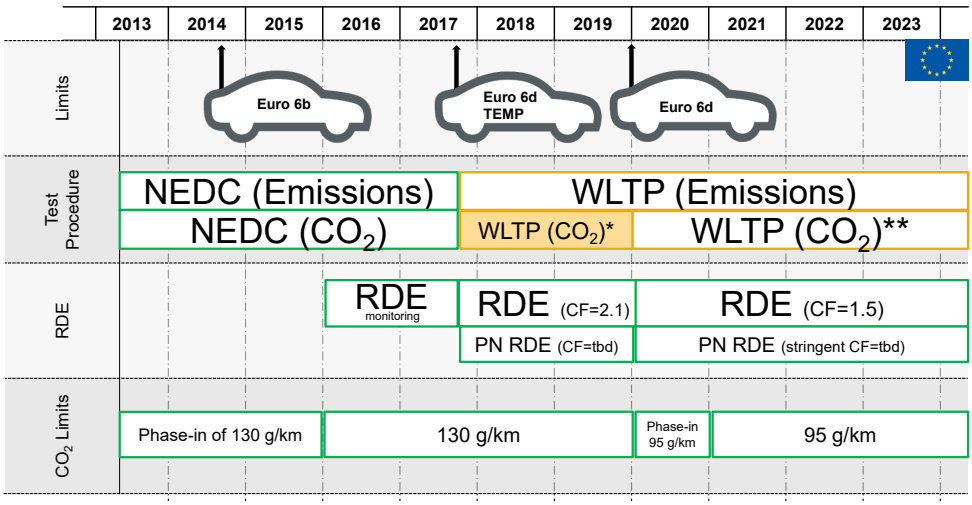

Figure 2.4: EU emission regulation time line.

In Fig. 2.5 the evolution of HSDI engines, since 1974 until 2004, with the achieved emissions goals are depicted [47]. USA regulations evolution has been included in the figure as they are previous to European standards and in general more restrictive. Both gasoline and diesel engines have to achieve the same pollutant goals. Oxidative catalytic converter is not included in the chart as it was already mandatory in 1975. Figure pollutant milestones are focussed on both PM and NOx reduction. Since roughly 2000 until today, aftertreatment systems such as Diesel Particulate Filter (DPF), Lean NOx Trap (LNT) and the recent Selective Catalytic Reduction (SCR) technology have been necessary to fullfill both USA and EU standards. The evolution of those technologies is not included in the figure.

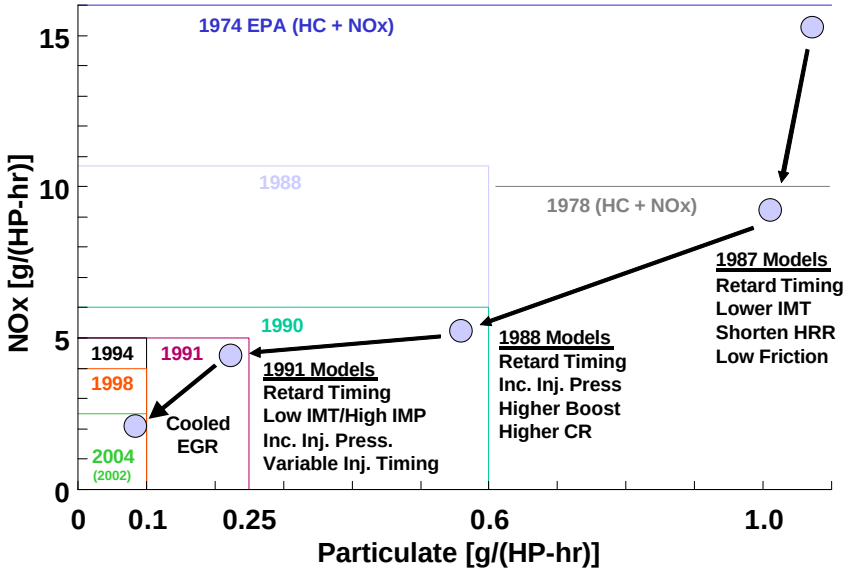

Figure 2.5: Evolution of diesel engines technology and pollutant reduction achivements. IMT: Intake Manifold Temperature. CR: Compression Ratio. HRR: Heat Release Rate.

Bibliography

[4] T. J. Crowley. "Causes of climate change over the past 1000 years". *Science* 289.5477 (2000), pp. 270–277.

[5] J. Cook, N. Oreskes, P. T. Doran, W. R. Anderegg, B. Verheggen, E. W. Maibach, J. S. Carlton, S. Lewandowsky, A. G. Skuce, S. A. Green, et al. "Consensus on consensus: a synthesis of consensus estimates on human-caused global warming". *Environmental Research Letters* 11.4 (2016), p. 048002.

[6] S. Manabe and R. T. Wetherald. "The effects of doubling the CO2 concentration on the climate of a general circulation model". *Journal of the Atmospheric Sciences* 32.1 (1975), pp. 3–15.

[7] S. H. Schneider. "The Greenhouse Effect: Science and Policy". *Science* 243.4892 (1989), pp. 771–781.

[8] R. Dickerson, S Kondragunta, G Stenchikov, K. Civerolo, B. Doddridge, and B. Holben. "The impact of aerosols on solar ultraviolet radiation and photochemical smog". *Science* 278.5339 (1997), pp. 827–830.

[9] R. Atkinson and A. C. Lloyd. "Evaluation of kinetic and mechanistic data for modeling of photochemical smog". *Journal of physical and chemical reference data* 13.2 (1984), pp. 315–444.

[10] C. B. Field, V. R. Barros, D. Dokken, K. Mach, M. Mastrandrea, T. Bilir, M Chatterjee, K. Ebi, Y. Estrada, R. Genova, et al. *IPCC, 2014: Climate Change 2014: Impacts, Adaptation, and Vulnerability. Part A: Global and Sectoral Aspects. Contribution of Working Group II to the Fifth Assessment Report of the Intergovernmental Panel on Climate Change*. 2014.

[11] E. W. Team et al. "ESRL Global Monitoring Division-Global Greenhouse Gas Reference Network" (2005).

[12] P. Tans and R. Keeling. *ESRL Global Monitoring Division-Global Greenhouse Gas Reference Network*. `www.esrl.noaa.gov/gmd/ccgg/trends/` and `scrippsco2.ucsd.edu/`. 2018.

[13] T. Laepple, S. Jewson, and K. Coughlin. "Interannual temperature predictions using the CMIP3 multi-model ensemble mean". *Geophysical Research Letters* 35.10 (2008).

[14] A. McEvoy, T. Markvart, L. Castañer, T Markvart, and L. Castaner. *Practical handbook of photovoltaics: fundamentals and applications*. Elsevier, 2003.

[15] J. Hansen, R. Ruedy, M. Sato, and K. Lo. "Global surface temperature change". *Reviews of Geophysics* 48.4 (2010).

[16] *GISS Surface Temperature Analysis (GISTEMP)*. 2018. URL: `https://data.giss.nasa.gov/gistemp/`.

[17] I. Union. *Communication from the Commission to the European Parliament, the Council, the European Economic and Social Committee and the Committee of the Regions*. Brussels, 2016.

[18] R. Hannappel. "The impact of global warming on the automotive industry". In: *AIP Conference Proceedings*. Vol. 1871. 1. AIP Publishing LLC, 2017, p. 060001.

[19] Council of European Union. *Proposal for a regulation of the european parlamient and of the council setting emission performance standards for new passenger cars and for new light commercial vehicles as part of the Union's integrated approach to reduce CO2 emissions from light-duty vehicles and amending Regulation (EC) No 715/2007*. 2017.

[20] H. Vikström, S. Davidsson, and M. Höök. "Lithium availability and future production outlooks". *Applied Energy* 110 (2013), pp. 252 –266.

[21] O. Egbue and S. Long. "Barriers to widespread adoption of electric vehicles: An analysis of consumer attitudes and perceptions". *Energy Policy* 48 (2012), pp. 717–729.

[22] D. Mage, G. Ozolins, P. Peterson, A. Webster, R. Orthofer, V. Vandeweerd, and M. Gwynne. "Urban air pollution in megacities of the world". *Atmospheric Environment* 30.5 (1996), pp. 681–686.

[23] H. Mayer. "Air pollution in cities". *Atmospheric Environment* 33.24-25 (1999), pp. 4029–4037.

[24] OECD. *The Economic Consequences of Outdoor Air Pollution*. OECD Publishing, Paris, 2016.

[25] M. J. Molina and L. T. Molina. "Journal of the Air and Waste Management Association Megacities and Atmospheric Pollution Megacities and Atmospheric Pollution". *Journal of the Air and Waste Management Association* 546 (2004), pp. 644–680.

[26] B. Gurjar, A. Jain, A. Sharma, A. Agarwal, P. Gupta, A. Nagpure, and J. Lelieveld. "Human health risks in megacities due to air pollution". *Atmospheric Environment* 44.36 (2010), pp. 4606–4613.

[27] WHO. *Health effects of transport related air pollution.* Ed. by B. K.-D. Michal Krzyzanowski and J. Schneider. WHO Regional Office for Europe, 2005.

[28] I. A. for Research on Cancer et al. "IARC: Diesel engine exhaust carcinogenic". *Press release* 213 (2012).

[29] J. G. Hemmingsen, P. Møller, K. Jantzen, B. A. Jönsson, M. Albin, A. Wierzbicka, A. Gudmundsson, S. Loft, and J. Rissler. "Controlled exposure to diesel exhaust and traffic noise–Effects on oxidative stress and activation in mononuclear blood cells". *Mutation Research/Fundamental and Molecular Mechanisms of Mutagenesis* 775 (2015), pp. 66–71.

[30] D. T. Silverman, C. M. Samanic, J. H. Lubin, A. E. Blair, P. A. Stewart, R. Vermeulen, J. B. Coble, N. Rothman, P. L. Schleiff, W. D. Travis, et al. "The diesel exhaust in miners study: a nested case–control study of lung cancer and diesel exhaust". *Journal of the National Cancer Institute* 104.11 (2012), pp. 855–868.

[31] S. Steiner, C. Bisig, A. Petri-Fink, and B. Rothen-Rutishauser. "Diesel exhaust: current knowledge of adverse effects and underlying cellular mechanisms." *Archives of toxicology* 90.7 (2016), pp. 1541–53.

[32] J. G. Hemmingsen, P. Møller, J. K. Nøjgaard, M. Roursgaard, and S. Loft. "Oxidative stress, genotoxicity, and vascular cell adhesion molecule expression in cells exposed to particulate matter from combustion of conventional diesel and methyl ester biodiesel blends". *Environmental science & technology* 45.19 (2011), pp. 8545–8551.

[33] T. R. Dallmann and R. A. Harley. "Evaluation of mobile source emission trends in the United States". *Journal of Geophysical Research: Atmospheres* 115.D14 (2010).

[34] K. M. Nichols, L. M. Thompson, and H. L. Empie Jr. "A review of NOx formation mechanisms in recovery furnaces" (1991).

[35] G. A. LAVOIE, J. B. HEYWOOD, and J. C. KECK. "Experimental and Theoretical Study of Nitric Oxide Formation in Internal Combustion Engines". *Combustion Science and Technology* 1.4 (1970), pp. 313–326.

[36] C. Fenimore. "Formation of nitric oxide in premixed hydrocarbon flames". In: *Symposium (International) on Combustion*. Vol. 13. 1. Elsevier. 1971, pp. 373–380.

[37] F. Payri and J. María. *Motores de combustión interna alternativos*. 2011.

[38] A. Abdel-Rahman. "On the emissions from internal-combustion engines: a review". *International Journal of Energy Research* 22.6 (1998), pp. 483–513.

[39] M. E. R. Perea. "Assessment of fuel consumption reduction strategies on a gasoline turbocharged direct injection engine with a cooled EGR system". PhD thesis. 2016.

[40] *Citizens to Preserve Overton Park, Inc. v. Volpe*. 1971.

[41] A. Faiz, C. S. Weaver, and M. P. Walsh. *Air pollution from motor vehicles: standards and technologies for controlling emissions*. World Bank Publications, 1996.

[42] T. J. BARLOW, S Latham, I. McCrae, and P. Boulter. "A reference book of driving cycles for use in the measurement of road vehicle emissions". *TRL Published Project Report* (2009).

[43] M Nesbit, M Fergusson, A Colsa, J Ohlendorf, C Hayes, K Paquel, and J. Schweitzer. "Comparative study on the differences between the EU and US legislation on emissions in the automotive sector". *Policy Department A: Economic and Scientific Policy, European Union* (2016).

[44] E. Directive. "90/C81/01,Emission Test Cycles for the Certification of light duty vehicles in Europe, EEC Emission Cycles". *EEC Emission Cycles, 1999* (1999).

[45] E. Regulation. "No 595/2009 of the European Parliament and of The Council of 18 June 2009 on type-approval of motor vehicles and engines with respect to emissions from heavy duty vehicles (Euro VI) and on access to vehicle repair and maintenance information and amending Regulation (EC) No 715/2007 and Directive 2007/46/EC and repealing Directives 80/1269". *EEC* 55 (2005).

[46] "Commission Delegated Regulation (EU) 2017/1502 of 2 June 2017 amending Annexes I and II to Regulation (EC) No 443/2009 of the European Parliament and of the Council for the purpose of adapting them to the change in the regulatory test procedure for the measurement of CO2 from light duty vehicles". *Official Journal of the European Union* L 221 (26 August 2017), pp. 4–10.

[47] P. Flynn. *Diesels-Promises & Issues.* Tech. rep. Cummins Engine Company (US), 2000.

Chapter 3

Methods and experimental

Contents

3.1 Introduction

In this chapter the experimental facility, the engine layout and the laboratory measurement devices are described. Test procedure and analytic tools needed for data analysis are explained too. Finally error propagation from exhaust gas sampling uncertainty is analysed for EGR and exhaust mass flow calculation.

3.2 Engine description

Experiments with two in line 4 cylinders, turbocharged HSDI diesel engines were conducted. The main features of both engines are depicted in Table 3.1. Engine 1 is a DW10C PSA Euro 5. Engine 2 is a R9M Euro 6 engine.

Table 3.1: Engine specifications

Feature	Engine 1	Engine 2
Cylinder number	In-line 4	In-line 4
Bore x stroke (mm)	80x79.5	85x88
Displacement (cm3)	1598	1997
Compression ratio	15.4	17.6
Maximum power (kW/rpm)	96/4000	120/3750
Maximum torque (Nm/rpm)	320/1750	340/2000
Torque at maximum power (Nm)	315	300
Specific power (kW/l)	60.86	81.5
Valve number	16	16
Valvetrain	Double cam shaft over head	
Fuel delivery system	Common rail. Direct injection	
EGR system	HP and LP cooled EGR	
Intake boosting	Turbocharger with VGT	
Intake cooling system	Water charge air cooler (WCAC)	

Both engines are equipped with aftertreatments systems that include a DOC and DPF. Engine 1 has been used for experimental characterization

of the current automotive technology operating at low ambient temperature using the original calibration and engine architecture of the carmaker. Engine 1 outcomes are analysed in Chapter 4, where raw emissions are sampled, and Chapter 5, where DOC performance is studied at low temperatures. All novelties, engine (EGR) calibration and thermal systems hardware and software, for emissions reduction were applied in the engine 2. Results are shown in Chapter 6. Concerning the engine 2, the intake manifold is a cutting edge design where the classic intercooler has been replaced by a water/air heat exchanger, known as Water Charge Air Cooler (WCAC), that is joined to a short intake manifold. High pressure exhaust gas recirculation (HP EGR) duct connects at one side of this short manifold and mixes the exhaust gases with the fresh air trying to avoid HP EGR dispersion between cylinders. A deeper description of the system can be found at [48]. The result is a compact Air Intake Module (AIM) in which lengths are reduced and therefore time response under transient operation points too. Replacing the intercooler by a WCAC allows the application of several thermal management systems, where WCAC coolant works as a heat recovery fluid [49]. Fig. 3.1 shows a drawing of the AIM. Engine on board measurement devices, such as common rail

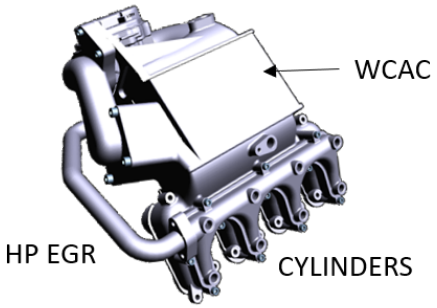

Figure 3.1: Air intake module

pressure sensor, coolant thermoresistances and lambda sensor, were recorded by INCA software through ETAS hardware for ECU handling. The main use of these variables was to ensure the repetitiveness of the performed tests in order to detect anomalies during test performing. In addition, special access to ECU settings allowed the calibration modification in engine 2 where thermal management novelties were applied.

3.3 Test cell

Ambient temperature controlled tests were carried out in a climatic chamber. Temperature sensitive devices such as gas sampling analysis and fuel balance were placed outdoors at constant temperature of 20 ^{o}C. Engine coolant and oil were cooled at the climatic chamber. Fuel was cooled down by a heat exchanger using a ethylene glycol flow coming from a vessel of 1 m^3 placed in the test cell. Engine speed and torque were controlled by an electrical dynamometer at both steady and transient conditions. Section 3.5 digs on how NEDC and WLTC driving cycles are performed by the dynamometer. The engine is controlled in the test bench by using an interface developed by Horiba called STARS that communicates the engine dynamometer control management with the engine pedal sensor and actuator. Electrical dynamometer torque and speed and pedal position are set by a PID controller working in closed loop. Vehicle speed is converted into an engine speed target knowing the gear ratio of the simulated vehicle. Following, engine torque is set by means of the electrical dynamomenter load that takes into account the tire-road friction, powertrain transmission losses, aerodynamic drag and vehicle mass. As torque varies, engine speed is modified leading the pedal position actuator to work for reaching the target engine speed.
In addition to on board engine measurement devices, several measurements were connected to the engine. All laboratory measurements devices were sampled at 10 Hz and handled by a PLC.
The fuel measurement system employed in this research work was an AVL 733S fuel balance. Fuel mass flow measure is based on the principle of gravimetric measurement. The amount of fuel consumption is determined directly by measuring the time related weight decrease of the measuring vessel by means of a capacitive sensor. The fuel consumption is determined using an appropriate weighing vessel linked by a bending beam to a capacitive displacement sensor. Due to the fact that the weighting vessel has to be refilled for each measurement this is a discontinuous measurement principle. The mass of fuel consumed is therefore determined gravimetrically, which means that the density does not have to be determined in addition. The fuel consumption can thus be determined with and uncertainty of 0.12%. The built-in calibration unit is standard scope of supply and allows calibration and accuracy check according to ISO 9001 which helps to reduce downtimes. The operation of this system is automatically performed by STARS software, controlling the filling of the volume used to measure the fuel mass flowing into the engine. The accuracy and specifications of the fuel balance are presented in Table 3.2

Table 3.2: Fuel balance features

Characteristics	Units	Value
Measuring range	kg/h	0 to 150
Vessel capacity	g	1800
Measurement uncertainty	%	0.12
Ambient temperature	ºC	0 to 60
Fuel temperature	ºC	-10 to 70
Max. fuel supply flow	kg/h	100

Regarding air mass flow measurement, an ABB Sensy flow FMT700-P meter was used to measure the air mass flow that goes into the engine. Measurement physical principle relies on hot-film anemometry. The heated platinum film resistor is maintained at a constant overtemperature in relation to an unheated platinum sensor inside the gas flow. The heating power required for maintaining the overtemperature depends directly on the flow rate and the material properties of the gas. With a known, and constant, gas composition the mass-flow can be determined by electronically evaluating the heater current/mass-flow curve without additional pressure and temperature compensation. This sensy flow has a measure uncertainty of less than 1% of the measured value and a time response less than 12 ms, which suits perfectly to perform transient tests such as driving cycles.
Intake, exhaust gas, coolant and fuel temperatures among others were measured by type K thermocouples. With a range of temperature that goes from -270 to 1260 ºC and a uncertainty of 0.75% for temperatures above zero and 2.2% for sub-zero temperature measurement. K-thermocouples are the most popular and suitable thermometry devices for temperature measurement on engine research. Like temperature, pressure measurement in the aforementioned locations are needed. Average pressure sensors PME transmitter P40, with a measure uncertainty of 0.3%, were used. Engine speed was measured using a Kistler crank-angle encoder type 2613A with an uncertainty of 0.006%. Engine torque was measured by the SHENCK DYNAS dynamometer with an uncertainty of 0.1%.
Concerning pollutant emissions, Horiba 7100, MEXA-ONE and OBS-ONE gas analysers were used. All measurements were obtained in volumetric concentration, so emissions rates have to be calculated by means of the total gas mass flow. Humidity correction coefficient has to be applied to raw data in case of 7100 and MEXA-ONE as measurement is done in dry conditions.

In case of OBS-ONE no correction is required as measurement is done in wet conditions. Gas sampling devices comprises several optical techniques for chemical analysis. In the following lines the main features and physical principles of the gas sampling techniques are described. More details about gas analysers operation can be found at [50]. CO and CO_2 concentration is obtained by means of Non Dispersive Infrared (NDIR) spectroscopy. The physical principle in what this technique relies is know as absorption spectroscopy. Beams coming from an infrared source are directed to a sampling gas. According to Beer-Lambert's law the ratio between the transmitted and the incident radiation intensity, known as transmittance, depends on the concentrations of the attenuating species in the material sample. Gas radiation absorbance is governed by a frequency depending absorbance coefficient specific for each chemical compound. Spectra features intensity, obtained by the Beer-Lambert's law, at constant pressure, temperature and absorption length (i.e the path length of the beam of light through the material sample) are proportional to the concentration compound. Knowing this relation, molar concentration by chemical compound can be inferred by comparing the measured features with previous calibrated conditions of the same compounds where molar concentration is known. By means of the CO_2 measure at the engine intake and the exhaust manifold the recirculated exhaust gases rate (EGR) is calculated. EGR is one of the most popular techniques to reduce NOx emissions in diesel engines. By EGR enabling, in cylinder oxygen concentration is diluted and combustion rate is reduced driving to lower peak combustion temperature that eventually causes lower NOx formation [51], [52] and [53]. EGR is defined as the ratio between the recirculated mass flow and the total intake mass flow rate. By applying the species continuity conservation equation between the intake and the exhaust manifold the EGR can be obtained in terms of the CO_2 concentration. EGR may be calculated from any chemical specie e.g CO, O_2, NOx. But, as CO_2 is the main chemical specie released as combustion product, its measurement is more reliable than other species whose concentrations remain hundred of times lower. In addition, the definition of EGR based on CO_2 may be applied at any combustion condition, as CO_2 is always produced no matter the type of combustion e.g SI, CI. The following EGR definition considers equal the molecular mass for both fresh air and exhaust gases. An exhaustive study of the influence on considering both molecular mass different was carried out by Vera García [54]. By considering the same air and exhaust gas molecular mass the maximum error was below 0.3%

$$EGR = \frac{\dot{m}_{EGR}}{\dot{m}_{air} + \dot{m}_{EGR}} = \frac{[CO_{2in}] - [CO_{2amb}]}{[CO_{2exh}] - [CO_{2amb}]} \tag{3.1}$$

where *in* and *exh* refers to the CO_2 measured at the intake and exhaust manifold respectively and *amb* is the ambient CO_2.
Regarding hydrocarbons, Flame Ionization Detection (FID) technique is applied to the exhaust stream. FID uses the phenomenon that HC combustion in a hydrogen flame generates HC ions. The FID response is in approximate proportion to the number of carbon atoms contained in the sample. The FID method is commonly used for measuring HC contained in the engine exhaust gas as Total Hydrocarbon (HC) in ppmC units Fig. 3.2. shows the configuration of an FID.

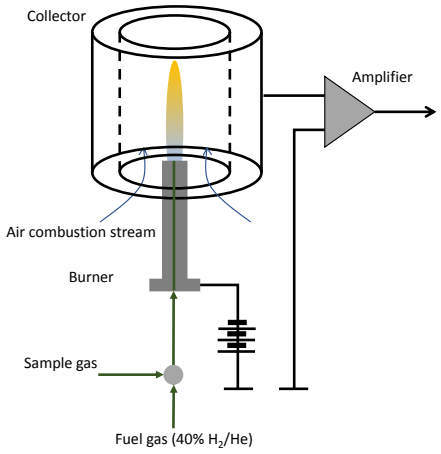

Figure 3.2: FID details

The hydrogen-based flame is formed at a burner nozzle by supplying fuel gas (H_2, or a mixture of H_2 and an inert gas such as He or N_2) and combustion air. The sample gas is introduced into the hydrogen flame with the fuel gas, where HCs in the sample gas are ionized. An electric potential is applied across the nozzle to the collector electrode surrounding the nozzle; therefore, an electric current is generated between the nozzle and the electrode due to HC ions in the flame. This ion current is nearly proportional to the amount of carbon introduced into the flame as HCs; hence, the HC concentration can be known as "THC" in "ppmC" units. The sensitivity of FID depends on each HC component. In engine exhaust gas measurement, the FID sensitivity for each HC is represented by a response factor that indicates the relative sensitivity compared to propane used as calibration gas. Generally, the FID has lower

sensitivity to oxygenated HC components such as methanol. The FID response factor can also be influenced by detector structure and sample condition (e.g., detector temperature and gas flow rate at the detector).The FID sensitivity depends not only on the concentration and type of HC in the sample gas but also on the flow rates of the combustion air and fuel gas. The FID shows negligible interference form inorganic components such as CO,CO_2, H_2O and NO.
Concerning nitrogen oxides, Chemiluminescence Detection (CLD) technique is used for NO and NO_2 measurement. Chemiluminescence detection address any reaction that involves light emission. A simplified schema of a NO detector using the CLD is shown in Fig. 3.3.

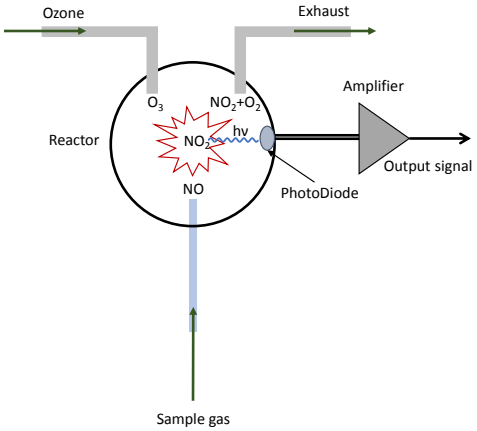

Figure 3.3: Chemiluminiscent detector schematic

In the reactor, the NO sampling gas is oxidized to NO_2 by ozone (O_3), which is also introduced into the reactor. This reaction produces a small fraction (approx. 10%) of excited $NO_2^\bullet$. As this excited $NO_2^\bullet$ decays to its ground state, excitation energy is emitted as photons. Eq. (3.2) displays this reaction.

$$\begin{aligned} NO + O_3 &\longrightarrow NO_2^\bullet + O_2 \\ NO_2^\bullet &\longrightarrow NO_2 + h\nu \end{aligned} \tag{3.2}$$

The intensity of luminescence is proportional to the amount of NO reacted with O_3 therefore, detecting the luminescence intensity with a photoelectric element provides the NO concentration in the sample gas. The CLD can be used to measure NOx as well as NO. In this case, a converting unit (NOx converter) packed with a carbon-based material is located before the detector

to convert NO_2 into NO. NO_2 in the sample gas is deoxidized by reacting with carbon in the NOx converted, as is shown in the following reactions:

$$\begin{aligned} NO_2 + C &\longrightarrow NO + CO \\ 2\,NO_2 + C &\longrightarrow 2\,NO + CO_2 \end{aligned} \tag{3.3}$$

The output of a CLD with a NOx converter provides total concentration of NO and NO_2 which is NO_x. The NO_2 concentration also can be obtained by subtracting the NO concentration from the NOx concentration, if two analysers, one for NO and one for NOx are used.
Finally, Oxygen concentration at the exhaust is measured by a Magnetopneumatic Detector (MPD) which working principle relies on oxygen ParaMagnetic Detection (PMD). MPD is based on magnetics susceptibility of an oxygen carrier sampling gas. Current flows through an electromagnet creating an alternating magnetic field, between magnetic poles. When the sample gas is introduced in the magnetic field, components with high magnetic susceptibility, such as O_2, are drawn toward the magnet pole. Consequently, the pressure near the magnetic pole rises in relation to the concentration of drawn components, mainly O_2 in the case of a diesel engine exhaust gas. Non-uniform oxygen concentration entails a pressure difference that causes a mechanical displacement of a dumb-bell pressure sensor. Measurement of all aforementioned chemical compounds is needed for accomplish this work. In Table 3.3 the sample location, the experimental technique and the purpose of carrying out the measurement by chemical compound is shown.

Table 3.3: Measured chemical compounds

Specie	Technique	Sampling point	Aim
THC	FID	PRE and POST Aftertreatment	Pollutant emissions and DOC performance analysis
CO	NDIR	PRE and POST Aftertreatment	Pollutant emissions and DOC performance analysis
NOx	CLD	PRE and POST Aftertreatment	Pollutant emissions and DOC performance analysis
O_2	MPD	PRE and POST Aftertreatment	DOC performance analysis
H_2O	NDIR	PRE and POST LP EGR cooler	Recovery enegy analysis of exhaust water vapor latent enthalpy
CO_2	NDIR	PRE Aftertreatment and intake manifold	EGR rate calculation

Sensor locations are displayed in the engine setup layout presented in Fig. 3.4. All sampling gas lines are heated by electrical resistors to avoid in-line condensation. Pressure and temperature probes are placed at the centre of pipes and tubes where sensors are located. Air flow meter inlet air is previously filtered to remove any presence of ambient dust or dirt. In some tests WCAC cooling lines are connected to a glycol vessel (not depicted in Fig. 3.4) to control the WCAC coolant temperature. In this thesis LP EGR cooler is also used as an Exhaust Gas Heat Recovery (EGHR) system in some low temperature tests. For this reason the heat exchanger is named as LP EGR/EGHR in the figure.

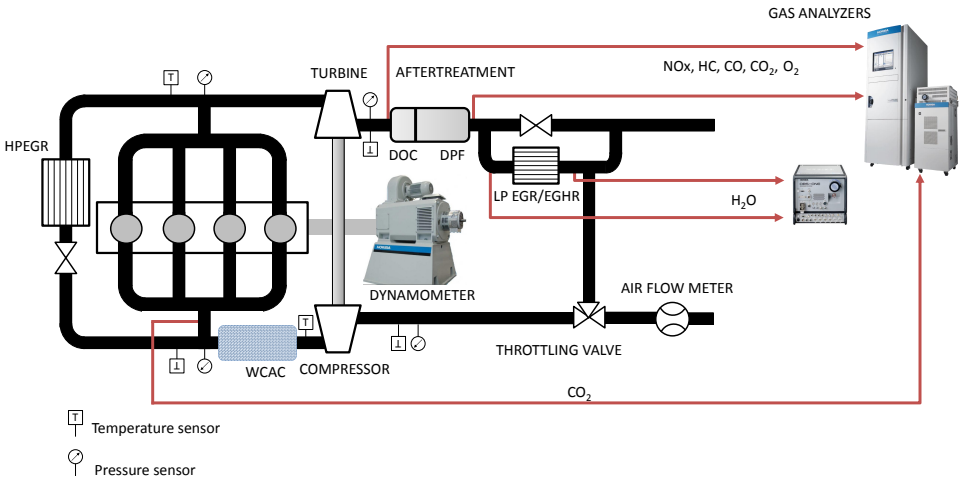

Figure 3.4: Engine layout

3.4 Thermal management solutions description

Two different thermal management configurations were tested in the test cell. The first one, named as engine cooling management layout, is based on the engine coolant flow management for avoiding overcooling during cold starts, specially at low ambient temperatures. The second lays on the exhaust gas heat recovery (EGHR) by means of a modified LP EGR cooler. Comparing both systems, the thermal management approaches are very different. On one hand, the engine cooling management is aimed to temperature increase by reducing heat transfer losses between the gas flow and the coolant flows. On the other hand, the EGHR system is aimed to intake temperature heating by means of two heat exchangers, one placed at the exhaust line and the other at the intake manifold. Intake air heating focusses on initial combustion conditions enhancement by increasing the initial reaction temperature.

3.4.1 Engine coolant management layout

The engine coolant management layout is depicted in Fig. 3.5. Coolant flow is managed by means of an electric valve. Four different coolant regulation strategies can be set depending on the electric valve position:

- Radiator cooling down: enabled when engine coolant temperature reaches 80 ^{o}C.
- Radiator bypass: enabled when engine coolant flow is recirculated.
- Microflow: very low coolant flow is performed for cooling down EGR.
- 0 flow: no coolant flows through the engine.

0 flow configuration requires an additional electric pump for avoiding EGR coolers overheating. Regardless the tested thermal layout, once high loads are performed, e.g EUDC of the NEDC, the thermal strategy is switched to the radiator bypass for avoiding engine coolant overheating. In case of coolant temperature reaches 80 ^{o}C, radiator cooling position is enabled for removing the engine heat surplus.

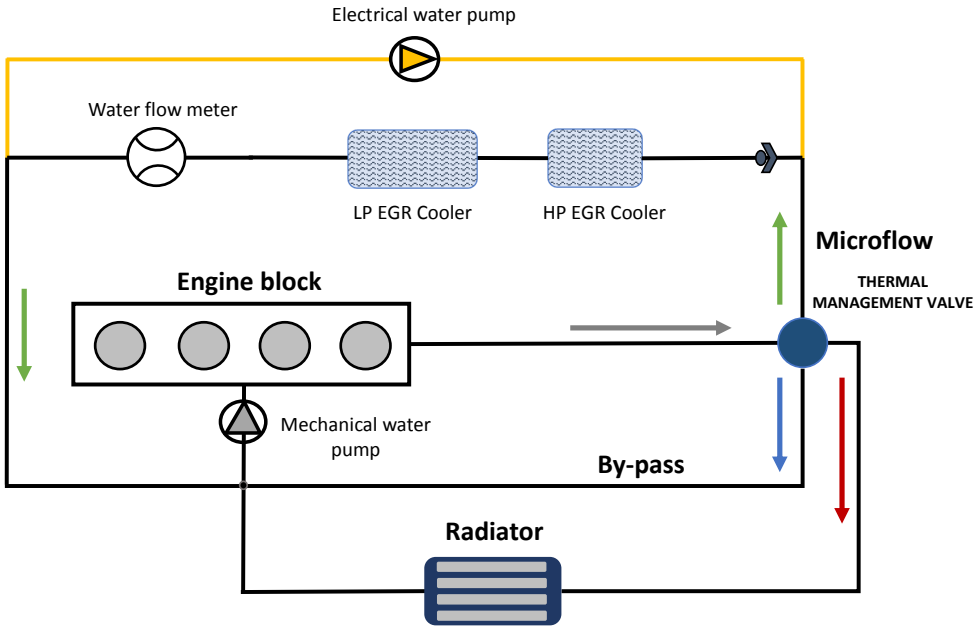

Figure 3.5: Engine coolant thermal management layout. Coloured arrows show the coolant flow directions. Red: radiator flow. Blue: bypass flow. Green: microflow. Gray: common flow of all strategies with the exception of 0 flow.

Coloured arrows show the coolant flow direction. Flow in red arrow is only enabled when heatsurplus removing is needed. Green arrow represents the microflow system, where low coolant flow is passed thought the EGR coolers. Blue arrow represents the bypass strategy, the most popular automotive layout of today for engine coolant management at cold conditions, where engine coolant is recirculated. Gray coloured arrow shows the common coolant flow path of the three aforementioned systems. Finally, no arrow is depicted in case of 0 flow layout. When 0 flow strategy is performed an additional coolant circuit is needed for cooling down recirculated exhaust gases. The extra EGR coolant flow is supplied by an electrical pump. In Section 6.3 the influence of the engine coolant management systems on engine emissions and fuel consumption is analysed running in NEDC at low ambient temperature.

3.4.2 Exhaust Gas Heat Recovery and WCAC coolant management layout

EGHR system is based on exhaust waste heat recovery by means of a coolant flow for intake air heating. The aim of intake heating is the increase of the initial combustion reactiveness by rising in cylinder gas temperature. The EGHR coolant layout is depicted in Fig. 3.6. Exhaust heat exchanger is denoted as EGHR/LP cooler as it works as both exhaust heat recovery exchanger and LP EGR cooler depending on the intake air temperature. When no heat recovery is needed, a bypass placed at the EGHR heat exchanger opens releasing the exhaust gas outdoors. Exhaust bypass is depicted in Fig. 3.4. Both, intake and exhaust heat exchangers work in counterflow. The intake air heat exchanger is known as Water Charge Air Cooler (WCAC). A WCAC is a liquid-gas heat exchanger placed downstream the compressor. Using a WCAC instead of a intercooler, where intake gas is cooled down by ambient air, shows several advantages:

- Active cooling regulation may be carried out. Coolant flow can be easily set by means of the electrical pump control. WCAC coolant management allows applying thermal strategies that come from the 0 flow, when engine is running in cold conditions, to the maximum coolant supply, when high loads and/or high outdoor temperatures are reached.
- The heat capacity of the ethylene glycol and water solution is roughly 3.3 times higher than air. It means that the mass flow rate needed to remove the intake heat surplus can be lowered in the same proportion. Therefore, the intake heat exchanger size can be reduced by using a WCAC.

On the other hand, the installation of a WCAC requires the installation of an electrical pump, hydraulic pipes, and an expansion tank for active cooling performing strategies.
In this work two different thermal layouts based on intake heating by means of a WCAC are addressed. On one hand, the WCAC 0 flow layout is analysed. This layout works in similar way as the engine coolant 0 flow. But, in this case avoiding the intake air cooling down at cold conditions. The WCAC 0 flow strategy is performed by switching off the WCAC electrical pump. On the other hand, the EGHR configuration is implemented by the WCAC and the EGHR heat exchanger. The EGHR requires the installation of an additional hydraulic circuit that manages the coolant flow between both heat exchangers by means of a pair of electrovalves. When intake air temperature is low, the EGHR coolant flow is driven by the WCAC electrical pump. Once the intake air temperature reaches a threshold, the EGHR heat exchanger switches to the engine coolant circuit, releasing the recovered heat from the exhaust to the engine coolant by means of the mechanical engine pump. As warming up proceeds, the EGHR evolves through different operation modes. In Table 3.5 the EGHR thermal modes that the system evolves are presented. The EGHR mode control is based on the outlet WCAC coolant temperature. In spite of the EGHR is aimed to control the intake air temperature, the air temperature is not used as target variable. The reason behind this decision is the low heat capacity of intake air. Under transient engine load conditions, compressor outlet air temperature varies quickly with the engine load. Managing the EGHR modes switch by means of the air temperature risks the thermal control as it alternates constantly between two adjacent thermal stages. By setting the WCAC coolant temperature as the target variable an stable control is accomplished.

In Fig. 3.6 the EGHR coolant layout is shown. The EGHR system is handled by two directional control valves, V0 and V1, that are commanded by the same signal. Regarding the WCAC coolant circuit, a proportional valve, denoted as P0 in the diagram, is placed between the bypass and the cooling path. This kind of control valves allow infinite position between the two edges. By means of the P0 valve a continuous coolant flow control between the bypass and the WCAC cooler is allowed. This continuous control is crucial for commanding the thermal regulation mode. Coloured arrows in the layout display the flow direction depending on the EGHR thermal stage. At cold conditions, when WCAC coolant outlet temperature is below 35 ^{o}C, EGHR coolant flow from the exhaust heat exchanger to the WCAC. EGHR coolant flow is supplied by the WCAC electrical pump. EGHR coolant flow is spotted in the figure as red coloured arrow that comes from the EGHR heat exchanger to the WCAC

Table 3.5: EGHR system thermal modes. WCAC T. refers to WCAC coolant outlet temperature.

Thermal mode	Condition	Description
Heating	WCAC T. $\leqslant 35^{o}$C	- Heat recovered at the EGHR heat exchanger is directed to the WCAC.
Standby	35^{o}C < WCAC T. $\leqslant 40^{o}$C	- WCAC coolant bypassed. - EGHR connected to the engine block.
Regulation	40^{o}C < WCAC T. $\leqslant 45^{o}$C	- WCAC coolant partially bypassed and cooled. - EGHR connected to the engine block.
Cooling	WCAC T. > 45^{o}C	- WCAC coolant is cooled down. - Exhaust bypass is opened. - EGHR connected to the engine block.

inlet. When WCAC coolant temperature rises 35^{o}C the thermal stage is switched to the stand by position. During standby, EGHR heat exchanger stops releasing recovered heat to the WCAC. EGHR coolant is directed to the coolant engine by means of the V0 and V1 activation. EGHR flow direction to the engine block is depicted as green arrows. Regarding the WCAC, the P0 is commanded to open the bypass port. The coolant flow path is marked in orange arrows. Once WCAC coolant temperature reaches the threshold of 40 ^{o}C, the regulation thermal stage is activated. In this mode, P0 controls the opening of the bypass and the cooler ports. P0 manages the mix of both coolant flows in order to keep the WCAC coolant outlet temperature in the range of 35 - 40 ^{o}C. Finally when WCAC coolant temperature is over 45 ^{o}C, P0 commands the full opening of the WCAC cooler port, reaching the cooling stage. In this condition only green and blue coloured flows remain, the others vanish. In addition, when engine coolant temperature reaches 80

ºC, EGHR heat exchanger bypass, depicted in Fig. 3.4, is opened for heat surplus removing. In this condition the EGHR heat exchanger becomes a regular LP EGR cooler, where only the exhaust recirculated gas flow is cooled down.

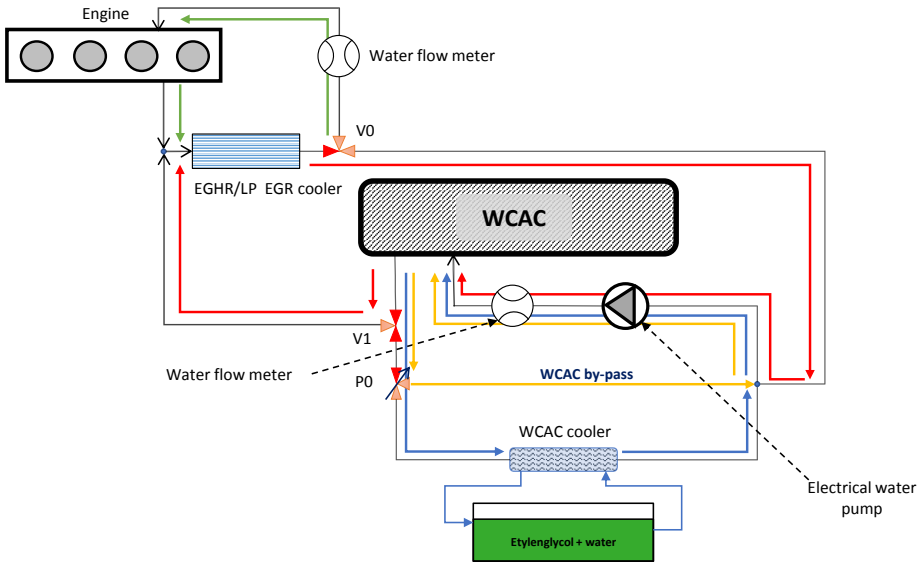

Figure 3.6: EGHR coolant layout. Coloured arrows belong to the different coolant flows depending on the enabled thermal mode.

3.5 Driving cycles test procedure

In the European Union, type approval emission tests are required by law for all new light-duty vehicle models and for the engines used in heavy-duty vehicles. Since 2000 the EU type approval driving cycle has been the NEDC, a modification of the original MVEG-A, but from 2017 to 2019 the new type approval Worldwide harmonized Light vehicles Test Cycle (WLTC) is enforced in law. The new type approval differs from the NEDC in the higher intensity of transient conditions and the longer cycle duration. In this thesis the effect of ambient temperature on engine performance is addressed for both NEDC and WLTC. All engine tests in this thesis are performed at transient conditions of

NEDC and WLTC cycles in an engine test bench. Tests were performed in two different engines. In Fig. 3.7 and Fig. 3.8 vehicle speed profiles are shown for NEDC and WLTC respectively. Driving cycles are one of the main tools that engineers have to analyse engine performance mainly from the point of view of efficiency and pollutant emissions. In spite of the current rise of Real Driving Emissions (RDE) approach on engine analysis, laboratory engine test bench is still a worth procedure for detecting enhancement and anomalies in engine performance. The high repeatability of laboratory tests along with the great availability and accuracy of non portable measurement devices make test bench approach the most suitable for getting reliable conclusions on the analysis of new automotive technologies.

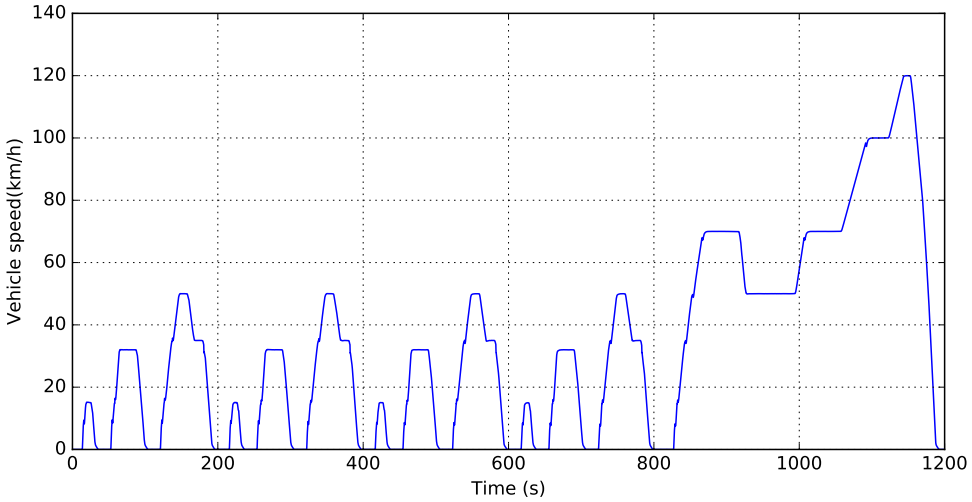

Figure 3.7: NEDC vehicle speed profile

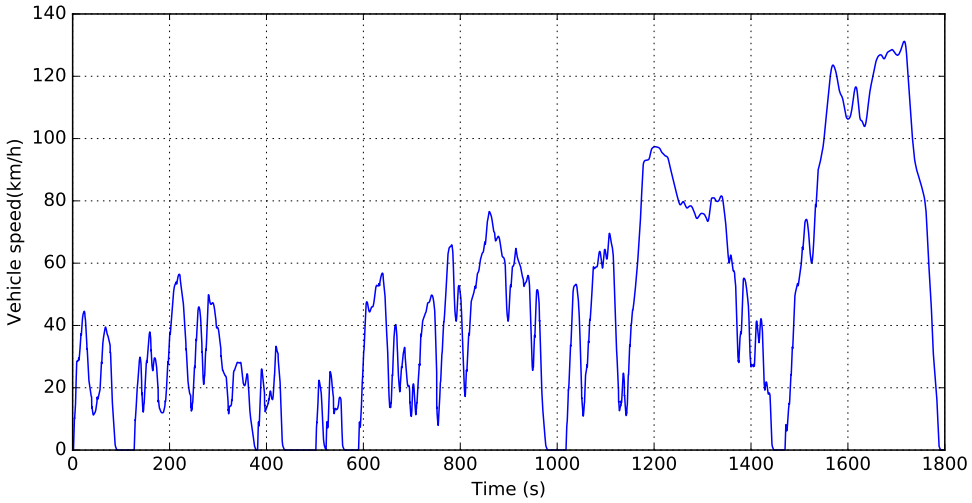

Figure 3.8: WLTC vehicle speed profile

Driving cycles are performed by means of the electric dynamometer. Speed and torque are the engine target variables needed to perform the driving cycles. Both variables are calculated from the vehicle velocity and the gear ratio defined by the driving cycles and the features of the vehicle. The vehicle model used for testing was a typical mid-size car from the European market. Engine speed is calculated from the vehicle speed and gear according to Eq. (3.4).

$$n = \frac{u}{\pi \cdot D \cdot Z} \tag{3.4}$$

where n is the engine speed, u is the vehicle speed, D is car wheel diameter and Z is the gearbox ratio between the driven and the driving gear. The engine power demand is calculated at Eq. (3.5) from the increase of vehicle kinetic energy, the inertia of transmission and carwheel, the loss terms and the mechanical efficiency of the gearbox.

$$P = \left(\frac{\frac{m}{2} \cdot \left(u_{t+1}^2 - u_t^2\right)}{t} + I \cdot \alpha + P_{road} + P_{aerodynamic} \right) \cdot \frac{1}{\eta_m} \tag{3.5}$$

where P is the effective dynamometer power, m is the vehicle mass, u the vehicle speed, t is the time step between two points, I is the combined momentum inertia term of the powertrain transmission, the gear box and the carwheel, α is the angular acceleration of the aforementioned components,

P_{road} is the road friction power loss, $P_{aerodynamic}$ is the aerodynamic power loss and η_m is the mechanical efficiency of the gear box. The first term of the sum represents the increase of kinetic energy of the vehicle. In case of no velocity variation, the demand of power is only owing to the frictional losses. Road and aerodynamic friction losses are vehicle speed dependent. Once the crankshaft power and the engine speed are obtained, the engine torque, N, is calculated as:

$$N = \frac{P}{2 \cdot \pi \cdot n} \tag{3.6}$$

The output signal of a PID controller handles the engine pedal position for reaching the target engine speed calculated in Eq. (3.4). For a given gear ratio, when the dynamometer load toque is increased, i.e in an acceleration,engine speed goes down. To avoid the speed down the position of the pedal actuator moves to increase the injected fuel rate. When the engine speed target is reached the pedal actuator stops running.
After running a driving cycle the DPF is regenerated by applying high engine loads, with high exhaust temperatures, during half an hour. DPF pressure difference is monitored to ensure the regeneration is carried out. After the regeneration, the test cell is cold down for 8 hours.

3.6 Data analysis procedure

In this section the procedure carried out for data analysis is described in detail. Firstly, pollutant emissions rates calculation is described at Section 3.6.1, where raw concentration measurements in dry conditions are converted to flow rates in wet basis. Secondly, experimental test–retest reliability, also known as experimental repeatability, is analysed in terms of sampling standard deviation. Process variability is caused by inherent and random instabilities of a process. In order to detect biased test outcomes, an outlier detection procedure designed for relatively low amount of available samples is proposed in Section 3.6.2. Finally, the experimental uncertainty of measurement devices is analysed for error propagation analysis in Section 3.6.3.

3.6.1 Pollutant emissions calculation

Once chemical pollutants have been measured by the gas analyser, it is necessary to process the data to ensure the right time span and avoid the mismatch between pollutant emissions and the other engine variables such as

air and fuel mass flow [20]. The existence of a delay in pollutant analysis is due to two different sources [21]. On one hand, there is an internal delay necessary to analyse the sample that depends on the type of pollutant. On the other hand, the distance between the sample point and the gas analyser forces the existence of a delay defined by the gas velocity and the length of the sample pipes. The gas speed through the sample pipes is produced by the vacuum pressure generated by the gas analyser pump, which remains equal during the whole cycle. Some authors have implemented physical behaviour models [22] while other authors analyse the delay by correlation methods comparing the pollutant measurement with other related variables like engine speed and air mass flow rate [23]. In this study a correlation method is used, based on the convolution between pollutants and air mass flow signals [24]. Convolution expresses the amount of overlap between two functions; it is defined as the integral of the product of two signals when one of these functions is shifted over the other:

$$(p * m) = \int_{-\infty}^{+\infty} p\,(t) \cdot (t - \phi)\, d\tau \approx \sum_{i=0}^{i=n} p_i \cdot m_{i-k} \tag{3.7}$$

where p and m are the pollutant and air mass flow signals in the time domain. ϕ is the shift variable. The right hand side of the equation is an approximation of the convolution between functions in case there are finite discrete signals. p_i and m_{i-k} are expressed in vector notation, where i is any point of the signal of the n measured points, k works as shift coefficient. The point where the convolution function is maximum indicates the mismatch delay between signals that must be corrected to synchronize both measurements.
Mass flow rate emissions are calculated using the pollutant concentrations and the air and fuel mass flow rate, according to the equation below.

$$\dot{m}_{pollutant} = \frac{M_{pollutant}}{M_{air}} \cdot (\dot{m}_{air} + \dot{m}_{fuel}) \cdot C^*_{pollutant} \tag{3.8}$$

where $M_{pollutant}$ and M_{air} are the molecular mass of pollutants and air respectively, $\dot{m}_{air}$ and $\dot{m}_{fuel}$ are the mass flow of fresh air and fuel respectively and $C^*_{pollutant}$ is the corrected pollutant concentration. Species concentration that are measured in dry basis have to be corrected in order to take into account the exhaust gas water vapour content. Pollutant measurements are corrected according to European Commission Directive 2001/63/EC adapting to technical progress Directive 97/68/EC [25].

3.6.2 Test repeatability and experimental uncertainty

In addition to the errors of the measurement devices, engine performance and boundary test conditions variability affects the result obtained. Beyond the accuracy of the engine actuators and sensors such as fuel injectors, variable geometry turbine position control and engine speed encoder among others, it is observed a variability when the same test is performed several times. Repeatability is defined at the National Institute of Standards and Technology (NIST) Guidelines for Evaluating and Expressing as [55]: closeness of the agreement between the results of successive measurements of the same measurand carried out under the same conditions of measurement. Repeatability may be expressed quantitatively in terms of the dispersion characteristics of the results. Repeatability condition include:

- The same measurement procedure.
- The same observer.
- The same measuring instrument, used under the same conditions.
- The same location.
- Repetition over a short period of time.

A procedure for anomalous results detection was defined to quantify the natural variability of the process avoiding the presence of exceptions. The outlier detection methodology is divided in two parts. The first part calculates the weighted average of the relative error of test variables. The relative error is weighted by means of the instantaneous variable measurement magnitude. The mathematical expression is shown below, where the right hand side is the discrete approximation according to Riemann sum.

$$\epsilon = \frac{\int_0^T \bar{\beta}\left(t\right) \cdot \bar{x}\left(t\right) dt}{\int_0^T \bar{x}\left(t\right) dt} \approx \frac{\sum_{i=0}^{i=n} \bar{\beta}\left(t\right) \cdot \bar{x}_i}{\sum_{i=0}^{i=n} \bar{x}_i} \tag{3.9}$$

where $\bar{x}$ is the instantaneous measured average variable, $\bar{\beta}$is the instantaneous average relative error of each variable, both obtained from the mean of several repetitions of the same test, and n is the number of test measurement points. $\bar{\beta}$ is calculated as follows:

$$\bar{\beta} = \frac{1}{m} \cdot \int_{j=0}^{j=m} \alpha_j \tag{3.10}$$

Where m is the number of test repetitions by case and α is the instantaneous relative error of each test repetition defined as:

$$\alpha_j = \frac{|x_j - \bar{x}|}{\bar{x}} \tag{3.11}$$

where x is the variable under study at the j test repetition. By merging both Eq. (3.10) and Eq. (3.11), the Eq. (3.9) can be rewritten as:

$$\epsilon = \frac{\frac{1}{m}\sum_{i=0}^{i=n}\sum_{j=0}^{j=m}(x_{i,j} - \bar{x}_i)}{\sum_{i=0}^{i=n}\bar{x}_i} \tag{3.12}$$

The above parameter is a modification of the original definition of the Symmetric Mean Average Percentage Error (SMAPE) defined by Flores [56]. The ratio shows how high is the dispersion (expressed as an absolute error) of the whole tests set related to the averaged variable value. Measured variables, such as pressures, temperatures, fuel mass flow, air mass flow, engine speed and engine torque show a relative error (ϵ) lower than 5%. The second part of the outlier detection method focusses on pollutant emissions variability. Because pollutants emissions variation between test repetitions can be high compared to the rest of the test variables [57], an additional analysis based on cumulative emissions instead of instantaneous measurements is applied. The pollutant mass is calculated at each speed part of the cycles. Pollutants data spread is analysed by means of boxplots, also known as box and whiskers plots, where data is divided in quartiles. The threshold to consider a measurement as an outlier occurs when the distance between the pollutant mass and the closest quartile is higher than 1.5 times the interquartile range. In addition, extreme values existence is studied though the comparison of the mean and median of the data set. In case of adding an anomalous test in a sample, the median remains with low variations while the mean is strongly modified. The comparison between median and mean is characterised by the ratio of the absolute difference between the median and mean divided by the median of the data set:

$$SK = \frac{|m - \mu|}{m} \cdot 100\,(\%) \tag{3.13}$$

where SK is the median-mean skewness coefficient, m and μ are the pollutant median and average by test respectively, calculated at each phase driving. This coefficient measures the central tendency of the data set distribution. Considering the experimental variability as a symmetric distribution, the higher this coefficient, the skewed the data set because of the presence of an outlier. The threshold of this coefficient, to consider a measurement as an outlier, is defined at 4%. The threshold value is obtained by Monte

Carlo method approach: first, considering the hypothesis of normal error pollutants distribution [58], a normal distribution is created with a mean and a standard deviation obtained from the experimental data set. Then, a large data set is randomly sampled and used to calculate the average of the median-mean skewness coefficient. This procedure is applied at each driving phase by pollutant emission. Finally, the highest value obtained of the averaged skewness coefficients is defined as threshold of the SK coefficient.
Once the absence of outliers is ensured, mean results are obtained by averaging the dataset of each test type. For small dataset size, lower than 10, the standard deviation can be inferred from the sample range as follows.

$$\frac{R}{d_{2,n} \cdot \sqrt{n}} \tag{3.14}$$

where R is the sample range, $d_{2,n}$ is the control limit factor and n is the sample size. Population mean and standard deviation is calculated by phase driving. For getting reliable conclusions, data spread of pollutants and fuel have to be addressed. Results analysis at Chapter 6 show the mean value by phase driving along with the errorbar. Errorbars are obtained, by considering a 2-sigma significance level (95% of confidence interval), from the inferred standard deviation Eq. (3.14). As outcomes in this theses are presented in ratios between the emissions and fuel consumption at -7 ^{o}C and 20 ^{o}C, the uncertainty is calculated for the ratio of two stochastic variables. Ratio error bar is calculated as follows.

$$\delta r = \frac{M_0}{M_1}\sqrt{\frac{\delta M_0}{M_0} + \frac{\delta M_1}{M_1}} \tag{3.15}$$

where r is the ratio of variables, M_0 and M_1 are the mean variables at -7 ^{o}C and 20 ^{o}C.

3.6.3 Error propagation

Error propagation, also known as propagation of uncertainty, is the effect of variables' uncertainties (random errors) on the uncertainty of a function based on them. When the variables are the values of experimental measurements they have uncertainties due to measurement limitations (e.g., instrument precision) which propagate to the combination of variables in the function. The error propagation is analysed by means of the first order Taylor expansion of the absolute error function, that is the mathematical definition of total differential of a function.
In this work, the propagation of error plays an important role in the total

exhaust mass flow calculation as it is obtained from EGR. Based on CO_2 gas analyser uncertainty, the EGR propagated error is obtained at Eq. (3.16), where the process of EGR relative error calculation is described regarding the dependence of the error with the measured intake and exhaust CO_2.

$$\begin{aligned} dEGR &= \left|\frac{\partial EGR}{\partial CO_{2in}}\right| \cdot dCO_{2in} + \left|\frac{\partial EGR}{\partial CO_{2exh}}\right| \cdot dCO_{2exh} \\ dEGR &= \frac{dCO_{2in}}{CO_{2exh} - CO_{2amb}} + \frac{CO_{2in} - CO_{2amb}}{(CO_{2exh} - CO_{2amb})^2} \cdot dCO_{2exh} \end{aligned} \tag{3.16}$$

Differential terms are approximated to finite differences:

$$\begin{aligned} dEGR &\approx \delta EGR \\ dCO_{2in} &\approx \delta CO_{2in} \\ dCO_{2exh} &\approx \delta CO_{2exh} \end{aligned} \tag{3.17}$$

As finite differences represent the absolute measurement error, they can be expressed in terms of the relative error. Relative error of CO_2 is the same independently of the gas sampling point, at the intake or exhaust manifold. The common relative error is denoted as η_{CO_2}.

$$\begin{aligned} \delta EGR &= \eta_{EGR} \cdot EGR \\ \delta CO_{2in} &= \eta_{CO_2} \cdot CO_{2in} \\ \delta CO_{2exh} &= \eta_{CO_2} \cdot CO_{2exh} \end{aligned} \tag{3.18}$$

$$\eta_{EGR} \cdot EGR = \eta_{CO_2} \cdot \left(\frac{CO_{2in}}{CO_{2exh} - CO_{2amb}} + \frac{CO_{2in} - CO_{2amb}}{(CO_{2exh} - CO_{2amb})^2} \cdot CO_{2exh} \right) \tag{3.19}$$

Replacing EGR definition leads to:

$$\eta_{EGR} = \eta_{CO_2} \cdot \frac{(2 \cdot CO_{2in} \cdot CO_{2exh} - (CO_{2in} + CO_{2exh}) \cdot CO_{2amb})}{(CO_{2in} \cdot CO_{2exh}) - (CO_{2in} + CO_{2exh}) \cdot CO_{2amb}} \tag{3.20}$$

Rearranging terms, the above expression can be presented as:

$$\eta_{EGR} = \eta_{CO_2} \cdot \frac{2 - \frac{(CO_{2in} + CO_{2exh}) \cdot CO_{2amb}}{CO_{2in} \cdot CO_{2exh}}}{1 - \frac{(CO_{2in} + CO_{2exh}) \cdot CO_{2amb}}{CO_{2in} \cdot CO_{2exh}}} \tag{3.21}$$

As $CO_{2amb} << CO_{2int,exh}$ the expression of above can be reduced to:

$$\begin{aligned} k &= \frac{(CO_{2in} + CO_{2exh}) \cdot CO_{2amb}}{CO_{2in} \cdot CO_{2exh}} \\ \lim_{k \to 0} \eta_{EGR} &= 2 \cdot \eta_{CO_2} \end{aligned} \tag{3.22}$$

So, neglecting the ambient CO_{2amb} the relative EGR error is expressed as:

$$\eta_{EGR} = 2 \cdot \eta_{CO_2} \tag{3.23}$$

The relative error of EGR is twice the gas analyser measurement uncertainty. As total exhaust mass flow is calculated from the EGR, the error propagation to the total exhaust mass has to be addressed too. Exhaust mass flow calculation only accounts of LP EGR, in case of HP EGR the exhaust mass flow is the sum of the air mass flow and the injected fuel mass flow. By rearranging terms at Eq. (3.1), and adding the fuel mass flow, the total exhaust gas mass flow is obtained as:

$$\dot{m}_{exh} = \frac{\dot{m}_{air}}{1 - EGR} + \dot{m}_{fuel} \tag{3.24}$$

The injected fuel mass flow is several times lower than the air and the recirculated exhaust flow and the fuel balance measurement uncertainty is roughly 8 and 17 times lower than the air flow meter and the CO_2 gas sampling device respectively. The effect of adding the fuel uncertainty on the error propagation is around 0.095% in average. Regarding the low influence of the fuel mass flow rate on the total exhaust mass flow it has been decided to neglect this term in the propagation error analysis. By applying the same procedure as in Eq. (3.16) the propagated error leads to:

$$\begin{aligned} \delta\dot{m}_{exh} &= \frac{\dot{m}_{air}}{(1 - EGR)^2} \cdot \delta EGR + \frac{1}{1 - EGR} \cdot \delta\dot{m}_{air} + \cancel{\delta\dot{m}_{fuel}} \\ \delta\dot{m}_{exh} &= \frac{\dot{m}_{exh}}{(1 - EGR)} \cdot \delta EGR + \frac{1}{1 - EGR} \cdot \delta\dot{m}_{air} \end{aligned} \tag{3.25}$$

By applying the same relation as Eq. (3.18), the finite differences are expressed in terms of the relative error and measured values.

$$\begin{aligned} \eta_{\dot{m}_{exh}} &= \frac{EGR}{1 - EGR} \cdot \eta_{EGR} + \frac{1}{1 - EGR} \cdot \eta_{\dot{m}_{air}} \cdot \frac{\dot{m_{air}}}{\dot{m_{exh}}} \\ \eta_{\dot{m}_{exh}} &= \frac{EGR}{1 - EGR} \cdot \eta_{EGR} + \frac{1}{1 - EGR} \cdot \eta_{\dot{m}_{air}} \cdot (1 - EGR) \end{aligned} \tag{3.26}$$

Replacing the Eq. (3.23) at Eq. (3.26) leads to a total exhaust mass flow relative error expression dependent on the gas sampling relative measurement error, the air mass flow error and the EGR rate. According to the expression Eq. (3.27), total flow relative error grows non linearly as EGR rate increases.

$$\eta_{\dot{m}_{exh}} = 2 \cdot \frac{EGR}{1 - EGR} \cdot \eta_{CO_2} + \eta_{\dot{m}_{air}} \tag{3.27}$$

In Fig. 3.9 exhaust mass flow relative error is shown, from Eq. (3.27), for an EGR range from 0 to 100%. At 0 % of EGR the relative error reaches the minimum that is equal to the air mass flow measurement relative error, 0.12%. As EGR approaches 100% the exhaust mass flow error tends to infinite. NEDC experimental values, at -7^{o}C of ambient temperature, are depicted over the relative error line. Uncertainty analysis is focused in NEDC tests as main results of this thesis are obtained by NEDC test procedure. More details about the selection of the experimental testing conditions can be found at Chapter 6. In the figure, a zoom window is included showing the total exhaust mass flow error for the 99% of NEDC points. Most of experimental values are located in a relative error region lower than 18%. Only few points are located at the high EGR region where relative error may punctually rise to 1400%. Those points are neglected to avoid high propagation error into the outcomes.

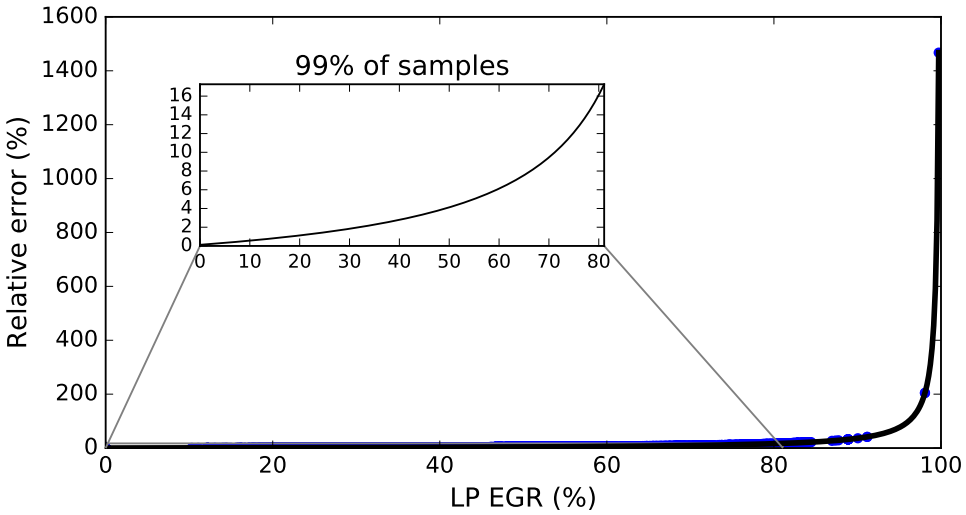

Figure 3.9: Total mass flow relative error dependence with EGR

In Fig. 3.10 LP EGR normalized histogram is depicted. Exhaust mass flow only accounts to LP EGR, NEDC points where HP EGR is running are set to 0 in the histogram as they don't influence on the exhaust mass flow calculation. According to the figure, in 16% of the NEDC test no LP EGR is performed. When LP EGR is running the data set mode is lower than 55%, representing the 14% of the total NEDC points. By combining both Fig. 3.9 and Fig. 3.10 the percentage of samples under an error threshold can

be inferred. For example, regarding Fig. 3.10, in 95% of NEDC points the LP EGR rate is below 55%. Knowing this rate and looking at Fig. 3.9 the exhaust mass flow error for the 95% of NEDC points is close to 6%.

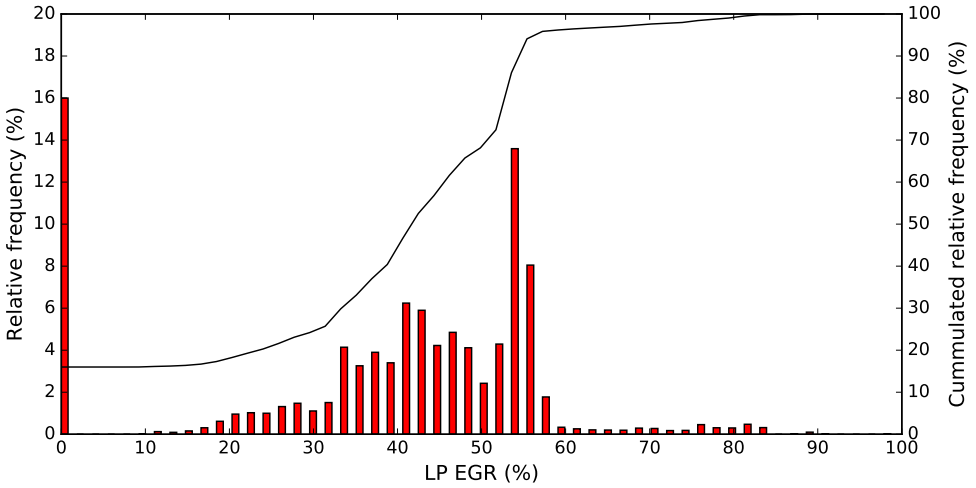

Figure 3.10: LP EGR histogram. Normalized relative frequency on left axis. Cumulated relative frequency on right axis.

Bibliography

[48] J. M. Luján, H. Climent, B. Pla, M. E. Rivas-Perea, N.-Y. François, J. Borges-Alejo, and Z. Soukeur. "Exhaust gas recirculation dispersion analysis using in-cylinder pressure measurements in automotive diesel engines". *Applied Thermal Engineering* 89 (2015), pp. 459–468.

[49] J. M. Luján, H. Climent, V. Dolz, A. Moratal, J. Borges-Alejo, and Z. Soukeur. "Potential of exhaust heat recovery for intake charge heating in a diesel engine transient operation at cold conditions". *Applied Thermal Engineering* 105 (2016), pp. 501–508.

[50] M. Adachi and H. Nakamura. *Engine Emissions Measurement Handbook: HORIBA Automotive Test Systems.* SAE International, 2014.

[51] A Maiboom, X Tauzia, and J.-F. Hétet. "Influence of high rates of supplemental cooled EGR on NOx and PM emissions of an automotive HSDI diesel engine using an LP EGR loop". *International Journal of Energy Research* 32.15 (2008), pp. 1383–1398.

[52] K. Narusawa, M. Odaka, N. Koike, Y. Tsukamoto, and K. Yoshida. "An EGR control method for heavy-duty diesel engines under transient operations". *SAE transactions* (1990), pp. 991–1004.

[53] D. W. Dickey, T. W. Ryan, and A. C. Matheaus. *NOx control in heavy-duty diesel engines-what is the limit?* Tech. rep. SAE Technical Paper, 1998.

[54] F. P. González and J. M. D. Fernández. *Motores de combustión interna alternativos.* Editorial Universitat Politècnica de València, 2011.

[55] B. N. Taylor and C. E. Kuyatt. *Guidelines for evaluating and expressing the uncertainty of NIST measurement results.* Citeseer, 1994.

[56] B. E. Flores. "A pragmatic view of accuracy measurement in forecasting". *Omega* 14.2 (1986), pp. 93–98.

[57] K. Robinson, S. Ye, Y. Yap, and S. T. Kolaczkowski. "Application of a methodology to assess the performance of a full-scale diesel oxidation catalyst during cold and hot start NEDC drive cycles". *Chemical Engineering Research and Design* 91.7 (2013), pp. 1292–1306.

[58] I. P. Kandylas, A. M. Stamatelos, and S. G. Dimitriadis. "Statistical uncertainty in automotive emissions testing". *Proceedings of the Institution of Mechanical Engineers Part D-Journal of Automobile Engineering* 213.D5 (1999), pp. 491–502.

Chapter 4

Effect of low ambient temperature on engine performance

Contents

4.1 Introduction

Combustion rate is greatly affected by reaction temperature. While oxidation rate is linearly dependent on reactants concentration, temperature influences on chemical kinetics in exponential manner. The general expression of a reaction rate, where the Arrhenius coefficient is included, is shown below:

$$\frac{-d[HC]}{dt} = [O_2] \cdot [HC] \cdot A \cdot e^{\frac{-E_a}{R \cdot T}} \tag{4.1}$$

where $[O_2]$ and $[HC]$ is the concentration of oxygen and a generic hydrocarbon, A is the pre-exponential factor, E_a is the activation energy, R is ideal gas constant and T is the reaction temperature. The temperature effect on the reaction rate is analysed by the ratio of two combustion rates at different initial temperatures. The above expression Eq. (4.1) is converted to:

$$RR = e^{\frac{E_a}{R} \cdot \frac{\Delta T}{T_1 \cdot (T_1 - \Delta T)}} \tag{4.2}$$

where RR is the reaction rate ratio, T_1 is the reference temperature, set at 293 K, ΔT is the temperature difference between the warm to the cold reaction rate. The reaction rate ratio variation owing to the variation of reaction temperature is depicted in Fig. 4.1. As engine fuel is a mixture of different hydrocarbons the reaction rate is calculated along a range of activation energies for typical diesel composition. Activation energy limits are set according to [59], where activation energy for diesel fuel is obtained by experimental approach. The temperature has been swept from -7 ^{o}C to 20^{o}C as all tests outcomes analysed in this work have been conducted at those ambient temperatures. This analysis only accounts to the starting reaction rate. The effect of temperature on the reaction rate is remarkable by regarding the surface slope on the ΔT axis direction.

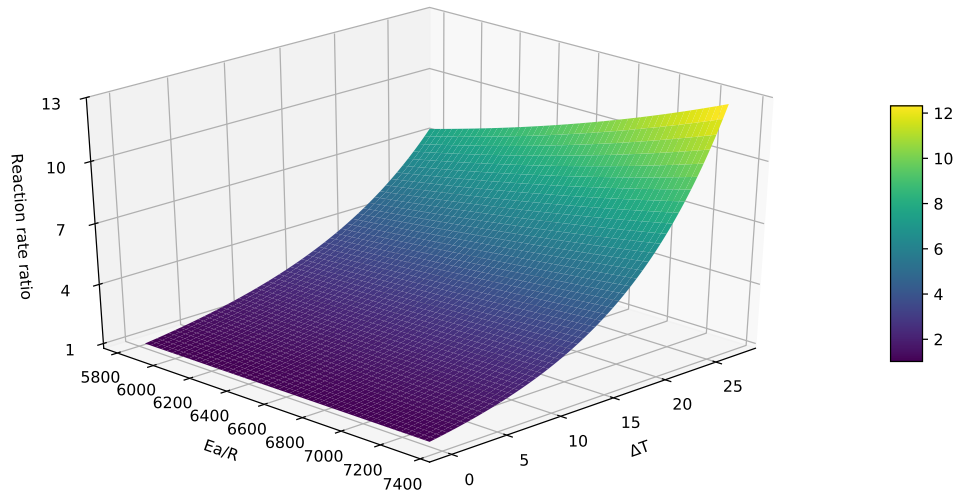

Figure 4.1: Reaction rate. Temperature and activation energy dependence

This analysis is aimed only to remark the significant influence that initial temperature has over the reaction rate and consequently over the emissions formation and thermal efficiency. The effect of lowering the ambient temperature gets more complex when the analysis is carried out at real engine operation conditions, where initial reaction temperature is influenced by cylinder line heat transmission losses, trapped air mass, in cylinder turbulence among others. In addition EGR systems control performance in different manner depending on the ambient temperature, as EGR enabling depends on several engine temperatures such as engine coolant and intake temperature. Therefore, the aim of this work is to conduct an experimental analysis on the influence of the ambient temperature effect over all aforementioned systems and features that eventually show an impact on the pollution emissions and engine thermal efficiency.

Increasingly stringent emissions regulations are constantly motivating the automotive industry to develop new systems and strategies. As automotive cycles are being more restrictive, it is expected that future driving test procedures will consider the effect of running at lower ambient temperature. Currently, the U.S Environmental Protection Agency includes a cold cycle of FTP-75 carried out at -7 ^{o}C [60]. On the other hand, European regulation enforces, only in petrol engines, a cold start low temperature emissions test

[61]. Regarding the current state of the law, it is expected that future regulations will consider low temperature emissions as regular testing. Under low ambient temperatures, fuel consumption and pollutant emissions during the engine warm-up are critical [62]. According to the literature [63] and [64], unburned hydrocarbons and carbon monoxide are mainly emitted when engine temperatures remain low. Many researchers have studied the effect on pollutant emissions and engine performance in cold driving cycles. In a project initiated by the Swedish Environmental Protection Agency (SEPA), Ludykar et al. [65] reported a notable increase in the tailpipe emissions of CO, HC and NOx in a gasoline engine running in European Urban Driving tests at -7 ºC and -20 ºC. Weilenmann et al. [66] carried out an extensive study of low ambient temperature (-7 and -20 ºC) tailpipe emissions in a fleet of gasoline (Euro 0 and Euro 3) and Diesel engines (Euro 2). Several tests were performed such as ECE, FTP-75, IUFC15 and IRC15. Pollutants were sampled according to the bag technique, so instantaneous data were not available. CO and HC results shown that, in general terms, cold start extra emissions were lower for diesel than for gasoline vehicles. On the other hand, a relevant trend of NOx increase was spotted in cold start diesel emissions for low temperatures. The authors couldn't find an explanation of this trend as the EGR system was not considered in the analysis. Dardiotis et al. [67] performed a similar study in a fleet of gasoline and diesel engines running in a NEDC at 20 and -7 ºC. CO and HC shown the same tendency spotted by Weilenmann [66], being higher the effect of ambient temperature in gasoline than in diesel engines. Regarding NOx, the authors identified the EGR rate reduction as the main cause of pollutants increase in diesel engines running at low temperatures. In case of gasoline engines, a clear tendency couldn't be found.

Some authors, have analysed the engine performance start at different temperatures fuelled by other fuels beyond the gasoline and diesel. Armas et al. [68] analysed the effect of diesel blends on HC, CO and particle emissions in a diesel engine running a NEDC. The results shown an improvement of emissions at warm conditions but a deterioration of combustion stability at cold starts that eventually caused an increase of all pollutants. García-Contreras et al. **??** analysed the influence of the ambient temperature on the combustion process start in diesel and gas to liquid fuels by means of the indicated mean pressure and rate of the heat released rate. Results shown a significant sensitivity to the cetane number when running at -7 ºC.

Most of low temperature emissions bibliography is focused in NEDC testing. But world current legislation is turning towards a more realistic emission driving analysis which includes new procedures such the WLTC and real

driving engine emissions. Some authors have analysed the effect of replacing the NEDC by the new WLTC. Giakoumis et al [69] presented the experimental validation of an empirical emissions and engine efficiency model where NEDC and WLTC performance were compared. Diesel engine out pollutants emissions were measured in a non-controlled ambient temperature test bench showing an increase of 55% NOx and 10.8% in soot in the WLTC. Ko et al. [70] analysed the performance of a Diesel Lean NOx Trap (LNT) measuring the NOx concentration at both inlet and outlet. NEDC and WLTC tests were performed at 23, 14 and -5 ^{o}C of ambient temperatures. Tailpipe NOx emissions increased up to 11 and 13 times for the NEDC and WLTC respectively when running at -5^{o}C. In addition to the NOx analysis the authors remarked the general trend of CO and HC increase as ambient temperature gets lower.
This chapter is aimed to compare the effect of low ambient temperature on pollutants formation by analysing the raw engine emissions. In addition, engine efficiency is also evaluated by means of the fuel consumption in the NEDC and the WLTC. Emissions were sampled upstream the DOC to identify the cause of pollutants formation in combustion processes fired at low surrounding temperatures. The content is structured as follows. Section 4.2 is devoted to the driving cycles description. Section 4.3 contains the results and analysis of the ambient temperature effect on the raw pollutant emissions and engine performance. Finally, the main conclusions are presented in Section 4.4.

4.2 NEDC and WLTC driving conditions

Designed to represent the typical usage of a car in Europe, the NEDC is composed by four repetitions of the Urban Driving Cycle (UDC) and an Extra Urban Driving Cycle (EUDC). The first Urban Driving Cycle (UDC) was introduced in 1970 under the United Nations Economic Commission for Europe (UNECE) vehicle regulation program. The Extra-Urban Driving Cycle EUDC, introduced by ECE in 1990 has been designed to represent more aggressive, high speed driving modes. The combination of UDC and EUDC conformed what is known as MVEG-A cycle that was used for EU type approval testing of emissions and fuel consumption in light duty vehicles until 2000. In 2000, the MVEG-A was modified by removing the initial idling period at the engine start, i.e. engine cold start emissions are sampled from the beginning of the cycle. This modified cold-start procedure is referred to as the New European Driving Cycle (NEDC) or as the MVEG-B test cycle [44]. NEDC has been widely criticized of not being representative of a real

driving behaviour where transient conditions get more important [71] and [72]. Aimed to create a realistic driving cycle, the developing of a worldwide harmonized light duty test cycle (WLTC), that represents the average driving characteristics around the world, was launched by the World Forum for the Harmonization of Vehicle Regulations (WP.29) of UNECE through the working party on pollution and energy transport program (GRPE) [73]. The WLTP replaces the European NEDC based procedure for type approval testing of light-duty vehicles, with the transition from NEDC to WLTP occurring over 2017-2019. Dynamic behaviour of NEDC and WLTC is assessed by the acceleration histogram depicted in Fig. 4.2. Histogram bars are represented in

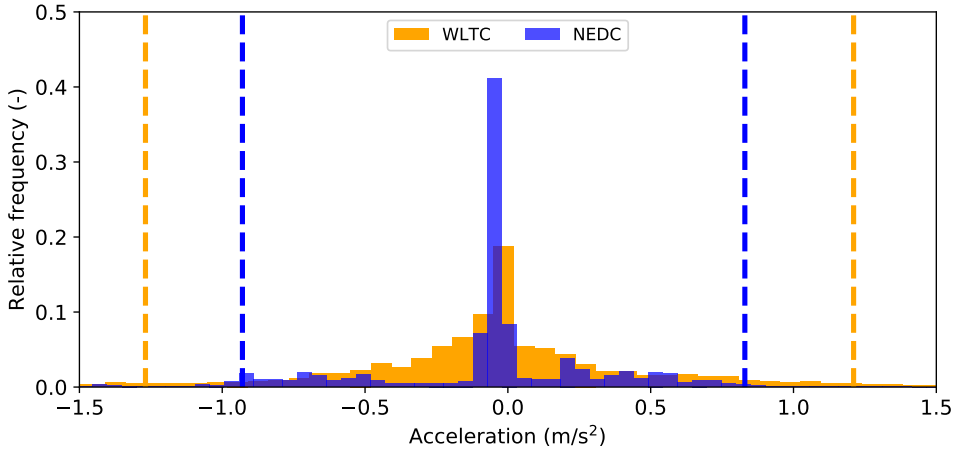

Figure 4.2: Acceleration normalized histogram of both driving cycles. Dotted lines mark the 95% of values.

relative frequency, dividing each interval repetition by the total. The relative frequency histogram shows how dynamic is the behaviour of the driving cycles. NEDC performs with low transient conditions during half of the cycle with accelerations bounded between -0.1 and 0.05 m/s^2. Acceleration distribution is skewed to the left side, pointing that decelerations get more importance than accelerations, which are critical regarding engine efficiency and pollutant emissions. Regarding the WLTC, the higher dispersion of the histogram is noticeable owing to the more intense dynamic behaviour. Low transient points, delimited in the region of -0.02 to 0.6 m/s^2, represent just the 20 % of the whole WLTC. Regarding the highest acceleration, the acceleration is limited to 0.83 m/s^2 in the NEDC while in the case of WLTC it reaches 1.25 m/s^2. The main

engine variables such as: torque, engine speed and power are shown in Fig. 4.3 for both driving cycles. All variables have been averaged by driving phase. Regarding the low load part, requested power is similar, 3.25 and 4.5 kW for NEDC and WLTC respectively, being the engine speed higher at the NEDC and therefore the engine torque lower than the WLTC. Concerning high load parts comparison, EUDC at the NEDC performs like the high load driving phase of the WLTC. Engine demand power rises to 11 kW in both cycles and the torque is slightly lower in the NEDC. In the case of WLTC, extra-high load is performed at the last part of the cycle with a power demand increase to 22.5 kW where the average torque almost reaches 100 Nm.

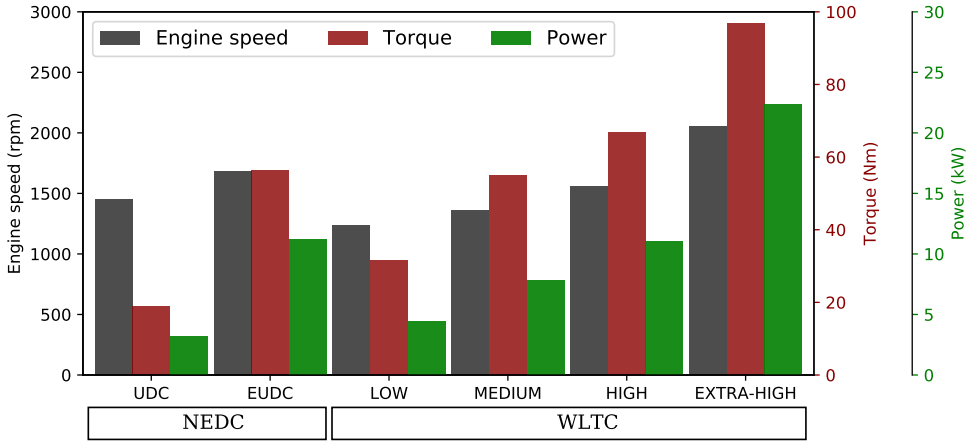

Figure 4.3: Averaged main engine variables by driving schedule in the NEDC and WLTC.

4.3 Results

This section describes the effect of ambient temperature on both, NEDC and WLTC, driving cycles by comparing the pollutant emissions and engine efficiency at -7 ºC and 20 ºC. First, the effect of the ambient temperature on the air management system is addressed. Secondly, the effect of low ambient temperature on pollutant emissions and brake thermal efficiency is analysed. Finally, a deep analysis on the cold start and first instants of warm up is included remarking the effect of load transients on emissions increase.

4.3.1 Effect of low ambient temperature on air management

EGR plays a crucial role on the air mass flow performance. When EGR is enabled, air management by the intake manifold pressure is shifted to the air mass flow meter based control. Indeed, under EGR running conditions, air mass flow is not set by the VGT position but by the EGR valves position [74, 75, 75]. Aimed for NOx reduction, EGR has become one of the most popular active systems for pollutants reduction in diesel engines. Nevertheless, lowering peak combustion temperature along with oxygen dilution at cold running conditions may drive to combustion instabilities that increase emissions such as HC, CO and particle matter, and eventually result in misfiring events [76, 77].
Fig. 4.4 and Fig. 4.5 show the instantaneous air mass flow ratio between -7 ºC and 20 ºC for NEDC and WLTC respectively. Values have been smoothed by means of a Gaussian convolution filter. In addition to the air mass flow ratio, the EGR valves position have been depicted. EGR system performs in similar way in both driving cycles. At 20 ºC, HP EGR is enabled from the beginning and once the coolant temperature reaches 60 ºC, around 500 seconds for both cycles, the HP is replaced by the LP EGR. Engine coolant and intake manifold temperature is generally used by carmakers as EGR control variable. Regarding -7 ºC tests, the HP EGR is enabled when engine coolant temperatures are over 60 ºC. Concerning the NEDC, EGR is enabled at 1000 seconds, at the last half term of the EUDC, when high engine loads are performed. In case of WLTC, as the engine warming up proceeds faster, owing to the higher power demand, the EGR is enabled earlier, at roughly 850 seconds, during the middle engine load. The effect of EGR on the air mass flow is noticeable looking at the air flow ratio. On one hand, as the EGR remains disabled at -7 ºC, the air flow ratio shows great values and performs in unsteady manner. During transients, the ECU control demands lower EGR rates commanding the EGR valve closing. In consequence at these points, the air flow ratio drops. On the other hand, boost control is directed by the intake manifold pressure during EGR cut-off operation points [75]. So, the lower ambient temperature entails higher air density that increases the air mass flow rate. Comparing both, the EGR disabling and the higher air density, the effect of EGR disabling is more meaningful. The 85% and 72% of air flow increase in the NEDC and WLTC respectively is caused by the EGR disabling at low temperatures. During the EGR cut off, air mass flow ratio is bounded between 1.4-2.4 and 1.2-2.2 in NEDC and WLTC respectively. Once EGR is enabled at -7 ºC, air mass flow ratio fluctuations vanish, and amplitude drops to around 1.3 in both driving cycles.

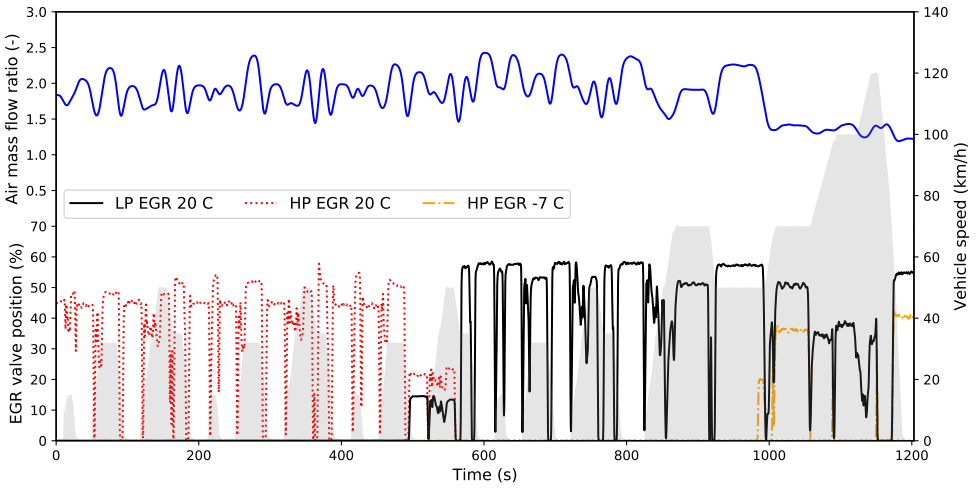

Figure 4.4: Air mass flow ratio between -7 ºC and 20 ºC in NEDC and EGR valves positions. Vehicle speed depicted as a surface in grey.

The EGR cut-off at low temperature is a conservative engine calibration strategy for avoiding combustion instabilities that lead to engine efficiency reduction and pollutant emissions rise in CO, HC and particles. The results shown in Fig. 4.4 and Fig. 4.5 cannot be extrapolated to the whole automotive technology state of the art as it represents the ECU calibration of a specific engine. Nevertheless, all carmakers apply similar EGR calibration procedures where EGR operation is enabled once coolant temperature reaches a threshold. Temperature threshold varies between carmakers but the EGR disabling at low temperature is a common strategy in all cases. Conclusions obtained from these data should be used as a guide for getting general trends of engines performance at low ambient temperatures.

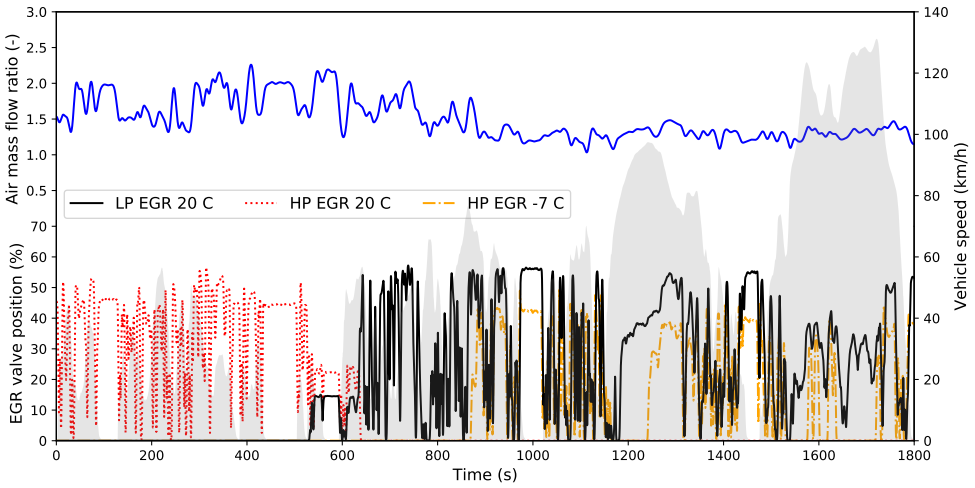

Figure 4.5: Air mass flow ratio between -7 ºC and 20 ºC in WLTC and EGR valves positions. Vehicle speed depicted as a surface in grey.

4.3.2 Engine out pollutants emissions and fuel consumption analysis

Fig. 4.6 and Fig. 4.7 show the pollutants ratios of HC, NOx, CO and fuel consumption, by driving phase, between the cold and warm cases for the NEDC and WLTC respectively. Regarding the NEDC, Fig. 4.6, the evolution of emissions shows similar patterns between HC, CO and fuel consumption. With the exception of NOx, the rest of pollutants ratios show a general trend of reduction as the cycle proceeds.

In the case of hydrocarbons, the emission peak is not placed at the beginning of the cycle but in the second UDC. During cold starts, even at 20 ºC of ambient temperature, significant emissions of HC are released as consequence of the enriched fuel and low temperature combustion [66] that drives to incomplete combustion [66]. In the 20 ºC case, the enabling of EGR in the beginning of the engine cold start, for NOx reduction, carries an increase of HC in detriment. The maximum difference in HC emission is observed during the second UDC. The engine warm up reduces HC at both ambient temperatures, being the HC decrease more significant at 20 ºC than at -7 ºC during the first 400 seconds. Beyond this point, HC reduction tends to slow down at 20 ºC in comparison to the -7 ºC case. That's the reason why emissions at -7 ºC tends to approach the 20 ºC case, being the lowest difference on HC emissions at the last driving

schedule, when high loads are performed, with a ratio of 1.8.
Concerning CO, the ratio decreases monotonically from 3.4 at the beginning to 1.4 at the end of the EUDC. In the case of fuel consumption, ratios perform in a flatter manner along the NEDC, being the highest ratio of fuel consumption 1.4 at the beginning and the lowest 1.1 when high loads are performed.
In contrast to carbon based emission, NOx ratios show a non-monotone evolution with high emissions at – 7 ºC during the EUDC. As the negative effect of cold start on emissions is greater at low ambient temperatures, NOx shows higher ratios at the first UDC than at the second and third UDC. According to Zeldovich mechanism [78], NOx is produced in conditions of high oxygen concentration and temperature. Both variables are lowered by EGR valve opening, driving eventually to NOx reduction. As was shown in Fig. 4.4, EGR remains disabled at -7 ºC until 1000 seconds. On contrast, EGR is running from the beginning in the 20 ºC case. At the last UDC, the increase of NOx ratio is driven by the switch from HP to LP EGR in the 20 ºC case. Finally, at the EUDC, NOx emissions get more important because of the higher engine loads. As LP EGR is enabled at 20 ºC, high EGR rates and low combustion temperatures can be achieved. In contrast, EGR is not enabled at -7 ºC until 1000 seconds by means of the HP EGR loop whose ability of NOx reduction is lower than LP EGR [79, 80, 81, 79, 82]
Evaluating the whole NEDC, the effect of lowering the ambient temperature to -7 ºC is an increase of 270% in HC, 125% in CO and 250% in NOx. Regarding fuel consumption, a drop of 10% in brake thermal engine efficiency is observed.

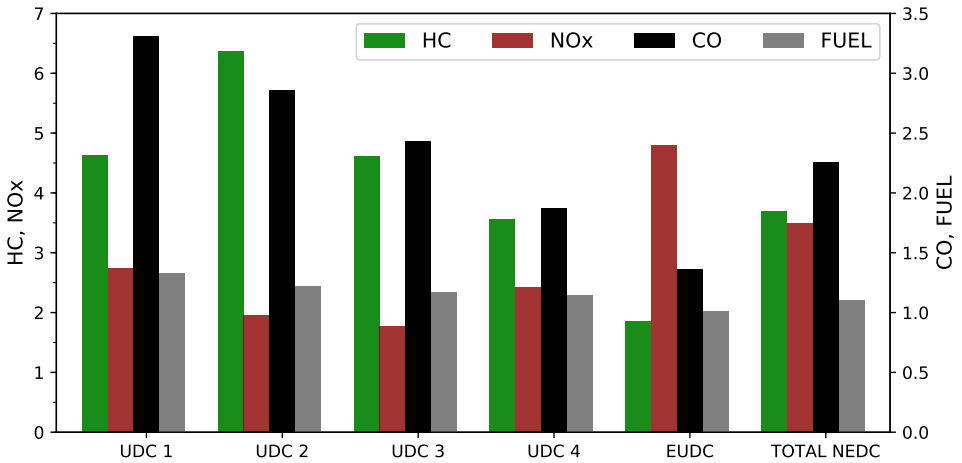

Figure 4.6: Pollutant ratio by driving schedule in NEDC. HC and NOx on the left axis. CO and fuel consumption on the right axis.

Concerning WLTC, ambient temperature effect on pollutants and thermal engine efficiency is shown in Fig. 4.7. Like in NEDC, HC and NOx emissions drastically increase when engine runs at low ambient temperature.
HC emissions evolve in opposite way than NOx, as engine warm up proceeds, hydrocarbons go down and NOx increases. Encouraged by the higher engine loads, the EGR is enabled prior in WLTC, at 875 seconds, than in NEDC, at 1000 seconds. Despite HP EGR is enabled during the WLTC middle driving schedule, performed EGR rates are not enough to reduce NOx emissions as LP EGR does. At the extra-high load, the NOx at -7 ^{o}C rises to 6.2 times the emission at 20 ^{o}C.
In the case of CO, emissions perform in a quite different manner. Maximum ratio is bounded to 1.3, at the low load WLTC term, and suddenly drops when higher loads are performed, being CO emissions at -7 ^{o}C lower than at 20 ^{o}C. The minimum ratio is obtained during the medium load term where HP EGR is not enabled until the last part of this driving schedule. Once EGR is enabled, a slight deterioration on CO emissions at -7 ^{o}C is observed owing to the oxygen concentration dilution [82]. CO and HC pollutants formation share similar dependence with combustion temperature and oxygen concentration. In case of NEDC, Fig. 4.6, both species evolve in the same way, being the engine warm up the main responsible of reduction. However, despite HC emissions are closely linked to CO emissions since they are both caused by low

quality combustion, [82, 83], in WLTC this correlation is not found. Results suggest that CO emissions are more sensitive to oxygen concentration than HC. Under strong load transient conditions air management control becomes crucial to ensure proper air cylinder filling and exhaust gases removing. When required AFR is not achieved, incomplete combustion occurs and consequently CO emissions increase. When EGR is enabled, air management becomes harder to control and ensure complete combustion. During transients, ECU commands the EGR valve closing (see Fig. 4.5) to fulfil power demands and avoid soot emissions increase [84, 85, 86]. The effect of transients on CO is more significant at 20 ^{o}C than at -7 ^{o}C owing to the higher EGR rates performed by the LP than HP EGR, as well as the lower intake temperature of the air-EGR mixture.
Evaluating the whole WLTC, the effect of lowering the ambient temperature to -7 ^{o}C is an increase of 150% in HC, 280% in NOx and a reduction in CO of 18%. Regarding fuel consumption, a drop of 1% in thermal engine efficiency is observed. As variation is lower than the test repeatability uncertainty threshold of 5% (See Chapter 3 for more details) deterioration of brake thermal engine efficiency cannot be considered.

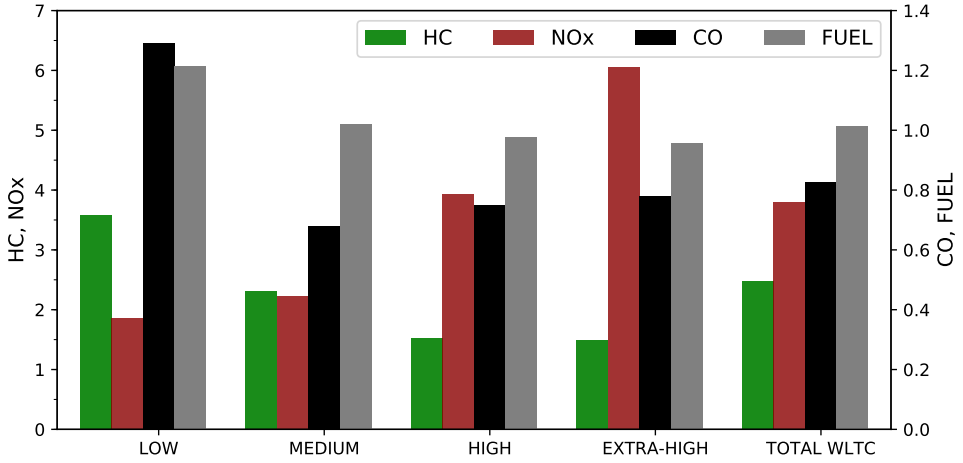

Figure 4.7: Pollutant ratio by driving schedule in WLTC. HC and NOx on the left axis. CO and fuel consumption on the right axis.

4.3.3 Comparison between NEDC and WLTC emissions

In this section cumulated emissions of both driving cycles are shown. As engine loads perform in very different manner between NEDC and WLTC, to compare the evolution of pollutants along the driving cycle the emissions must be rescaled previously. The comparison of pollutants between driving cycles is based on the ratio between the cold and warm cycle. The emissions ratio by cycle are rescaled as follows:

$$R_{x\ scaled} = \frac{R_x - min(R_x)}{max(R_x) - min(R_x)} \tag{4.3}$$

R_x is the ratio between the cold and warm cycle of each pollutant cumulated mass:

$$R_x = \frac{\int_0^{t_i} \dot{m}_{cold}\, dt}{\int_0^{t_i} \dot{m}_{warm}\, dt}, ti\epsilon[0, 0.1, 0.2...T] \tag{4.4}$$

T is the total duration of each cycle, 1200 for NEDC and 1800 for WLTC. In Fig. 4.8, pollutant emissions such as HC, NOx and CO are depicted for both NEDC and WLTC. HC evolves along the NEDC and the WLTC in a very similar way. At 400 seconds the peak emission is achieved in both cycles. Beyond this point the HC cumulated ratio reduces owing to the engine warm up at -7 ^{o}C. The fact that both cycles perform with great similarities suggests that HC are more sensitive to the engine warm up than to the EGR strategies.

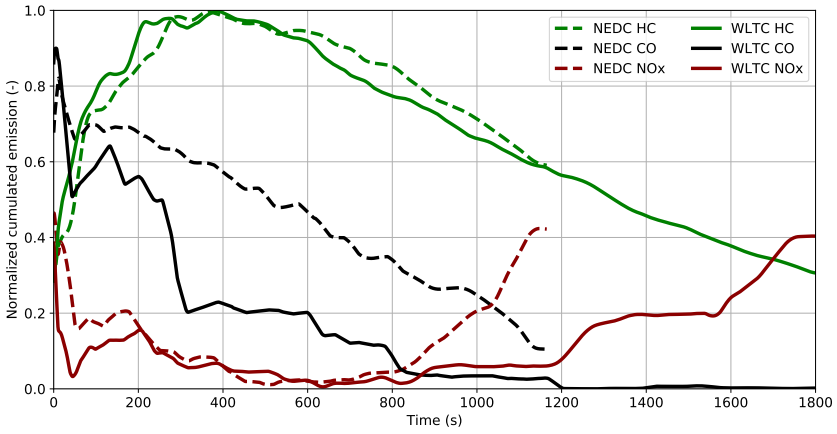

Figure 4.8: Rescaled cumulated emissions ratio. Dotted lines for NEDC and solid lines for WLTC.

The engine heating up has been analysed by the rejected thermal energy of the in-cylinder energy balance, according to the following expression.

$$RH = \dot{m}_f \cdot LHV + \dot{m}_{air} \cdot (c_p \cdot T_{in}) - (\dot{m}_{air} + \dot{m}_f) \cdot (c_p \cdot T_{exh}) - N \cdot 2 \cdot \pi \cdot n \quad (4.5)$$

Where RH is the rejected heat power, $\dot{m}_f$ and $\dot{m}_{air}$ are the fuel and air mass flow rate respectively, T_{in} and T_{exh} are the intake and exhaust manifold temperature, N is the torque, n is the engine speed, LHV is the Low Heating Value of the fuel and c_p is the heat capacity at constant pressure. The above expression is composed by four energy terms. From the left to the right: the two first terms are the in-cylinder energy inputs as the heat released at the combustion and the intake air enthalpy. The two last terms address the output energy terms such the mechanical shaft energy and the exhaust gases enthalpy. The rejected energy comprises the engine mass, coolant and oil heating up as well as the energy released to the surroundings. Rejected energy and engine coolant temperatures are shown in Fig. 4.9 for both NEDC and WLTC at -7 ºC. Regarding the rejected energy, both cycles follow the same tendency pointing that the warming up proceeds with the same heating rate in both cycles. This shared warming up behaviour is spotted also by comparing the coolant temperature of both driving cycles.

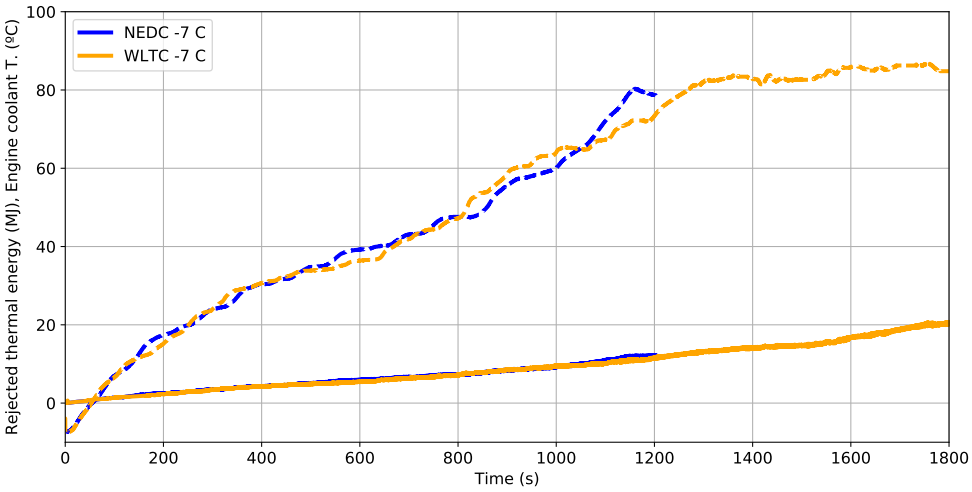

Figure 4.9: Rejected heat (solid lines) and Engine coolant temperature (dotted lines) of the NEDC and WLTC cycles at -7 ºC.

In the same way, NOx emissions behave in such quite similar manner too. Both cycles show the same peak emission at the beginning. As the cycles proceed, until 800 seconds, both NOx ratios reduce because of the cold start effect vanishing, the low intake temperature and the low loads performed that downplay the role of EGR on NOx reduction. Once higher loads are performed, beyond the 800 seconds in NEDC and 1200 in WLTC, HP EGR at -7 ºC is not enough to keep the NOx low and therefore an increase in the NOx ratio is observed in the last term of both cycles.
Unlike HC and NOx, CO shows quite different patterns. Reductions are stronger in WLTC where CO is even lower at -7 ºC than at 20 ºC, owing to the EGR disabling at low ambient temperatures, as already shown in Fig. 4.7. Higher emissions are measured at the beginning of the cold start. But, after 50 seconds significant reductions are observed comparing -7 ºC to 20 ºC. The EGR control along with the heavy transient conditions makes CO evolution at -7 ºC sharper comparing the WLTC to NEDC, where CO ratios evolve like HC does, with a quite constant and similar rate of decreasing. In the case of CO, the air management control, driven by the EGR system, plays the main role on emissions mostly during transient conditions, causing important differences between NEDC and WLTC.

4.3.4 Emissions during engine warm-up

In addition to the analysis by driving schedule and the cumulated pollutants along the cycles, the instantaneous emission rates are depicted in Fig. 4.10 and Fig. 4.11 for NEDC and WLTC respectively. Concerning the NEDC, the first two UDC, first 400 seconds, are shown. High CO and HC peak emissions are observed at the beginning of the cycle at -7 ºC. Great differences are observed between cold and warm cycles at steady state conditions, being remarkable the increase in HC. After the first 50 seconds both pollutants, HC and CO, perform in similar manner: most of pollutants are released during steady state conditions being the effect of transients less significant. In case of NOx, the emission rate evolves in opposite way being the effect of transients the main cause of emission. Despite emissions rate is a bit higher at 20 ºC in some points of vehicle acceleration, like at 50 ,120 and 215 seconds among others, the effect of transients is greater at -7 ºC than at 20 ºC.

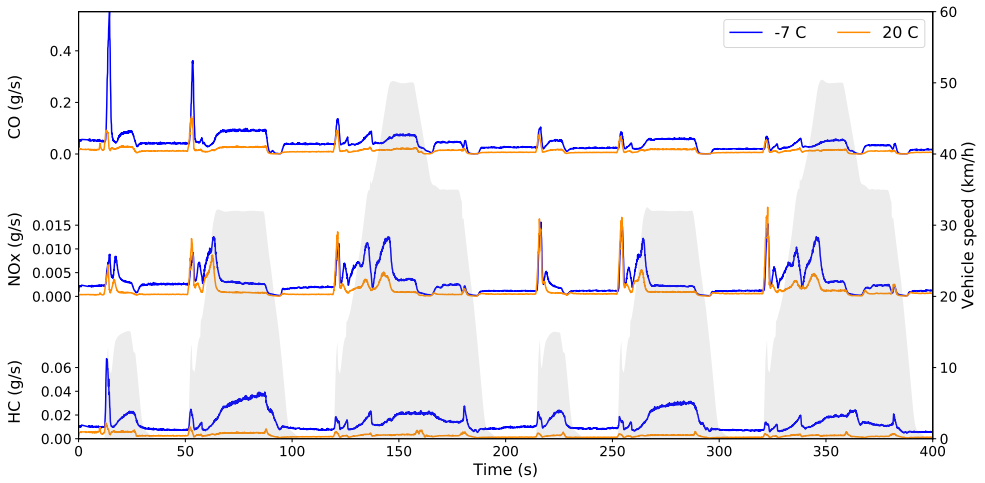

Figure 4.10: Instantaneous emission rates for HC, CO and NOx in NEDC. Vehicle speed depicted as a surface in gray.

WLTC emission flow rates are depicted in Fig. 4.11, for the first (low speed) part of the cycle, first 600 seconds. High HC peak is observed at the -7 ºC cold start. Unlike was seen in the NEDC, HC and CO emissions don't evolve with similar patterns in the WLTC. Hydrocarbons show similar dependence with time regardless the transient engine loads of the cycle. But, in the case of CO, transient conditions play the main role as emission source, being the CO emissions during transients up to 140 times the rates produced during steady operations. A zoom of the CO flow rates, between 50 and 120 seconds, is included in Fig. 4.11. During low transient points, CO emissions are higher at -7 ºC than at 20 ºC as in the NEDC. However, during strong transients, e.g. at 250 seconds, CO flow rates are considerably higher at 20 ºC, being up to twice the emission rate of -7 ºC. Transients make the accumulated CO emitted mass be higher at 20 ºC than at -7 ºC. In the case of NOx, emission rates evolve similar to the NEDC. Peak emissions are a bit higher at 20 ºC under strong transients, but this tendency flips in steady running conditions where NOx is much higher at -7 ºC and eventually makes the cumulate mass at -7 ºC higher than at 20 ºC.

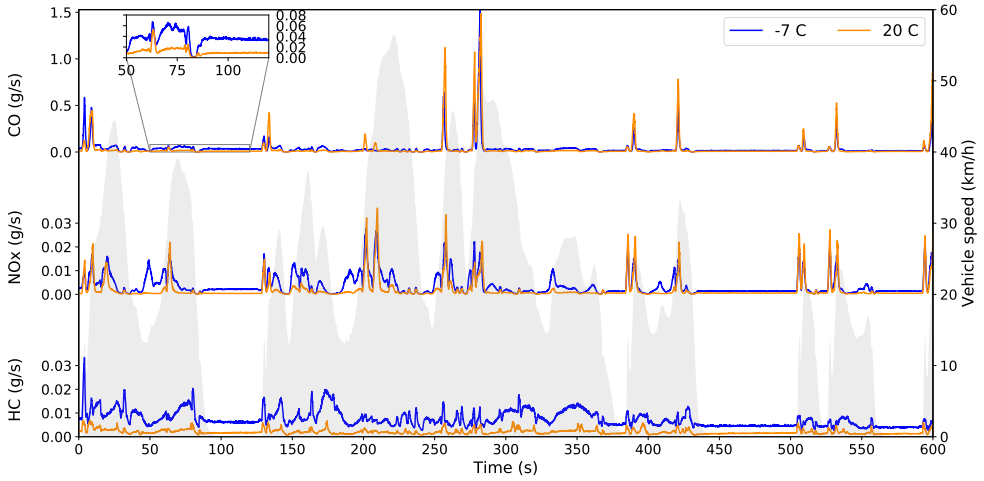

Figure 4.11: Instantaneous emission rates for HC, CO and NOx in WLTC. Vehicle speed depicted as a surface in gray.

4.4 Conclusions

The effect of low ambient temperature on pollutant emissions is analysed. WLTC and NEDC were carried out at two levels of ambient temperature: -7 ºC and 20 ºC. Pollutant analysis was focused on carbon monoxide, unburned hydrocarbons and nitrogen oxides. Thermal efficiency was evaluated by means of the fuel consumption. In general terms, emissions are increased and thermal efficiency is deteriorated when the engine runs at low ambient temperatures. Fig. 4.12 depicts the emissions ratio of the NEDC and WLTC for the whole cycle. The negative effect of low ambient temperatures is more significant in the NEDC than in the WLTC. Hydrocarbons emissions rise to 270% in the NEDC while in the WLTC are bounded to 150%. Regarding NOx, similar tendencies are observed being the increase around 250% and 280% for the NEDC and WLTC respectively. Concerning CO, opposite tendencies between both cycles are observed with the increase of 125% in the NEDC and the reduction of 18% in the WLTC. In the case of thermal efficiency, the effect of low temperatures is remarkable in the NEDC with a reduction in the 10%, while no variation is spotted in the WLTC. The analysis by pollutant shows a significant link between NEDC and WLTC regarding HC emissions. The engine warming up and load play the main role as emission source. Concerning

NOx and CO, the transient conditions of the cycles are the main cause of these pollutant emissions. At strong transient loads, where high demands of power must be met, the air management control is enforced to command the EGR valves closing producing an increase on NOx emissions. Despite the EGR valve closing, required oxygen concentration is not fulfilled and, consequently, emissions of CO rise. This effect is more noticeable in the WLTC where the role of air management control is critical. As EGR is performed with lower rates and higher temperatures at -7 ^{o}C, the effect of transients on the air management gets less important and the amount of CO is lower than at 20 ^{o}C.

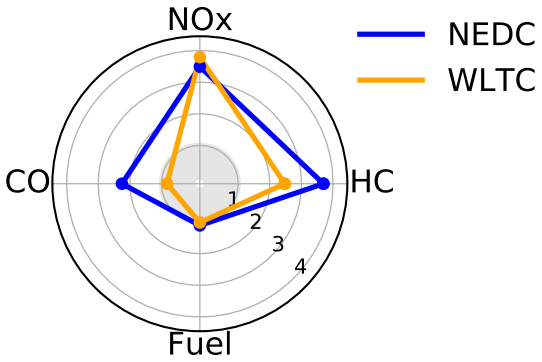

Figure 4.12: NEDC and WLTC whole cycle emissions ratio

Bibliography

[44] E. Directive. "90/C81/01,Emission Test Cycles for the Certification of light duty vehicles in Europe, EEC Emission Cycles". *EEC Emission Cycles, 1999* (1999).

[59] F. Soto, M. Alves, J. C. Valdés, O. Armas, P. Crnkovic, G. Rodrigues, A. Lacerda, and L. Melo. "The determination of the activation energy of diesel and biodiesel fuels and the analysis of engine performance and soot emissions". *Fuel Processing Technology* 174 (2018), pp. 69–77.

[60] *EPA regulation. 40 CFR Ch. I (7–1–12 Edition). 86.1828–01. Page 452.*

[61] *Commission Regulation (EC) No 692/2008 of 18 July 2008 implementing and amending Regulation (EC) No 715/2007 of the European Parliament and of the Council on type-approval of motor vehicles with respect to emissions from light passenger and commercial vehicles (Euro 5 and Euro 6) and on access to vehicle repair and maintenance information.* July 2008.

[62] A. J. Torregrosa, P. Olmeda, J. Martín, and B. Degraeuwe. "Experiments on the influence of inlet charge and coolant temperature on performance and emissions of a DI Diesel engine". *Experimental Thermal and Fluid Science* 30.7 (2006), pp. 633–641.

[63] A. J. Torregrosa, A. Broatch, P. Olmeda, and C. Romero. "Assessment of the influence of different cooling system configurations on engine warm-up, emissions and fuel consumption". *International Journal of Automotive Technology* 9.4 (2008), pp. 447–458.

[64] M. Weilenmann, J.-Y. Y. Favez, and R. Alvarez. "Cold-start emissions of modern passenger cars at different low ambient temperatures and their evolution over vehicle legislation categories". *Atmospheric Environment* 43.15 (2009), pp. 2419–2429.

[65] D. Ludykar, R. Westerholm, and J. Almén. "Cold start emissions at +22, -7 and -20°C ambient temperatures from a three-way catalyst (TWC) car: Regulated and unregulated exhaust components". *Science of the Total Environment* 235.1-3 (1999), pp. 65–69.

[66] M. Weilenmann, P. Soltic, C. Saxer, A.-M. M. Forss, and N. Heeb. "Regulated and nonregulated diesel and gasoline cold start emissions at different temperatures". *Atmospheric Environment* 39.13 (2005), pp. 2433–2441.

[67] C. Dardiotis, G. Martini, A. Marotta, and U. Manfredi. "Low-temperature cold-start gaseous emissions of late technology passenger cars". *Applied Energy* 111 (2013), pp. 468–478.

[68] O. Armas, R. García-Contreras, and Á. Ramos. "Pollutant emissions from engine starting with ethanol and butanol diesel blends". *Fuel Processing Technology* 100 (2012), pp. 63–72.

[69] E. Giakoumis and A. Zachiotis. "Investigation of a Diesel-Engined Vehicle's Performance and Emissions during the WLTC Driving Cycle—Comparison with the NEDC". *Energies* 10.2 (2017), p. 240.

[70] J. Ko, D. Jin, W. Jang, C.-L. Myung, S. Kwon, and S. Park. "Comparative investigation of NOx emission characteristics from a Euro 6-compliant diesel passenger car over the NEDC and WLTC at various ambient temperatures". *Applied Energy* 187 (2017), pp. 652–662.

[71] L. Sileghem, D. Bosteels, J. May, C. C. Favre, and S. Verhelst. "Analysis of Vehicle Emission Measurements on the New WLTC, the NEDC and the CADC". *Transportation Research: Part D: Transport and Environment* 32.0 (2014), pp. 70–85.

[72] J. Pavlovic, A. Marotta, and B. Ciuffo. "CO2 emissions and energy demands of vehicles tested under the NEDC and the new WLTP type approval test procedures". *Applied Energy* 177 (2016), pp. 661–670.

[73] D. Tsokolis, S. Tsiakmakis, A. Dimaratos, G. Fontaras, P. Pistikopoulos, B. Ciuffo, and Z. Samaras. "Fuel consumption and CO2 emissions of passenger cars over the New Worldwide Harmonized Test Protocol". *Applied Energy* 179 (2016), pp. 1152–1165.

[74] A.G.Stefnanopoulou, I.Kolmanovsky, and J. S. Freudenberg. "Control of Variable Geometry Turbocharged Diesel Engines for Reduced Emissions". *IEEE Transactions on Control Systems Technology* 8.4 (2000), pp. 733–745.

[75] M. Ammann, N. P. Fekete, L. Guzzella, and A. H. Glattfelder. "Model-based control of the VGT and EGR in a turbocharged common-rail diesel engine: Theory and passenger car implementation". *SAE transactions* 112.3 (2003), pp. 527–538.

[76] H. Peng, Y. Cui, L. Shi, and K. Deng. "Effects of exhaust gas recirculation (EGR) on combustion and emissions during cold start of direct injection (DI) diesel engine". *Energy* 33.3 (2008), pp. 471–479.

[77] A. S. Ramadhas and H. Xu. "Influence of Coolant Temperature on Cold Start Performance of Diesel Passenger Car in Cold Environment". In: *SAE Int. J. Engines*. 2016.

[78] Y. Zeldóvich. "The oxidation of nitrogen in combustion explosions". *Acta Pysichochimica USSR* 21 (1946), pp. 557–628.

[79] A. Maiboom, X. Tauzia, S. R. Shah, and J.-F. Hétet. "Experimental Study of an LP EGR System on an Automotive Diesel Engine, compared to HP EGR with respect to PM and NOx Emissions and Specific Fuel Consumption". *SAE International Journal of Engines* 2.2 (2009), pp. 2009–24–0138.

[80] Y. Park and C. Bae. "Experimental study on the effects of high/low pressure EGR proportion in a passenger car diesel engine". *Applied Energy* 133 (2014), pp. 308–316.

[81] D. Heuwetter, W. Glewen, C. Meyer, D. E. Foster, M. Andrie, and R. Krieger. "Effects of Low Pressure EGR on Transient Air System Performance and Emissions for Low Temperature Diesel Combustion". In: *SAE Int. J. Engines*. 2011.

[82] V. Bermúdez, J. M. Lujan, B. Pla, and W. G. Linares. "Effects of low pressure exhaust gas recirculation on regulated and unregulated gaseous emissions during NEDC in a light-duty diesel engine". *Energy* 36.9 (2011), pp. 5655–5665.

[83] B. Nitu, I. Singh, L. Zhong, K. Badreshany, N. A. Henein, and W. Bryzik. "Effect of EGR on Autoignition, Combustion, Regulated Emissions and Aldehydes in DI Diesel Engines". In: *SAE Int. J. Engines*. 2002.

[84] R. Schubiger, A. Bertola, and K. Boulouchos. "Influence of EGR on Combustion and Exhaust Emissions of Heavy Duty DI-Diesel Engines Equipped with Common-Rail Injection Systems". In: *SAE Int. J. Engines*. 2001.

[85] S. Wang, X. Zhu, L. Somers, and L. de Goey. "Effects of exhaust gas recirculation at various loads on diesel engine performance and exhaust particle size distribution using four blends with a research octane number of 70 and diesel". *Energy Conversion and Management* 149 (2017), pp. 918–927.

[86] X. Li, Z. Xu, C. Guan, and Z. Huang. "Impact of exhaust gas recirculation (EGR) on soot reactivity from a diesel engine operating at high load". *Applied Thermal Engineering* 68.1-2 (2014), pp. 100–106.

Chapter 5

Effect of low ambient temperature on DOC performance

Contents

5.1 Introduction

Catalytic converters have been used in engine exhaust aftertreatment systems since 1975 to reduce pollutant emissions [87]. Diesel oxidation catalysts (DOC) are used to control CO, HC and the organic fraction of diesel particulates to form harmless exhaust products. Additional reactions such as the oxidation of NO to NO_2 also occurs with the key interest attributed in facilitating passive diesel particulate filter (DPF) regenerations as well as in enhancing the performance of some selective catalytic reductions (SCR) catalysts [88]. Salomons et al. [89] studied the effect of CO and H_2 concentration on the catalysis performance, showing the increase of light off temperature with the CO concentration and the decrease of light off with the H_2 concentration. In addition to the pollutants concentrations effect, Zervas [90] analysed the impact of space velocity, average value and profile of exhaust temperature, on diesel engine tail-pipe emissions, pointing out the reduction of catalysis efficiency with the space velocity because of the lower dwell time as well as the increase of conversion efficiency with higher, both average and instantaneous, exhaust temperatures. Botsaris and Sparis [91] analysed the impact of the ambient temperature on the catalyst performance, by means of catalyst inlet-outlet temperature measurements, reporting an increase of efficiency with the ambient temperature. Karl Arnby et al. [92], studied the improvement of catalyst activity of CO performing at low temperatures by means of non-homogeneous supported catalyst.
This chapter addresses the effect of cold ambient temperature on DOC conversion efficiency. The pollutants studied are hydrocarbons and carbon monoxide. The tests were carried out at transient engine load conditions of NEDC and WLTC at -7 ^{o}C and 20 ^{o}C of ambient temperature. The content is structured as follows. Section 5.2 is devoted to the description of the heat transfer model in DOC temperature estimation. Section 5.3 contains the results and analysis of the ambient temperature effect on the DOC performance. Finally, the main conclusions are presented in Section 5.4.

5.2 Catalysis temperature estimation

DOC inner temperature plays an important role for DOC performance analysis. However, DOC inner measurements are difficult to achieve because of technical restrictions. On one hand, the small space available for temperature sensing makes it difficult to ensure the right position of the sensor during the tests realization. On the other hand, to perform the honeycomb bulk

temperature measurement it would be needed to drill the DOC housing with the risk of damaging the ceramic honeycomb. Taking into account the aforementioned drawbacks, a DOC temperature estimation model is proposed. The temperature estimation is based on a nodal heat transfer model where the thermal inertia, surrounding heat losses and internal heat generation are considered. The estimated temperature, named in this paper as DOC reference temperature, represents an average temperature of the whole DOC. The variables needed for the model implementation are: the exhaust gas temperatures and chemical species concentration at the inlet and outlet of the DOC, the exhaust mass flow and the surrounding air room temperature where the DOC is placed. The DOC reference temperature is averaged with the mean DOC internal exhaust gas temperature in order to obtain the estimated catalysis temperature. This temperature represents the mean temperature of the solid-gas interface where catalysis takes place. As catalytic oxidation is conducted in a heterogeneous solid-gas interface, the catalysis temperature is obtained from the average of the gas and the estimated DOC temperature. The catalysis temperature estimation is defined as follows:

$$T_{catalysis} = \frac{T_{DOC} + T_{gas_{mean}}}{2} \tag{5.1}$$

Where T_{DOC} is the DOC reference temperature and $T_{gas_{mean}}$ the mean gas temperature of the inlet and outlet of the DOC. Regarding the model for DOC reference temperature calculation, the DOC is formed by a ceramic honeycomb and a steel housing. Due to the small thickness of the steel housing, both parts are merged in the model and considered as one bulk. The heat released in the DOC comes from the exhaust gas enthalpy and the reaction enthalpy of the chemicals species oxidation. The heat losses to the surroundings are calculated considering only natural convection heat transfer. The DOC reference temperature evolution over time is calculated according to the following expression:

$$T_{DOC}^{t+1} = \left(\dot{H}^t - \left(T_{DOC}^t - T_{amb}^t\right) \cdot h_{ext}^t \cdot A_{ext}\right) \cdot \frac{\tau^t}{\rho_h \cdot V_h \cdot C_h + \rho_s \cdot V_s \cdot C_s} - T_{DOC}^t \tag{5.2}$$

Where $\dot{H}$ is the thermal power released in the DOC, including the internal generation, T_{amb} is the ambient temperature in the test cell, h_{ext} is the natural convection heat transfer coefficient, A_{ext} is the exterior surface of the DOC housing, $\rho_h \cdot V_h \cdot C_h$ and $\rho_s \cdot V_s \cdot C_s$ are the density, volume and specific heat of the honeycomb and the steel DOC housing respectively. The superscript indicates the time instant along the driving cycle. The heat transfer coefficient is calculated according to Morgan's correlations [93] of the Nusselt number by

means of the Grashof and Prandtl number calculation. The DOC internal generation has two energy terms. On one hand, the heat coming from the exhaust gases, calculated as:

$$\dot{H}_{exh} = \dot{m}_{exh} \cdot cp_{exh} \cdot (T_{DOC_i} - T_{DOC_o}) \tag{5.3}$$

Where $\dot{m}_{exh}$ is the exhaust mass flow passing through the DOC, cp_{exh} is the exhaust gases specific heat, T_{DOC_i} and T_{DOC_o} are the inlet and outlet DOC gas temperatures. The other term of the internal generation concerns the enthalpy released by the oxidation of carbon monoxide and hydrocarbon species. The proposed reaction mechanism is based on a set of one elementary step reactions. CO mechanism is shown below:

$$\mathrm{CO} + \frac{1}{2}\,\mathrm{O_2} \longrightarrow \mathrm{CO_2} \tag{5.4}$$

The specific reaction enthalpy is calculated from the balance of standard formation enthalpy of products and reactants:

$$\Delta H_r = H_f\,(CO_2) - H_f\,(CO) \tag{5.5}$$

Where ΔH_r is the specific reaction enthalpy and H_f is the formation enthalpy of the correspondent compound. In the case of hydrocarbons measurement, the FID technique presented in Chapter 3 doesn't allow to know the concentration of each hydrocarbon species. The HC measurement is obtained as an equivalent methane molar concentration. According to the bibliography, diesel engines hydrocarbon emissions are mainly formed by light alkenes along with medium-heavy alkanes [94] and [95]. The general reaction formulation for alkanes and alkenes (only monounsaturated considered) used is:

$$\begin{gathered} \mathrm{C_xH_{2x+2}} + \left(\frac{3\mathrm{x}+1}{2}\right)\mathrm{O_2} \longrightarrow \mathrm{xCO_2} + (\mathrm{x}+1)\,\mathrm{H_2O} \\ \mathrm{C_xH_{2x}} + \frac{3}{2}\mathrm{xO_2} \longrightarrow \mathrm{xCO_2} + \mathrm{xH_2O} \end{gathered} \tag{5.6}$$

The HC concentration measurement and the standard enthalpy of formation are weighted according to the hydrocarbons species distribution study by Stanislav V. Bohac et al. [96] for a conventional diesel combustion engine running at 1500 rpm and 3.9 bar of brake mean effective pressure (BMEP), that are representative conditions of the engine speed and BMEP average values of the performed driving cycles. The set of reactions include fifteen hydrocarbons, paraffin and olefin species, from methane to pentadecane. The enthalpy of formation of the products is corrected as follows:

$$H_f(X_i)_{corr} = H_f(X_i) \cdot \sum_{i=1}^{i=15} c_i \cdot A_i \tag{5.7}$$

Where $H_f(X_i)$ is the standard enthalpy of formation without correction for CO_2 or H_2O, c_i is the concentration of each species referred to the total amount of hydrocarbons and A_i is the products stoichiometric index according to the formulation shown at Eq. (5.6). In the case of reactants, the correction includes the standard enthalpy of formation of each hydrocarbon species as:

$$H_f(HC)_{corr} = \sum_{i=1}^{i=15} H_f(C_xH_y)_i \cdot c_i \tag{5.8}$$

where $H_f(C_xH_y)_i$ i is the standard enthalpy of formation of each hydrocarbon species. The stoichiometric index is not included because it is defined as one according to the formulation shown previously in Eq. (5.6).
In addition to the enthalpy of formation, the hydrocarbon concentration measured by the FID has to be corrected too. The hydrocarbons concentration is corrected taking into account the number of carbon atoms of each specie according to the following expression:

$$f = \frac{1}{\sum_{i=1}^{i=15} c_i \cdot n_i} \tag{5.9}$$

Where n_i is the number of carbon atoms by hydrocarbon specie. Once both the enthalpy of formation correction and the concentration factor are calculated, the corrected specific reaction enthalpy is obtained as:

$$\Delta H_{r_{corr}} = f \cdot (H_f\,(CO_2)_{corr} + H_f\,(H_2O)_{corr} - H_f\,(HC)_{corr}) \tag{5.10}$$

by multiplying the above expression, Eq. (5.10), by the FID methane equivalent moles, the released heat, because of hydrocarbons oxidation, is obtained.

5.3 Results

Pollutant emissions are analysed at the inlet and outlet of the DOC at both low (-7 ºC) and high (20 ºC) ambient temperature. DOC performance analysis is carried out for CO and HC emissions. The catalyst efficiency is defined as:

$$\eta = \frac{[X_i] - [X_o]}{[X_i]} \tag{5.11}$$

where $[X_i]$ and $[X_o]$ are the HC and CO molar concentrations at the DOC inlet and outlet respectively.
According to several authors [87] and [90], DOC temperature, dwell time,

[O2], [CO] and [HC] are the test variables that play a key role in the DOC performance. Dwell time is calculated as:

$$\tau = \frac{V_{DOC} \cdot \rho}{\dot{m}_{exh}} \tag{5.12}$$

where $\dot{m}_{exh}$ is the exhaust mass flow, V_{DOC} is the internal DOC volume and ρ is the gas density calculated from the ideal gas law:

$$\rho = \frac{p}{R \cdot T} \tag{5.13}$$

where p is the exhaust pressure, R the ideal gas constant and T the exhaust gas temperature.
According to the general expression of the chemical reaction rate, along with the Arrhenius constant rate expression, the efficiency of a chemical reaction depends on the DOC temperature, dwell time and oxygen concentration at the inlet of the DOC. The conversion efficiency equation can be obtained from the general reaction rate expression, considering a single-step reaction, as follows:

$$\begin{aligned} \frac{d[x]}{dt} &= [O_2]^a \cdot [X] \cdot K(T) \\ \frac{d[x]}{dt} \approx \frac{[X_i] - [X_o]}{\tau} &= [O_2]^a \cdot [X_i] \cdot K(T) \end{aligned} \tag{5.14}$$

The above expression is substituted in the conversion efficiency equation, Eq. (5.11), as:

$$\eta = [\mathrm{O_2}]^a \cdot K(T) \cdot \tau \tag{5.15}$$

Where $[\mathrm{O_2}]^a$ is the oxygen concentration raised to the a power, a is the stoichiometric coefficient of oxygen, τ is the dwell time of the gas in the DOC, $K(T)$ is the reaction rate constant, $[X_i]$ and $[X_o]$ are the DOC inlet and outlet pollutant concentration respectively. Despite Eq. (5.15) doesn't take into account the pollutant concentration on DOC efficiency, several authors have reported the influence of pollutant concentration on catalyst performance. According to [89] and [97], the light-off temperature increases with the pollutant concentration. In addition, pollutants interfere between them in the catalyst process [98], encouraging the conversion rate of CO_2, in case of high monoxide concentration, due to the higher reactivity of CO respect to some hydrocarbon species.
In the following lines results of DOC conversion efficiency at low temperature are presented for both WLTC and NEDC.

5.3.1 WLTC

The estimated catalysis temperature, is shown in Fig. 5.1 The catalysis temperatures show similar values from the beginning of the cycle. Higher temperatures are estimated at 20ºC after 800 seconds of the WLTC. The cause of such difference is twofold. On one hand the exhaust gas temperature is slightly higher at 20 ºC than at -7ºC, with an average difference of 17 ºC along the WLTC cycle. On the other hand, after 600 seconds the HP EGR is shifted to LP EGR in the case of 20 ºC case, and therefore the exhaust mass flow increases. Both higher exhaust temperature and exhaust mass flow increase drive to a higher release of thermal power in the DOC at 20 ºC when high engine loads are performed from the 800 seconds of the WLTC. The reasons why catalyst temperatures show so similar values no matter the ambient temperature are: the similar DOC inlet gas temperatures, the higher exhaust gas flow at -7ºC than at 20ºC, the relative low heating losses at the DOC driven by free convection heat transfer and the low thermal inertia of the DOC because of its low mass [**hamedi2014thermal**].

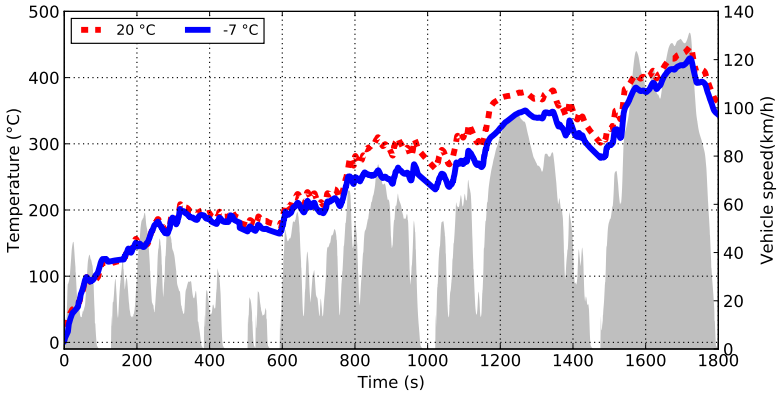

Figure 5.1: Catalysis temperature evolution for -7 ºC and 20 ºC ambient temperature. WLTC vehicle speed is depicted as a surface in gray.

DOC conversion efficiencies over the WLTC are depicted in Fig. 5.2 for HC and CO. DOC performs with relative high efficiency from the beginning of the cycle, mainly in the case of HC conversion (70%). The high HC efficiency in the first instants can be explained by the adsorption of some chemical species in the washcoat that retains pollutants in the DOC. Several authors have study the adsorption and desorption mechanisms on oxidation catalyzers, [99] and [100]. The adsorption effect on pollutants conversion is beyond the scope

of this work and it hasn't been considered in the DOC performance analysis. The evolution of the efficiencies shows very different profiles. On one hand the HC conversion efficiency performs in a quasi-steady behaviour along the WLTC cycle. On the opposite, the CO conversion efficiency shows an unstable pattern along most part of the WLTC. This unsteady operation is because of the dependence of the conversion efficiency with the CO inlet concentration [90] and therefore the CO conversion is strongly affected by the transient load conditions. In Fig. 5.3 the variables that play a main role in the conversion efficiency are shown: CO, HC, oxygen concentration and dwell time. CO concentration performs in a transient manner along the WLTC cycle. Lower CO peaks are observed at -7 ºC than 20 ºC because of the higher air to fuel ratio at low temperatures. HC concentration is greater at -7 ºC during the first 1200 seconds of the WLTC. The HC concentration at -7 ºC becomes lower as the warming up proceeds until it reaches the hydrocarbons level at 20 ºC. The differences observed in O_2 and in dwell time are because of the exhaust mass flow. During the first 600 seconds, exhaust mass flow is higher at -7 ºC causing lower dwell time and higher oxygen content because of the higher air to fuel ratio. Since 600 seconds until the end of the WLTC, -7 ºC case shows higher dwell time and exhaust oxygen concentration. The reason of this fact is because of the LP EGR enabling at 20 ºC causing the reduction of both the dwell time, because the higher exhaust mass flow, and the oxygen content, because of the reduction of air to fuel ratio.

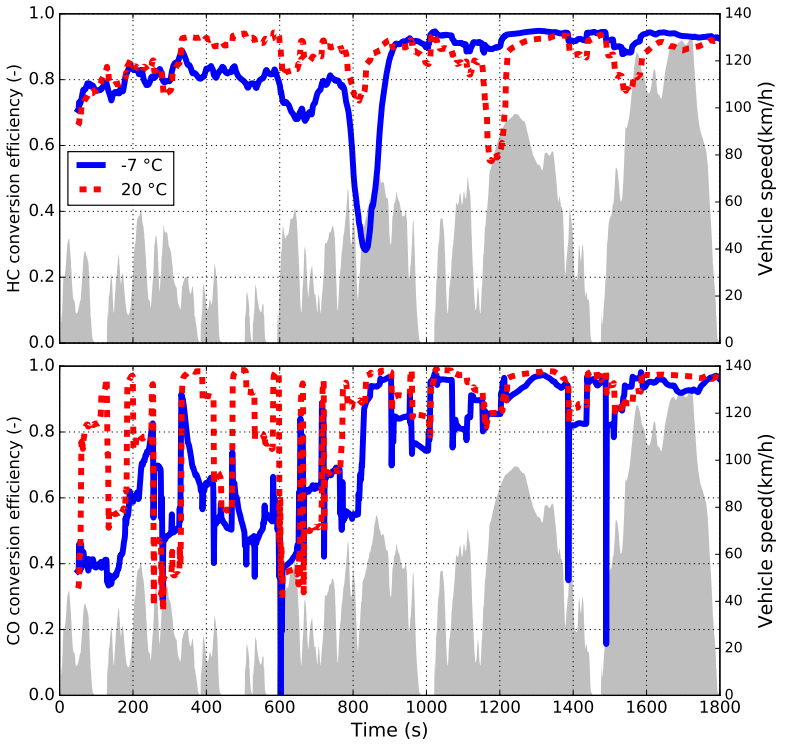

Figure 5.2: DOC conversion efficiency for HC and CO. WLTC vehicle speed is depicted as a surface in gray.

The conversion efficiency evolution over the WLTC in Fig. 5.2 can be deeply analysed by means of the explanatory variables of Fig. 5.3 The HC conversion efficiency shows quite high and very similar values since the beginning of the cycle for both ambient temperatures. Between 300 and 800 seconds the efficiency is higher in the case of 20 ^{o}C because of the higher dwell time and lower HC concentration. Despite the lower oxygen concentration at 20 ^{o}C compared to -7^{o}C, it is still high enough to avoid negative effects on HC conversion. An instant to highlight in the WLTC occurs at 800 seconds, when a notable reduction is detected on HC conversion efficiency at -7^{o}C. The reason of the efficiency reduction in this point is a combination of low dwell time, reduction of oxygen concentration and a sudden increase of CO emissions. The effect of CO concentration peaks on HC conversion is observed many times along the WLTC: 300, 600, 800, 1200 and 1550 seconds are points of HC conversion efficiency reduction because of the interference of CO concentration peaks. In case of 20 ^{o}C two significant efficiency reductions are observed at

1200 and 1550 seconds mainly because of the very low oxygen concentration at these points, which is around 6%. From 1000 seconds, when high and extra-high load are performed, until the end of the WLTC, the HC conversion efficiency is slightly higher in the case of -7ºC than 20 ºC. In the case of -7 ºC, the generation of HC falls to the hydrocarbon concentrations produced at 20ºC and the oxygen concentration keeps higher than 20 ºC. These factors drive to higher conversion efficiency in the case of -7 ºC. Regarding CO conversion is remarkable the strong transient performance of CO oxidation efficiency. The higher the CO peak, the stronger the CO conversion efficiency drop is [90]. This conversion dependence on CO peaks reduces as the WLTC proceeds.
One point of the cycle to highlight is at 600 seconds when CO DOC efficiency conversion drops at both ambient temperatures because of the change between the HP to the LP EGR system along with the presence of a CO emission peak. The LP EGR enabling at 20 ºC increases the exhaust mass flow and therefore the dwell time reduces, driving to lower DOC efficiencies. In the case of HC, as this change is not accompanied with a hydrocarbon emission peak the negative effect in the HC DOC efficiency is less noticeable. Once the WLTC reaches the 800 seconds the DOC conversion efficiencies become less important because of the high DOC interface temperature (250 ºC). As the cycle proceeds, the CO conversion efficiency differences between -7 ºC and 20 ºC vanish. In spite of this phenomena is more remarkable in CO, it is also spotted in case of HC oxidation efficiency at -7 ºC. When catalyst temperature reaches 250 ºC DOC efficiency enhancement is observed.

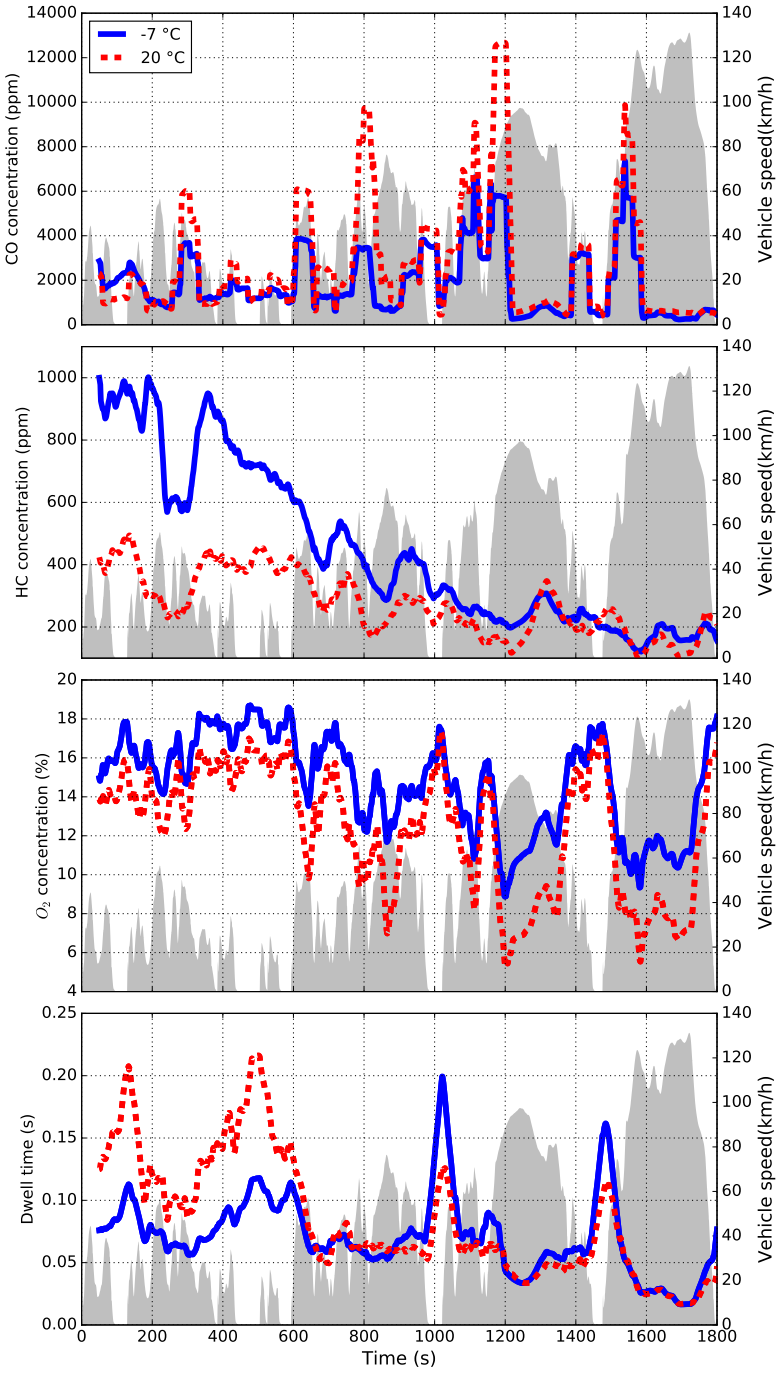

Figure 5.3: DOC performance explanatory variables. WLTC vehicle speed is depicted as a surface in gray.

5.3.2 NEDC

Regarding catalyst temperature, NEDC performs in similar manner than WLTC. DOC interface temperature evolves quite close at both ambient temperatures Fig. 5.4

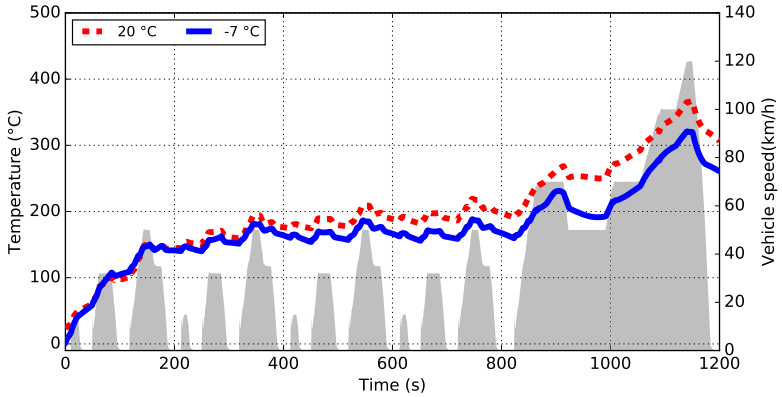

Figure 5.4: Catalysis temperature evolution for -7 ºC and 20 ºC ambient temperature. NEDC vehicle speed is depicted as a surface in gray.

Comparing to the WLTC, a flatter temperature evolution is observed in NEDC. While catalysis temperature rises to almost 425 ºC in WLTC, the highest temperature under NEDC is limited to roughly 350 ºC.
DOC conversion efficiencies over the NEDC are depicted in Fig. 5.5 for HC and CO. Regarding -7 ºC case, DOC performs with relative high efficiency from the beginning of the cycle, mainly in the case of HC conversion (60%). As was aforementioned in WLTC results Section 5.3.1, the high efficiency in the first instants can be explained by the adsorption of some chemical species in the washcoat that retains pollutants in the DOC. HC desorption can be observed between 850 to 950 seconds when EUDC is performed, pollutants measurements show higher concentrations at the DOC outlet than at the inlet, eventually causing negative conversion efficiencies. This phenomenon is caused by high intake temperatures that boost the pollutants release from the DOC washcoat. As DOC efficiency definition doesn't have any sense under this conditions the efficiency calculation has been neglected during the desorption process. Finally, during the EUDC, a notable DOC performance enhancement is observed owing to the catalyst temperature increase. During the last driving phase at roughly 900 seconds temperature reaches 250 ºC.

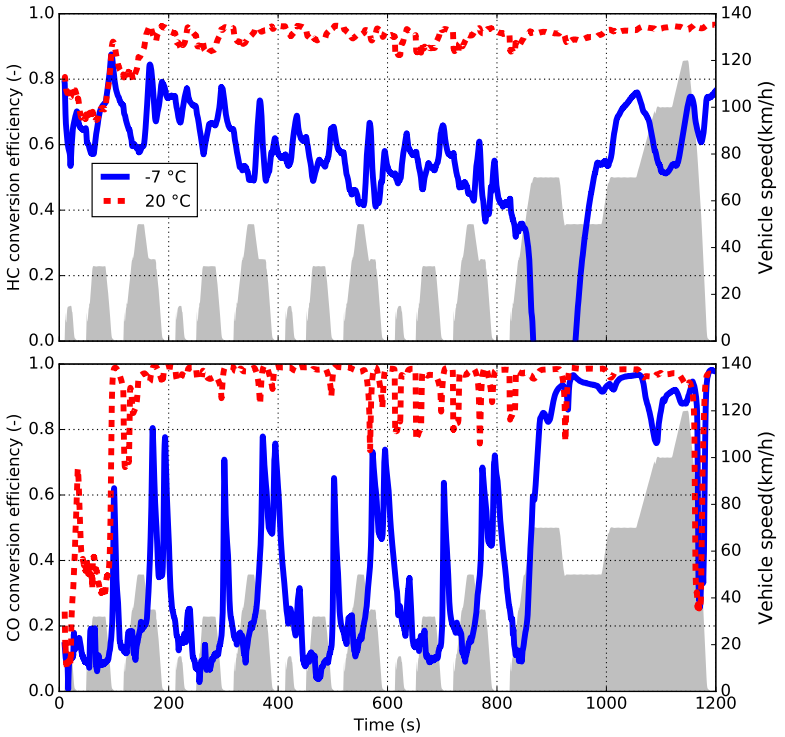

Figure 5.5: DOC conversion efficiency for HC and CO. NEDC vehicle speed is depicted as a surface in gray.

Comparing HC and CO conversion performance at low ambient temperatures, the evolution of the efficiencies show very different profiles. On one hand the HC conversion efficiency performs in a monotone reduction steady behaviour along the NEDC cycle. On the opposite, the CO conversion efficiency shows notable variations with a sort of pattern that repeats along the UDCs. Comparing to WLTC, CO conversion in NEDC is more stable because of the steadier driving conditions. Regarding DOC performance at 20 ^{o}C, both CO and HC efficiencies show high and almost constant oxidation efficiencies. Slight poor performance is spotted at the NEDC beginning. Nevertheless, since 100 seconds, DOC performance is roughly 0.95 and almost 1 for HC and CO respectively.

In Fig. 5.6 the variables that play a main role in the conversion efficiency are shown: CO, HC, oxygen concentration and dwell time. Significant correlation between $[O_2]$ and dwell time is spotted. During low loads, and mainly in idle condition, high oxygen concentration and dwell time are spotted. High CO

conversion efficiencies are linked with points of high dwell time and oxygen concentration. This relation is observed at low ambient temperatures with an enhancement of CO conversion during decelerations and idle conditions. As raw CO concentration evolves in a monotone decreasing manner, unlike the WLTC, no CO interference is spotted in case of NEDC. HC concentration is greater at -7 ºC during the first 1200 seconds of the NEDC. HC concentration at -7 ºC becomes lower as the warming up proceeds until it reaches the hydrocarbons level at 20 ºC. The differences observed in O_2 and in dwell time are because of the EGR differences. During the first 600 seconds, exhaust mass flow is higher at -7 ºC causing lower dwell time and higher oxygen content because of the higher air to fuel ratio. Since 600 seconds until the end of the NEDC, both ambient temperature cases show similar dwell times but different oxygen concentrations. The reason of this fact is because of the LP EGR enabling at 20 ºC causing the reduction of the dwell time owing to the higher exhaust mass flow. Comparing between ambient temperatures, higher DOC performance at 20 ºC is caused by the higher dwell time and the absence of peak emissions. Dwell time decrease between 600 and 800 seconds drives to CO oxidation efficiency reduction, manly during accelerations. Regarding low temperature performance, once EUDC is performed, pollutants concentration reduce and DOC interface temperature increases leading to DOC conversion enhancement of both CO and HC.

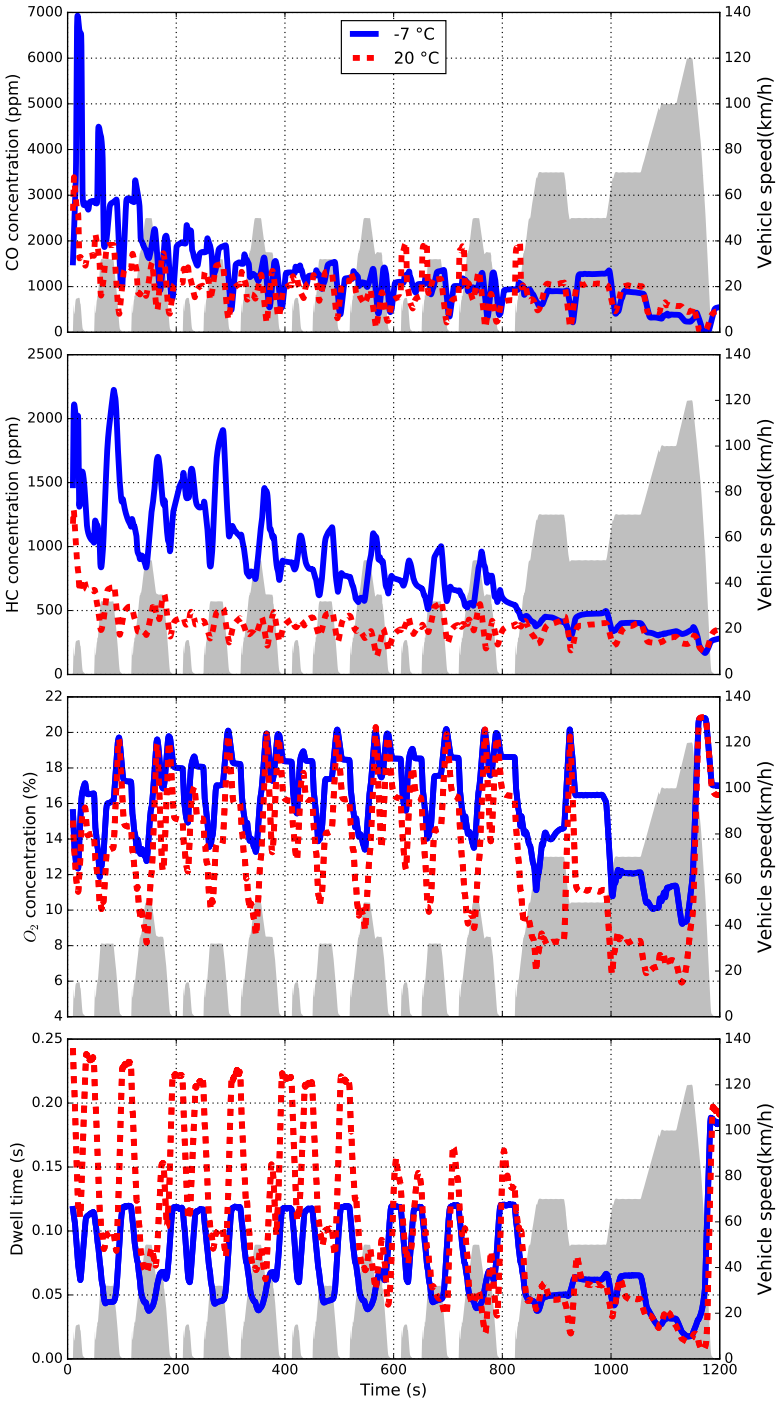

Figure 5.6: DOC performance explanatory variables. NEDC vehicle speed is depicted as a surface in gray.

5.4 Conclusions

Comparing both driving cycles, two different DOC efficiency patterns are spotted. On one hand, regarding CO, the conversion efficiency performs in a high transient manner owing to the high and transient peaks emissions of CO. Concentration peaks in WLTC can reach up to 3 times the concentrations in NEDC. In spite of the higher CO peaks, DOC performs with higher efficiencies in WLTC than in NEDC under low ambient temperatures. CO efficiency drops in the NEDC are observed during accelerations when high HC emissions are produced. Results suggest that HC peaks may reduce CO conversion rate. In case of running at 20 ^{o}C, the conversion efficiency is turned around, being the DOC efficiency notable higher and steadier, in NEDC. On the other hand, in case of HC conversion, DOC performance is slightly higher in the WLTC. HC conversion performs in steadier manner than CO at low ambient temperatures of both driving cycles. NEDC HC concentration is twice the WLTC. In case of running at 20 ^{o}C, the HC conversion efficiency is almost the same in both cycles.
Summing up, the negative effect of low ambient temperature on DOC conversion efficiency is greater in NEDC than in WLTC.

Bibliography

[87] H. Santos and M. Costa. "Evaluation of the conversion efficiency of ceramic and metallic three way catalytic converters". *Energy Conversion and Management* 49.2 (2008), pp. 291–300.

[88] J. M. Herreros, S. S. Gill, I. Lefort, A. Tsolakis, P. Millington, and E. Moss. "Enhancing the low temperature oxidation performance over a Pt and a Pt-Pd diesel oxidation catalyst". *Applied Catalysis B: Environmental* 147 (2014), pp. 835–841.

[89] S. Salomons, M. Votsmeier, R. E. Hayes, A. Drochner, H. Vogel, and J. Gieshof. "CO and H2 oxidation on a platinum monolith diesel oxidation catalyst". *Catalysis Today* 117.4 (2006), pp. 491–497.

[90] E. Zervas. "Parametric study of the main parameters influencing the catalytic efficiency of a diesel oxidation catalyst: Parameters influencing the efficiency of a diesel catalyst". *International Journal of Automotive Technology* 9.6 (2008), pp. 641–647.

[91] P. D. S. P. N. Botsaris. "Ambient temperature influence on catalytic outlet—inlet temperature difference". *Proceedings of the Institution of Mechanical Engineers, Part D: Journal of Automobile Engineering* 214.2000 (2000), pp. 95–100.

[92] K. Arnby, A. Törncrona, B. Andersson, and M. Skoglundh. "Investigation of Pt/γ-Al2O3 catalysts with locally high Pt concentrations for oxidation of CO at low temperatures". *Journal of Catalysis* 221.1 (2004), pp. 252–261.

[93] V. T. Morgan. "The Overall Convective Heat Transfer from Smooth Circular Cylinders". *Advances in Heat Transfer* 11.C (1975), pp. 199–264.

[94] J. Koop and O. Deutschmann. "Detailed surface reaction mechanism for Pt-catalyzed abatement of automotive exhaust gases". *Applied Catalysis B: Environmental* 91.1-2 (2009), pp. 47–58.

[95] F. Payri, V. R. Bermúdez, B. Tormos, and W. G. Linares. "Hydrocarbon emissions speciation in diesel and biodiesel exhausts". *Atmospheric Environment* 43.6 (2009), pp. 1273–1279.

[96] S. V. Bohac, M. Han, T. J. Jacobs, A. J. López, D. N. Assanis, and P. G. Szymkowicz. "Speciated Hydrocarbon Emissions from an Automotive Diesel Engine and DOC Utilizing Conventional and PCI Combustion". *SAE Technical Papers* 2006.2006-01-0201 (2006).

[97] I. Lefort, J. M. Herreros, and A. Tsolakis. "Reduction of low temperature engine pollutants by understanding the exhaust species interactions in a diesel oxidation catalyst". *Environmental Science and Technology* 48.4 (2014), pp. 2361–2367.

[98] M. J. Patterson, D. E. Angove, and N. W. Cant. "The effect of carbon monoxide on the oxidation of four C6 to C8 hydrocarbons over platinum, palladium and rhodium". *Applied Catalysis B: Environmental* 26.1 (2000), pp. 47–57.

[99] M. Kamijo, M. Kamikubo, H. Akama, and K. Matsushita. "Study of an oxidation catalyst system for diesel emission control utilizing HC adsorption". *JSAE Review* 22.3 (2001), pp. 277–280.

[100] Y. Hiramoto, M. Takaya, S. Yamamoto, and A. Okada. "Development of a New HC-Adsorption Three-Way Catalyst System for Partial-ZEV Performance". In: 2003.

Chapter 6

Analysis of thermal energy management solutions

Contents

6.1 Introduction

The effect of running in cold conditions on pollutant emissions and engine performance has been addressed by many researchers [101], [62] and [63]. Several authors have studied the effect of warm-up in engines and proposed methods and systems to reduce the time needed to get the nominal operation conditions. Jarrier et al. [102] explained that during the first minute of warm-up, around 65% of the combustion energy is used for mass heating, being negligible the heat transfer from the engine to the ambient. Referring to the improvement of cooling systems, researchers have been focused on cooling strategies in order to reduce the engine warm-up time, optimize the heat dissipation in each of the engine operation points and ensure the passenger comfort. Many authors have researched different ways to get improvements on engine thermal conditions for cold operation. Gumus [103] presented a thermal energy storage device (TESD) connected to the engine water jacket, that works on the effect of absorption and rejection of heat during the solid–liquid phase change of heat storage material ($Na_2SO_4 - 10H_2O$). By pre-heating the engine at cold start, at 2 ^{o}C, Gumus obtained a CO and HC emission decrease about 64% and 15% respectively. Broatch et al. [104] evaluated the potential of an intake air heating technology, by means of electrical heaters, for the reduction of pollutant emissions from diesel engine combustion during a NEDC cycle, showing a reduction of 13% in HC, 5% in CO and 3% in NOx. However, particulate matter increased about 4%. Kauranen et al. [105] proposed a double heat recovery system based on the combination of an exhaust gas heat recovery system and a latent heat accumulator for thermal energy storage, using the energy to heat the engine coolant during the cold start and low engine load operation.
Many authors, [106] and [107], have analysed the improvement on engine performance by engine coolant heating. In this work a different concept is proposed. Exhaust thermal energy is recovered by a heat exchanger placed on the tail of the exhaust line. Recovered heat is driven by a hydraulic installation to the intake manifold where a water/air heat exchanger releases the heat recovered to the intake air instead of heating the engine coolant. Regarding EGHR for engine coolant heating some advantages have to be highlighted:

- Increasing oil temperature reduces friction losses, due to its lower viscosity with temperature.
- Recovered energy is transferred to the engine block, reducing the transmitted heat from the combustion to the cylinder line and cylinder head.

On the other hand, some disadvantages still need to be addressed regarding the oil and coolant heating approach:

- High thermal inertia of block and coolant engine system as well as thermal losses along with low heat recovery during the first minutes of warming-up produces small temperature increases in engine coolant and oil.

- Initial combustion conditions are not improved. So, cold air is coming inside the cylinder, increasing the combustion time duration and therefore reducing the combustion performance.

The facility performed in this work was used to investigate the capability of an exhaust heat recovery system as well as to study the influence of the intake air temperature on the emissions and performance of a DI diesel engine working under transient load conditions at low ambient temperatures. The initial air temperature influences on the chemical reaction rate through the rate coefficient. According to Arrhenius expression [108] there is an exponential relation between rate constant and temperature. Higher intake air temperatures show a drawback effect on cylinder filling. The higher the temperature is, the lower the density is, and therefore the volumetric efficiency goes down [109]. However at low temperatures the negative effect on the volumetric efficiency is not significant, but on the rate of combustion it is. Therefore, the intake air temperature increase may be regarded as a solution for low combustion performance under low ambient temperature. The engine performance enhancement is addressed in this work by means of the fuel consumption and the measurement of pollutant emissions.
The aim of this chapter is to analyse how the improvement of combustion boundary and initial conditions, such as the engine coolant temperature and the air intake temperature, can enhance the engine performance under low ambient temperature. Two different thermal management approaches are considered. The first system, analysed in Section 6.3.1.1 and Section 6.3.1.2, comprises the WCAC and engine thermal management based on coolant flow regulation for avoiding overcooling during low temperature operation conditions. The second systems relies on the EGHR for intake air heating by means of an exhaust heat exchanger placed at the end of the exhaust tailpipe. Recovered energy and efficiency of the EGHR system is analysed in detail in Section 6.4. Finally, the EGHR performance is compared to the coolant management approach in Section 6.4.2.

6.2 Baseline case

Thermal management tests are assessed in NEDC at -7ºC. According to the results presented in Chapter 4 and Chapter 5, the negative effect of low ambient temperature is greater in NEDC than in WLTC. On one hand, CO and HC raw emissions are notable higher in NEDC than in WLTC. On the other hand, regarding DOC efficiency, CO and HC conversion performs worse in NEDC than in WLTC. So, considering the worst scenario for an engine running at low ambient temperatures, the NEDC comes up as the most suitable driving cycle to test the different thermal management solutions.
Unlike the outcomes of the carmaker calibration engine performance at low ambient temperatures, shown in Chapter 4 and Chapter 5, the baseline case proposed in this thesis encourages the prior EGR enabling to avoid NOx overshooting. In spite of the last NOx aftertreatment techniques such as LNT and SCR, NOx is still the main pollutant released [70] by diesel engines. Fig. 6.1 shows the pollutant ratios of three different EGR calibrations. On one hand, LP EGR case represents a late EGR enabling strategy where the low pressure loop is activated at 500 s. On the other hand, HP/LP EGR 200 s. case is a combination of HP and LP EGR, where loops are switched at 200 seconds. Finally, at the HP/LP 400 s. case a longer HP EGR strategy is performed at the expense of reducing the LP EGR enabling time. In all configurations, EGR is not enabled until the engine coolant temperature reaches -4ºC, that is around 100 s. in the NEDC, with the purpose of avoiding misfiring events at the cold start.
Comparing all proposed cases, LP 400 s. is dismissed as baseline because of the high increase on NOx as consequence of EGR delaying. In addition to the pollutant emission dependence, EGR setting needs to address the existence of interference between the HP EGR and the EGHR performance. Available exhaust gas energy reduces by HP EGR enabling as it reduces the exhaust gas flow.

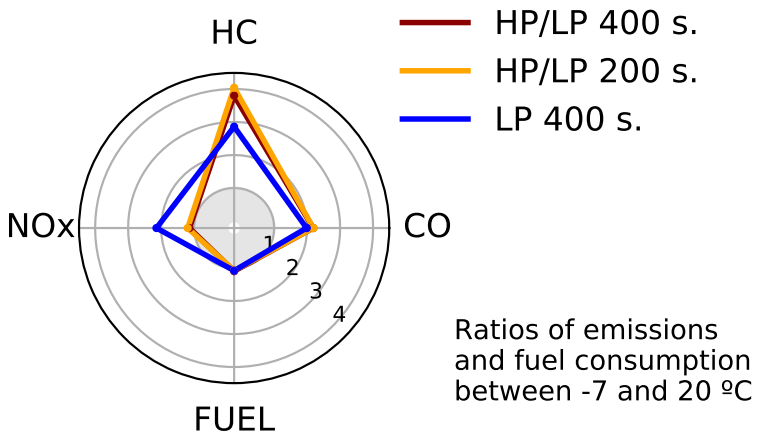

Figure 6.1: NEDC whole cycle emissions ratio between -7 to 20 ºC at several EGR calibration strategies

Comparing the HP/LP 200 s. to the HP/LP 400 s. strategies, the pollutant ratios are very similar no matter the time span of each EGR loop. As EGHR takes advantage of exhaust mass flow enthalpy, HP EGR enabling reduces the available exhaust energy to recover. HP EGR and EGHR system work in a competitive way unlike it happened by enabling the LP loop where the whole recirculated gas flows through the EGHR system. Therefore, regarding both NOx reduction and EGHR boosting, the baseline EGR calibration is set as HP/LP 200 s.
In this chapter, the results of the different thermal management systems are analysed by the ratio between the emissions at -7ºC divided the warm reference test at 20ºC with the serial calibration where the thermal management solutions weren't applied.

6.3 Coolant thermal management

In this section, coolant thermal management results are analysed. All configurations tested in this layout lay on the engine and WCAC coolant flow management. On one hand, in Section 6.3.1.1 several configurations are tested for the engine coolant thermal management depending on the thermal management valve position. Three cases were proposed: first, the reference case, that represents the most popular cooling layout nowadays, where no

thermal regulation is enabled. Engine coolant flows through a bypass from the beginning of the engine start until the coolant target temperature is reached. Once coolant temperature rises over 80ºC, the heat surplus is released to the ambient at the engine radiator by means of the thermostat regulation. Second, the microflow case, given this name because of the low coolant flow rate. In this layout, the engine coolant flows through the EGR coolers and the engine block. Finally, the coolant 0 flow case, where the thermal management valve avoids any coolant flow. In this last configuration, an external electrical pump is needed for avoiding EGR coolers overheating. In all aforementioned cases WCAC flow is recirculated through the WCAC bypass. On the other hand, the influence of different WCAC coolant flow strategies on engine performance is analysed at Section 6.3.1.2. The engine coolant reference case is compared to a WCAC 0 flow system where the WCAC electrical pump is turned off for avoiding intake air overcooling at cold ambient conditions. In addition, an AIRCAC reference running at - 7ºC has been added. This layout comprises the current most popular automotive technology where an air-air intercooler is placed downstream the compressor cooling down the intake air to the ambient temperature.

6.3.1 Effect on pollutant emissions and fuel consumption

6.3.1.1 Engine coolant management

Emissions ratios and fuel consumption by driving phase between -7 ºC and 20 ºC are shown in Fig. 6.2. In general terms, emissions and fuel consumption of all engine coolant thermal management cases evolve in similar way. As the cycle proceeds ratios reduce, pointing the performance enhancement of the cold tests with the warming-up. Regarding hydrocarbons, the emissions rates began in all cases between roughly 3.5 and 4.5. Due to the initial disabling of EGR at low ambient temperature, HC highest emission ratios are not placed at the first UDC but at the second, where ratios reach from 7 up to 8.5. While HP EGR is running since the beginning at 20 ºC, it is not enabled until 100 s. at -7 ºC. Beyond this point, ratios go down until reaching the lowest value at the last UDC when emissions are around 1.75 times higher at low ambient temperatures. Concerning CO, emission ratios are kept around 2.5 for the first three UDC. At the last UDC and EUDC ratios reduce to 1.25 and 1.6 respectively. In the case of NOx, notable reduction is spotted in the second UDC owing to the EGR enabling. NOx ratios are reduced from 3.75 to almost 1. Concerning BTE, a HC like evolution is observed, with a maximum of fuel consumption, close to 1.4, located at the second UDC. Beyond this point

engine efficiency increases until the end of the cycle reaching the same BTE than the 20 ºC case at the EUDC.
On the other hand, the AIRCAC case shows higher emissions than the rest of low temperature cases because of the low intake gas temperature. Intake temperature of AIRCAC case is analysed in Section 6.5. In contrast to the general tendency of enhancement of hydrocarbons and carbon monoxide with the warming-up, in the AIRCAC case a deterioration is spotted since the beginning until the third UDC. HC and CO emissions rise up to 12 and 4 times, respectively, the pollutants emitted at 20 ºC. Notable increase of CO and HC emissions are observed for all driving phases in the AIRCAC layout with the exception of the first UDC, where ratios perform close to the other low ambient temperature cases. Regarding BTE, engine efficiency reduction is spotted since the second until the last UDC. Concerning NOx, almost negligible differences with the rest of low temperature tests is observed in the EUDC.

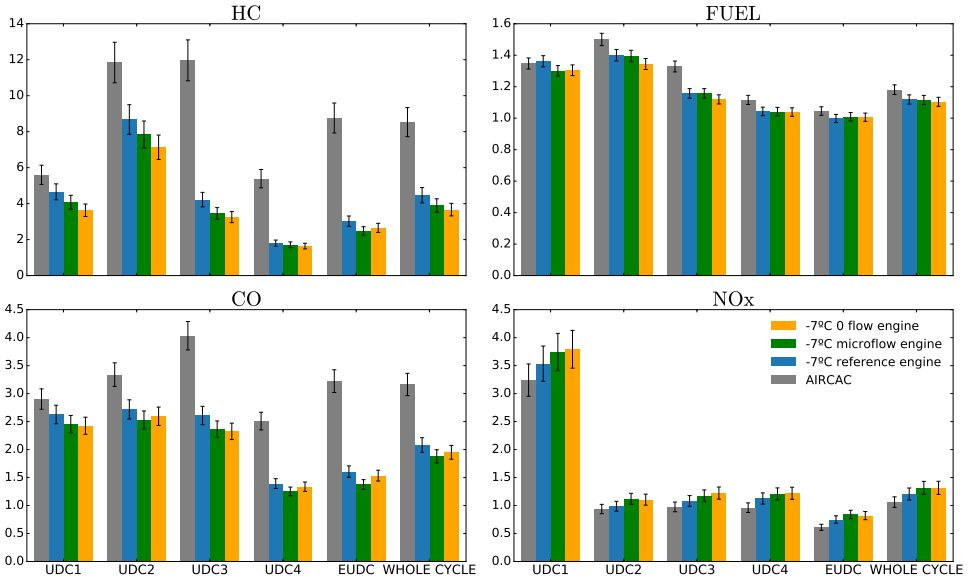

Figure 6.2: Pollutants and fuel ratio by NEDC driving phase. Different thermal management valve configurations

The notable CO and HC reduction in all coolant thermal management cases at the last UDC is because of twofold: on one hand, these emissions at low temperatures show the minimal emitted amount at the last UDC. On the other hand, carbon based emissions are not reduced beyond the third UDC

when the engine is running at 20 ºC. For better understanding of this effect, Fig. 6.3 shows the emitted mass amount by driving phase for hydrocarbons and carbon monoxide. In both pollutants, the lowest difference between the warm and cold cases is placed at the last UDC. All low ambient temperature cases

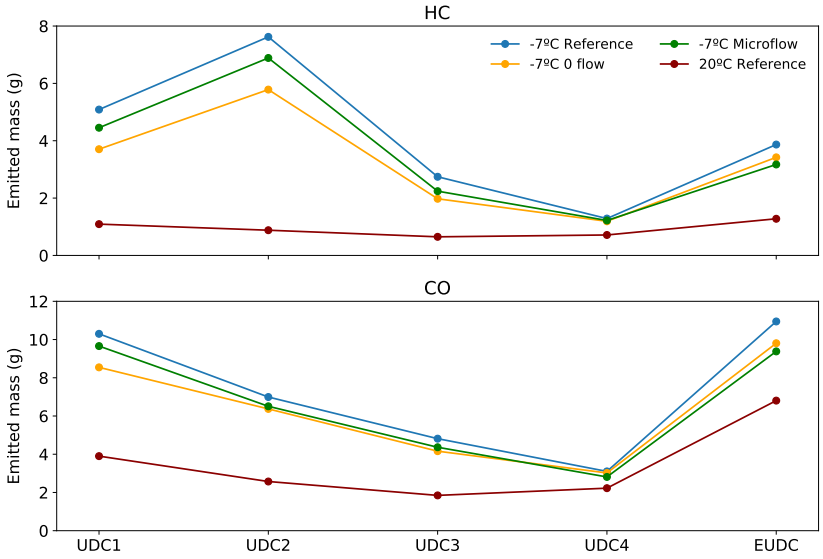

Figure 6.3: HC and CO emitted mass by NEDC driving phase

show similar reduction pattern of all ratios as the cycle proceeds. However, this tendency is switched when the EUDC is performed. HC and CO emissions ratios increase while NOx reduces because of different EGR rates between the cold and warm cases. As the original ECU calibration is kept, the air mass flow settings are the same in all cases independently of the inlet air temperature. The lower exhaust temperature of cold ambient tests entails lower LP EGR temperature that leads to increase the total intake mass flow, eventually comprising higher amounts of exhaust gas recirculation. This increase of EGR keeping constant the fresh air mass flow is known as additive EGR [110]. In Fig. 6.4 this phenomenon is depicted by showing the differences on emissions, EGR rates and LP EGR temperatures in a steady operation period of the EUDC. A difference on EGR of 3% causes the HC and CO rising and the NOx reduction. The LP EGR temperature difference is roughly 25 ºC. As

consequence of the additive EGR, according to Fig. 6.2, hydrocarbons ratio rise to 3 and carbon monoxide to around 1.5. In contrast, NOx ratios are reduced to 0.75 at the EUDC.

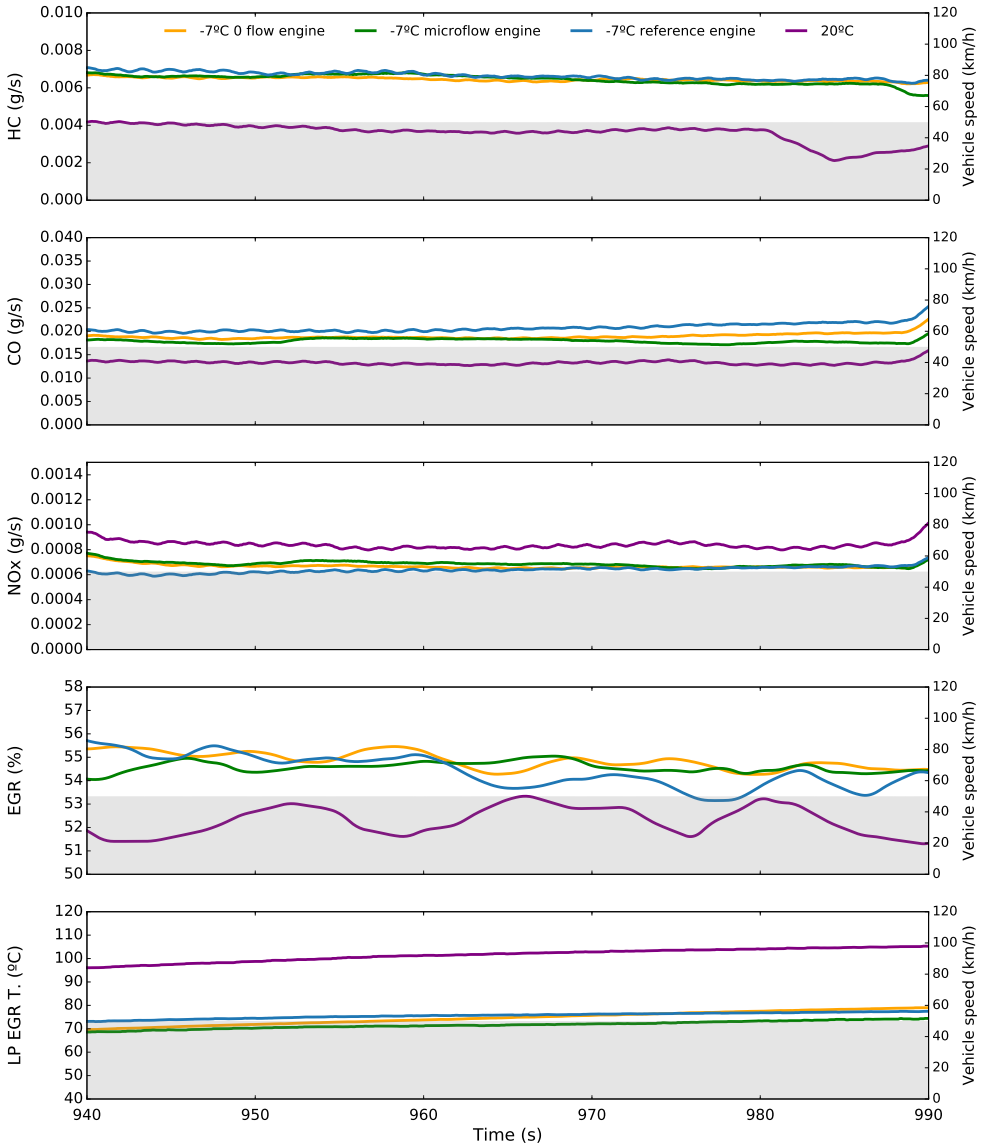

Figure 6.4: EGR, CO, HC and LP EGR temperature during a steady step of EUDC. Vehicle speed is depicted in gray area.

Comparing between thermal configurations, a statistical but slight significant difference is spotted in the 0 flow case compared to the reference. Regarding HC, emissions are lower for the first 3 UDC. In the case of CO, NOx and BTE, no statistical differences are observed between thermal management systems for all driving phases. Concerning the microflow case, non remarkable differences are observed comparing to the reference case. Negligible reductions are observed in HC at the third UDC and the EUDC. in the case of CO, a slight reduction is spotted at the EUDC. Regarding NOx and BTE, no statistical difference is obtained at any point of the NEDC. In several points, microflow ratio error bar is overlapped by the other two thermal configurations uncertainty. This overlapping makes impossible to determine any improvement or deterioration comparing to the two other thermal configurations.

6.3.1.2 WCAC coolant management

In this section the influence of two different WCAC coolant management strategies is analysed. On one hand, the reference case from Section 6.3.1.1, where WCAC coolant is recirculated for the whole test, is compared to the WCAC 0 flow strategy, where no coolant is flowing for the first 800 s. For the remaining 400 seconds of the cycle, the WCAC electrical pump is turned on for avoiding overheating during the EUDC high loads. Emission ratios and fuel consumption by driving phase for both cases are shown in Fig. 6.5

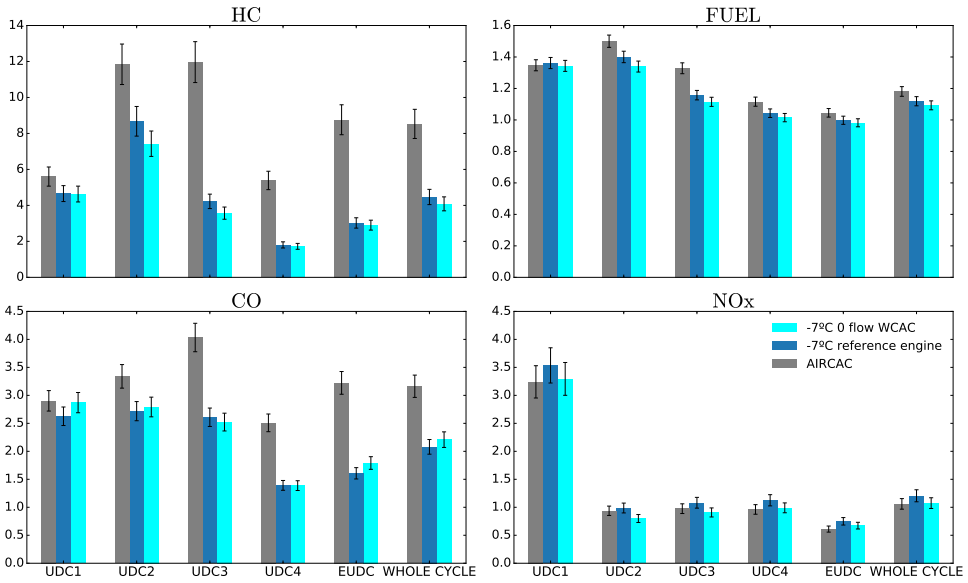

Figure 6.5: Pollutants and fuel ratio by NEDC driving phase. Different thermal management valve configurations

Regarding all emissions and fuel consumption of both thermal management systems, no difference is spotted in any driving phase. Only slight, and negligible, difference on NOx emissions at the second UDC is observed between both WCAC coolant strategies. In contrast, the low intake temperature of the AIRCAC case increases HC, CO and fuel consumption in a 100%, 43% and 8% respectively at the end of the NEDC.

6.4 Exhaust gas heat recovery

In this section, the EGHR is analysed. Firstly, in Section 6.4.1 an energy survey is carried out at the exhaust line, followed by the analysis of the EGHR efficiency, the enthalpy flows in the system and the recovered cumulated energy. In Section 6.4.2 the influence of the EGHR system on pollutant emissions is addressed. In addition, the EGHR performance is compared with the coolant thermal management systems. Finally, in Section 6.5 intake temperature evolution along the NEDC is shown for the EGHR, the coolant management systems and the most popular current automotive intercooler technology (AIRCAC).

6.4.1 Energy analysis

The energy balance at the EGHR is aimed for thermal efficiency calculation of the EGHR system. The available exhaust gas thermal energy reduces from the exhaust manifold, at the turbine inlet, to the tailpipe exhaust, at the EGHR heat exchanger outlet. Energy reduces because of twofold: Firstly, due to the heat transmission between the gas, the thermal inertia of exhaust line components and the surroundings heat losses. Secondly, owing to the output work that reduces the exhaust gas enthalpy as it happens in the turbine. Energy distribution along the exhaust line is depicted in Fig. 6.6. Energy is obtained from the sensible enthalpy between each exhaust line point

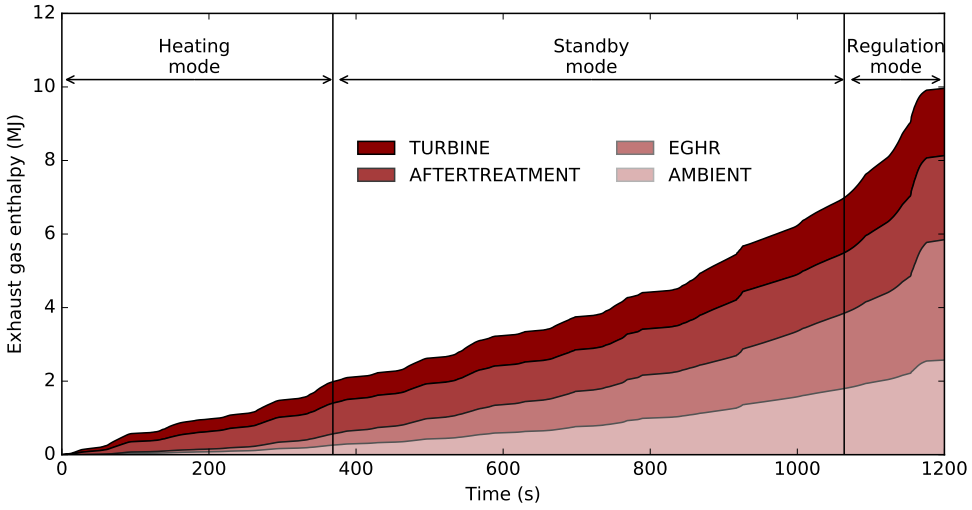

Figure 6.6: Gas sensible enthalpy along the exhaust line in the NEDC at -7 ºC. EHGR working modes are shown at the top of the figure

and the outdoors temperature. Four energy terms are depicted: turbine, aftertreatment, EGHR heat exchanger and finally the ambient energy release. The exhaust mass flow is obtained from the air mass flow, the LP EGR rate and the injected fuel mass flow. The total available sensible enthalpy rises to around 10 MJ at the end of the cycle, wich represents the 37% of the total heat of combustion (LHV was used for combustion heat release calculation as energy balance is based on sensible heat). Regarding the operation recovery modes of the EGHR, the available sensible heat recovery drops to 0.3 MJ at the end of the heating recovery mode, at 368 seconds, and to 2 MJ at

the standby ending, at 1063 seconds. As calculated energy only accounts for sensible heat, phase change heat release owing to water condensation and fusion is not addressed in Fig. 6.6. Relative energy distribution by exhaust line element is shown in Fig. 6.7. Exhaust gas enthalpy evolves in opposite

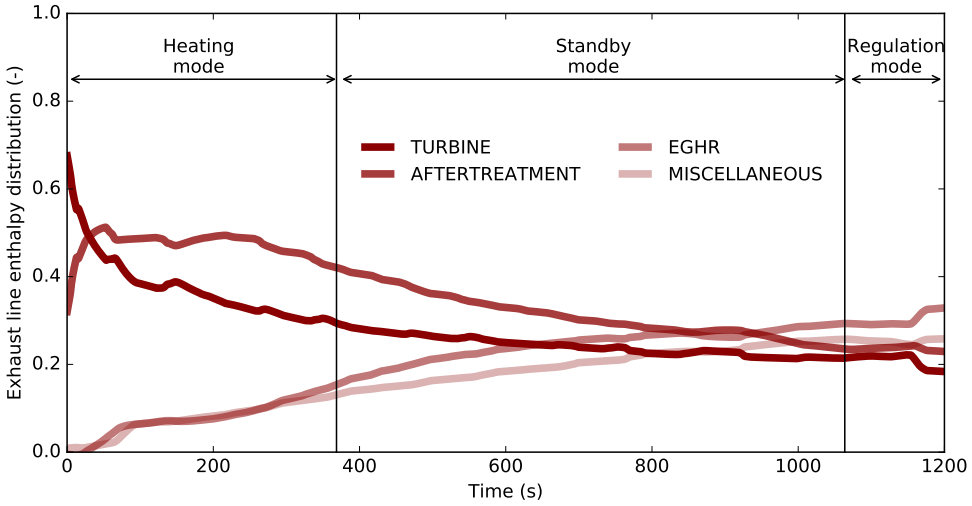

Figure 6.7: Relative exhaust gas sensible enthalpy distribution in the NEDC at -7ºC. EHGR working modes are shown a tthe top of the figure

trends: the enthalpy fraction exchanged at the turbine and aftertreatment decreases as the cycle proceeds while the enthalpy weight at the EGHR rises with time. At the end of the cycle the exhaust enthalpy variation at the EGHR heat exchanger becomes the highest, being the 33% of the total gas energy, followed by the ambient energy release at 25%, aftertreatment heat transmission at 23% and finally with the 18 % the turbine. However, regarding the key operation modes of the EGHR system, the relative energy weighs turn around. At the end of the heating mode, where exhaust energy is recovered for intake heating, the EGHR enthalpy represents the 15% of the total enthalpy. Concerning the standby operation, where exhaust energy is recovered for engine coolant heating, the EGHR enthalpy rises to 29%. Energy transfer at the EGHR heat exchanger along the NEDC is depicted in Fig. 6.8. Exhaust gas heat release calculation takes into account the latent heat of the water condensation and freezing. Exhaust gas and recovery coolant enthalpy flows are shown in the upper plot. Coloured areas in the plot highlight the differences between released and absorbed energy by the

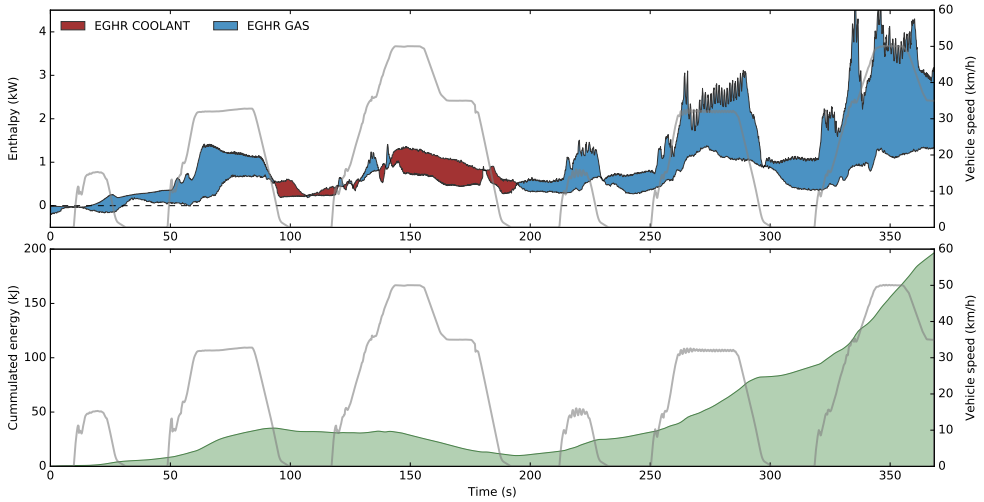

Figure 6.8: EGHR energy analysis. Upper plot: Enthalpy flow of exhaust gas and EGHR coolant. Coloured areas show the difference of gas and coolant enthalpy flow. Blue areas show higher enthalpy at the exhaust gas. Red areas spot instants where the coolant enthalpy increase is higher than the exhaust gas reduction. Lower plot: Cumulated energy difference between the gas and the EGHR coolant

gas and the coolant respectively. Blue areas in Fig. 6.8 spot where exhaust heat release is higher than coolant absorption. In contrast, red areas show the instants when coolant enthalpy increase is higher than gas enthalpy reduction. This apparently energy unbalance is explained by the heat exchanger thermal inertia. When decelerations and idles are performed exhaust gas temperature and flow reduce. Since the mass bulk temperature remains higher during these operation points, the heat exchanger mass becomes a heat source increasing the coolant temperature. These instants of low exhaust energy are mainly driven by HP EGR enabling that reduces the exhaust mass flow between the 100 to almost 200 seconds of the cycle. Once HP is switched to LP EGR, exhaust enthalpy increases. In addition to the increase of exhaust mass flow, as time proceeds, exhaust gas enthalpy at the EGHR rises, as was shown in Fig. 6.7. At the lower plot of Fig. 6.8 the difference of cumulated energy between the exhaust gas release and the coolant absorption shows an increasing evolution with time. Energy difference reduces for the 100 to 200 seconds because of the HP EGR enabling. Beyond this point, energy difference increase speeds up until reaching the maximum value of 200 kJ at the end of the heating recovery mode. Exhaust gas enthalpy flow at the EGHR exchanger

has been calculated by considering two different energy terms: sensible and latent enthalpy. Sensible enthalpy is obtained directly from the thermocouples measurement upstream and downstream the heat exchanger. Latent heat is calculated by measuring the water vapour concentration at the inlet and outlet of the heat exchanger. The concentration difference is caused by water condensation. In addition to the vapour to liquid phase change, fusion latent enthalpy is also considered when coolant and gas temperature remains subzero at the beginning of the cycle. The evolution in time of those heat sources is depicted in Fig. 6.9 as relative energy terms. The analysis is bounded to the heat recovery mode running time span. In the beginning, energy terms aren't

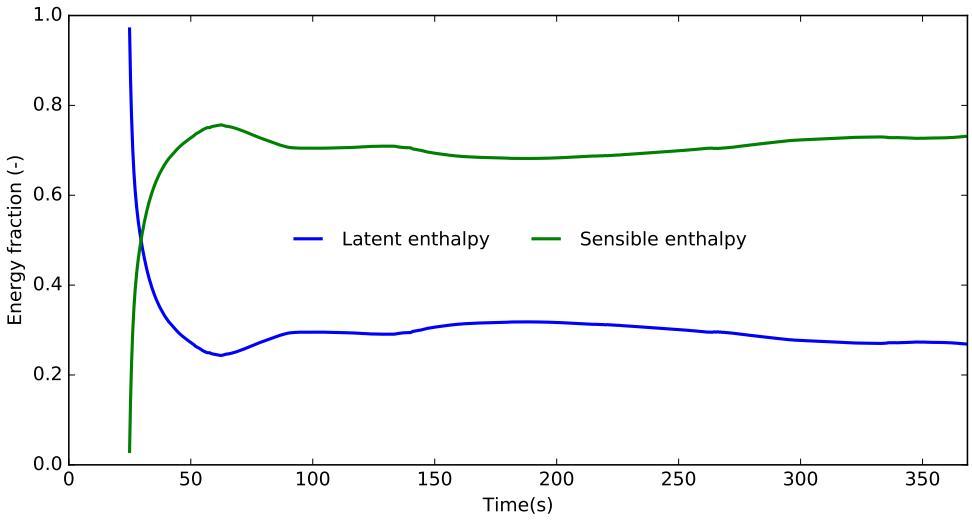

Figure 6.9: Relative distribution of exhaust gas heat sources. Only positive heat transmission points are depicted

shown as no heat is recovered from the exhaust. Since 25 seconds heat recovery comes up. At the first instants of heat recovery sensible enthalpy plays a minor role in the transmitted heat in contrast to the latent recovered heat. Between 25 and 50 s. energy sources weight is turned around. At 50 seconds, sensible term reaches the weigh of 75% and water condensation reduces to 25%. Beyond this point, energy distribution remains without significant variations for the rest of the heat recovery time span.

In Fig. 6.10 thermal efficiency, calculated as the ratio between recovered and released cumulated energy, is depicted. The existence of thermal inertia terms on the energy balance, working as sinks and sources of heat, make no possible

to analyse the efficiency by instantaneous enthalpy flows. Regarding Fig. 6.10 two efficiency lines are shown. The higher corresponds to the exhaust heat exchanger device efficiency calculated by the ratio between the gas and the coolant enthalpy. The lower line represents the global thermal efficiency of the EGHR system that comes from the ratio between the intake gas and the exhaust gas enthalpy. Efficiency values are only plotted for those

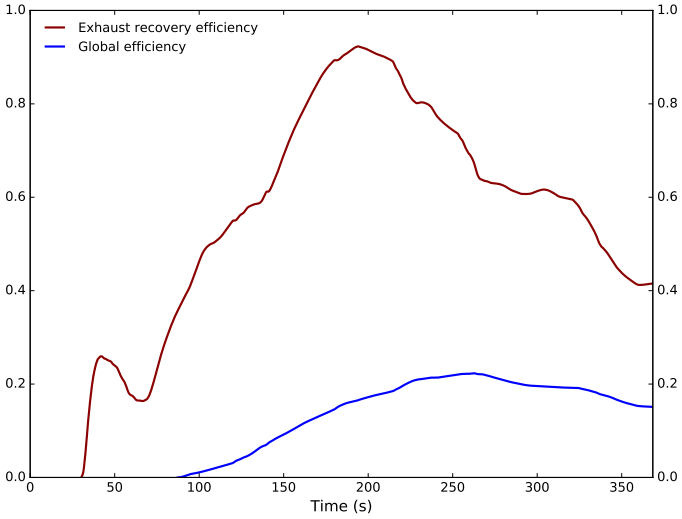

Figure 6.10: EGHR thermal efficiency. Red line: exhaust recovery efficiency. Blue line: global EGHR efficiency

points where heat is recovered from the exhaust. In case of negative enthalpy variation, i.e. EGHR heat exchanger coolant temperature reduction or intake gas enthalpy decrease, efficiency is not calculated. Regarding both lines, significant differences between the exhaust and global recovery are observed. The poor global efficiency is caused by the low heat transmission at the intake owing to the low temperature difference between coolant and gas flows, the high heat transmission losses driven by the large WCAC external area and the large intake heat exchanger size that entails a major role of the thermal inertia. Between the 50 to 200 seconds the exhaust heat recovery efficiency increases because of the heat exchanger thermal inertia as it's not included in the balance as an energy source. Beyond the 200 seconds, efficiency begins to reduce until reaching the 55% at the end of the heat recovery mode. Concerning the global efficiency, these increase and reductions of efficiency evolve in a slower way. At the end of the recovery mode the global thermal efficiency is around 15 %.

6.4.2 Effect on pollutant emissions and fuel consumption

In this section the EGHR engine out pollutant emissions are analysed and compared with the coolant 0 flow thermal management and the WCAC 0 flow strategy. The WCAC and engine coolant 0 flow represent the most simple thermal management application for warming-up speed up in comparison with the more complex EGHR layout that comprises an additional WCAC coolant control system aimed to intake temperature increase. Like Section 6.3.1, pollutant emissions and fuel consumption are analysed by driving phase in Fig. 6.11. Ratios are obtained by speed driving phase according to the Eq. (4.3). Like in Section 6.3, the AIRCAC case has been added to compare the thermal management systems with the most popular current automotive technology.
Pollutants as well as fuel consumption of the three thermal management

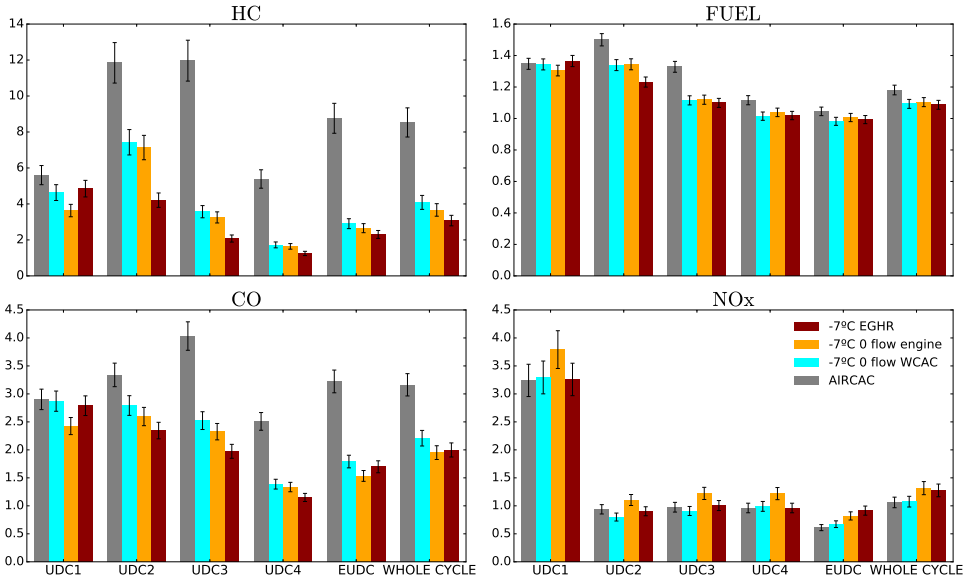

Figure 6.11: Pollutants ratio by NEDC driving phase

systems follow the same general trend: as the cycle proceeds, ratios reduce. At the first part of the cycle, all ratios are higher than one, pointing the notable negative effect of low ambient temperature cold start on emissions and engine efficiency. Regarding the EGHR system, HC is the pollutant that more increases being the emissions, at the low speed phase, 4.85 times the amount

emitted at 20 ºC. As the cycle proceeds, the emissions reduce reaching the minimal value of 1.5 at the last UDC. In the case of CO, emissions ratio began at almost 3 and reduces progressively until the last UDC where the minimal ratio is reached at around 1.15. Regarding NOx, the observed initial ratio is higher than 3 because of the EGR disabling at cold ambient temperatures. Once the EGR systems are running, NOx emissions turn around being the emissions slight higher at 20 ºC. NOx emission ratio performs in a quite steady manner in the range of 0.9 to 1 for the rest of the cycle. Concerning fuel consumption, a general monotone reduction tendency is spotted as the cycle proceeds. The fuel ratios evolves from the maximum of 1.3, at the first UDC, to the minimum value reached at the last UDC and EUDC of 1. Regarding the evolution of ratios by driving phase is remarkable the variation of HC and CO reduction tendency when EUDC is performed. Under relatively high engine loads, the aforementioned EGR rates differences in Section 6.3 between the cold and the warm cycles drives into quite different combustion performance. EGR rate increase at low ambient temperature, causes the rise of HC up to almost 2.3 times. The effect is less remarkable in case of CO where the increase is limited to 1.7. In contrast, as EGR rates are higher at low temperatures the NOx ratio goes down.

Comparing the EGHR system to the other two different thermal systems, the effect of the EGHR is more notable than the 0 flow layout. Reading the cycle step by step, differences at the first UDC between the EGHR and the engine coolant 0 flow case are spotted with a reduction of 25% in HC and 13% in CO at the engine coolant 0 flow. In spite of there is significant statistical difference the low variation between ratios along with the two 2 sigma criteria used in this work makes unprovable the existence of a difference between cases. The low recovered energy by the EGHR system along with the random and negative impact of engine start emissions hide any improvement in the first UDC. On the other hand, significant better performance is spotted by means of the EGHR between the second and the last UDC. The greatest difference comes up at the second and third UDC with the reduction of hydrocarbon emissions in 46% and 33% respectively. Concerning CO, non significant reductions are observed in the EGHR with a reduction of 13% and 15% in the second and third UDC. In the case of fuel consumption, EGHR improvement is limited to the second UDC, where the thermal efficiency improvement because of the heat recovery rises to the 8%. Finally, concerning NOx emissions, no statistical differences are spotted between all low temperature cases for the first and second UDC. For the rest of driving phases slight and almost negligible reduction in the EGHR comparing to the coolant engine 0 flow system is spotted. In spite of the low differences in

NOx between both thermal management layouts, an increase tendency in the engine coolant thermal management case is spotted. No explanation could be found in NOx variation between coolant thermal management and the rest of cases. All test related variable, such as air mass flow, injection law, EGR, exhaust manifold pressure, were under control performing the same values. Knowing the cause of the slight increase in the coolant management system requires a deeper statistical survey by including higher amount of NOx measurements and a more stringent confidence interval. The purpose of the proposed thermal management systems is directed to CO, HC and fuel consumption enhancement. The effect on NOx emissions is clearly governed by the EGR enabling. Finding the cause of differences on NOx emissions between the thermal management systems is a task to perform beyond the aim of this work focussed in carbon emissions.
Concerning both 0 flow thermal management systems. The same differences regarded for the EGHR at the first UDC for HC and CO are spotted too. Regarding fuel consumption, no differences are spotted between cases for all driving phases. In the case of HC, since the second UDC, no statistical differences are observed between both systems. Regarding CO, in addition to the first UDC slight reduction of emissions in the WCAC 0 flow are measured at the EUDC. Finally, in the case of NOx, slight reductions are observed by enabling the WCAC 0 flow since the second until the fourth UDC.
Comparing the EGHR system with the AIRCAC technology, remarkable reductions are obtained in HC and CO by the EGHR system. HC reduction comes from 64% up to 82% for the second and third UDC. CO reduction goes from 29% to 54% at the second and fourth UDC. Regarding fuel, reductions are spotted since second until the fourth UDC being the highest reduction around 18%. Finally in the case of NOx, no differences are spotted for all UDC driving phases. When EUDC is performed a 33% of increase is spotted by performing the EGHR system owing to the higher intake EGHR temperature.

6.5 Effect of thermal management in intake air temperature

Intake temperature of the different tests performed in this chapter is depicted in Fig. 6.12. As all engine coolant tests lay on the same WCAC configuration, only the temperature of the 0 flow engine coolant case is depicted. The rest of cases show the same intake temperature evolution. In addition to the low ambient temperature cases, the intake air temperature evolution of the warm case, 20 ^{o}C, is plotted too. In the 20 ^{o}C case, intake

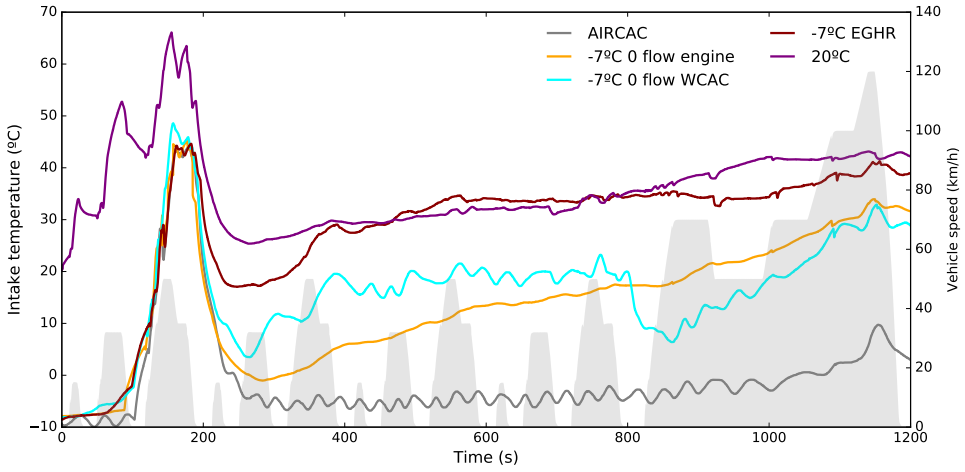

Figure 6.12: Intake temperature. Vehicle speed depicted as a surface in gray.

air temperature increases quickly since the beginning of the cycle because of the HP EGR enabling. EGR systems are not activated until engine coolant temperature reaches -4 ºC that's why intake temperature remains low in the -7 ºC cases. The effect of HP EGR enabling on the intake temperature is noticeable between the 100 s. to 200 s. when HP is shifted to LP EGR. The intake temperature increases in all cases when HP EGR is enabled, reaching 45ºC in the cold ambient case and 65 ºC in the warm case. Regarding the -7 ºC tests, for the first instants, intake temperature differences between the 0 flow and the EGHR case are negligible. Once the HP EGR is enabled, at 80 seconds, a rush, step like, temperature increase is spotted. When HP loop is switched to LP EGR the intake temperature at the engine coolant and WCAC 0 flow cases drops suddenly to 0 ºC and 3ºC respectively. In contrast, the intake temperature reduction in the EGHR case is not so notable because of the intake heating by the recovered exhaust energy. Air temperature remains at 18 ºC after disabling the HP EGR. Beyond this point the EGHR temperature control targets the intake to 35 ºC by releasing the recovered heat to the engine coolant and the intake air. At almost 400 s. the intake temperature target is reached and the EGHR control moves to the stand by position where recovered heat is delivered to the engine coolant. Regarding the engine coolant 0 flow case, since LP EGR is enabled, intake air temperature increases as the NEDC proceeds. At 900 seconds temperature reaches 20 ºC. Due to the higher engine loads performed in the last NEDC driving phase, compressor exhaust temperature

rises leading to increase the intake temperature that eventually reaches 30 ºC at the end of the driving cycle. Concerning the WCAC 0 flow, intake temperature rise speeds up in comparison to the WCAC recirculated flow of the engine coolant case. Owing to the lower heat transfer coefficient, intake air temperature reaches 20ºC at 380 seconds. Nevertheless, when WCAC flow is turned on at 800 seconds a sudden reduction of intake temperature occurs going down to 5ºC. As the EUDC evolves, intake temperature increases until reaching almost 30ºC meeting the same value as the WCAC recirculated flow strategy.
Comparing the EGHR case to the warm test, for roughly the first 400 seconds intake temperature is always higher in the warm case. In the case of EGHR system, the air temperature increases as thermal energy is recovered from the exhaust gas. At almost 400 seconds, -7 ºC EGHR case reaches the intake air temperature of the 20 ºC case. Beyond this instant, intake air temperature evolve similar between both cases. On the other hand, in the AIRCAC test, intake temperature is kept at -7 ºC with the exception of the HP EGR enabling time span where temperature increases to 45 ºC and the last part of the EUDC where the temperature is risen to 8ºC.

6.6 Conclusions

The effect of three different thermal management systems on pollutant emissions at low temperatures has been addressed in this section. Firstly, a set of different configurations of engine coolant flow have been tested keeping the same 0 flow WCAC coolant strategy based on flow recirculation. Secondly, a WCAC 0 flow system has been compared to the engine coolant management system. Finally, an EGHR system connected to the WCAC has been proposed for intake temperature increase.
Comparing all thermal systems for pollutant reduction at low ambient temperatures, the effect of the EGHR is more notable than the other layouts with a 46% and 33% reduction of hydrocarbons emissions during the second and third UDC. In addition, better engine efficiency was spotted at the second UDC with a reduction of 8% in fuel consumption. Regarding CO and NOx no significant differences were observed between both systems. Concerning NOx, the effect of the thermal management is negligible in comparison to the EGR enabling. When EGR is running NOx emissions reduce 3.5 times in average for all low temperature cases.
Regarding the AIRCAC system, the penalties of running at low ambient temperature are noticeable mainly in HC and CO. HC emissions may be

up to 12 times higher the emission at 20 ºC. Regarding the whole NEDC, HC and CO emissions are roughly 57% and 35%, in average, lower by using any thermal management system compared to the AIRCAC. In the case of fuel consumption, a 7% of reduction is spotted. Concerning NOx, negligible increases are observed at the engine coolant 0 flow and the EGHR respectively. Looking at the NEDC by driving phase the highest differences between the thermal management and the AIRCAC are placed at the third UDC where HC emissions may be up to 3.35 and 5.57 times lower by enabling the coolant thermal management systems and the EGHR respectively.

Bibliography

[62] A. J. Torregrosa, P. Olmeda, J. Martín, and B. Degraeuwe. "Experiments on the influence of inlet charge and coolant temperature on performance and emissions of a DI Diesel engine". *Experimental Thermal and Fluid Science* 30.7 (2006), pp. 633–641.

[63] A. J. Torregrosa, A. Broatch, P. Olmeda, and C. Romero. "Assessment of the influence of different cooling system configurations on engine warm-up, emissions and fuel consumption". *International Journal of Automotive Technology* 9.4 (2008), pp. 447–458.

[70] J. Ko, D. Jin, W. Jang, C.-L. Myung, S. Kwon, and S. Park. "Comparative investigation of NOx emission characteristics from a Euro 6-compliant diesel passenger car over the NEDC and WLTC at various ambient temperatures". *Applied Energy* 187 (2017), pp. 652–662.

[101] C. A. Romero, A. Torregrosa, P. Olmeda, and J. Martin. "Energy Balance During the Warm-Up of a Diesel Engine". *SAE Technical Paper* 2014-01-06 (2014), pp. 2–11.

[102] L. Jarrier, J. C. Champoussin, E. C. D. Lyon, R. Yu, and D. R. Renault. "Warm-Up of a D . I . Diesel Engine : Experiment and Modeling". *SAE Technical Paper* 2000-01-02 (2000).

[103] M. Gumus. "Reducing cold-start emission from internal combustion engines by means of thermal energy storage system". *Applied Thermal Engineering* 29.4 (2009), pp. 652–660.

[104] A. Broatch, J. M. Luján, J. R. Serrano, and B. Pla. "A procedure to reduce pollutant gases from Diesel combustion during European MVEG-A cycle by using electrical intake air-heaters". *Fuel* 87.12 (2008), pp. 2760–2778.

[105] P. Kauranen, T. Elonen, L. Wikström, J. Heikkinen, and J. Laurikko. "Temperature optimisation of a diesel engine using exhaust gas heat recovery and thermal energy storage (diesel engine with thermal energy storage)". *Applied Thermal Engineering* 30.6-7 (2010), pp. 631–638.

[106] P. Diehl, F. Haubner, S. Klopstein, and F. Koch. "Exhaust heat recovery system for modern cars". *Sae Transactions* 110.3 (2001), pp. 988–998.

[107] N. S. Ap and N. C. Golm. "Insulated Expansion Tank (IET) and Thermal Storage for Engine Cold Start". In: *SAE Technical Paper*. SAE Technical Paper., 1995.

[108] S. Arrhenius. "Über die Dissociationswärme und den Einfluss der Temperatur auf den Dissociationsgrad der Elektrolyte". *Zeitschrift für Physikalische Chemie* 4.1 (1889).

[109] G. De Nicolao, R. Scattolini, and C. Siviero. "Modelling the volumetric efficiency of ic engines: Parametric, non-parametric and neural techniques". *Control Engineering Practice* 4.10 (1996), pp. 1405–1415.

[110] B. Pla Moreno. "Análisis del proceso de la recirculación de los gases de escape de baja presión en motores Diesel sobrealimentados." PhD thesis. 2009.

Chapter 7

Conclusions and future work

Contents

7.1 Introduction

In this chapter main accomplished goals are summarized. In addition, work in progress is described for future approaches of the low ambient temperature analysis.
This work doesn't intend to address all issues concerning low ambient temperature emissions. A broad study has been carried out by analysing the influence of low ambient temperatures on the pollutant formation and the DOC performance. Two different thermal management approaches have been proposed for engine performance enhancement by engine and WCAC coolant management and by intake gas heating with the installation of an EGHR system.

7.2 Conclusions

As was described in Chapter 4, pollutant emissions in thermal engines increase when running at low ambient temperatures. Expected more stringent emissions regulations boost searching new engine technology for pollutant reduction. According to the NEDC and WTLC testing procedures a general trend of emissions increases is spotted by lowering the temperature from 20 ºC to -7 ºC. In the following lines the main conclusions of comparing NEDC to WLTC are presented:

- The negative effect of running at low temperature is more significant in NEDC than in WLTC owing to the higher engine loads performed in the WLTC. While NEDC shows significant increases of NOx, CO, HC and also in fuel consumption. WLTC detriment is limited to HC and NOx. Fuel consumption is not significantly affected.

- Regarding CO, one point to highlight is the reduction in WLTC. The reason behind this enhancement is the role that air management plays on carbon monoxide emissions. Unlike unburned hydrocarbons, CO formation is high sensitive to oxygen concentration. As cold conditions entails higher air mass flow, in-cylinder oxygen concentration is higher at low temperatures.

- Higher air mass flow rate is caused mainly by EGR enabling differences between the cold and warm test. On one hand, HP EGR is activated since the beginning in case of running at 20 ºC. In case of low ambient temperature, HP EGR is not enabled until the half and almost the end of

the driving cycle for the WLTC and NEDC respectively. On the other hand, EGR is enabled at low temperatures by running the HP loop. In case of warm testing, LP EGR is enabled driving to higher EGR rates. An additional, and minor, cause of air mass flow increase at low temperature is the higher air density at -7 ^{o}C than at 20 ^{o}C. Disabling or lowering the EGR rate in cold conditions boost the reduction of CO but, in contrast, rise NOx emissions significantly.

On the other hand, tail pipe emissions were analysed in Chapter 5 by the ambient temperature influence on DOC efficiency.

- DOC performance detriment was spotted in both NEDC and WLTC. Catalyst temperature evolved similar at both ambient temperatures. The low DOC bulk mass along with the low heat transmission losses, driven by natural convection, and the close evolution of both exhaust gas temperatures makes the warming-up process evolve in quite similar manner.
- DOC efficiency differences are caused indirectly by ambient temperature reduction. On one hand, lowering ambient temperature leads to EGR disable that entails a reduction of the dwell time.
- High pollutant concentrations of CO and HC may drive to a competitive oxidation leading to a reduction of catalytic efficiency.
- The higher air mass flow rate at cold ambient conditions leads to increase the oxygen concentration at the exhaust manifold and eventually boosts the DOC oxidation rate. The final balance of all theses three terms is a higher and negative effect on DOC efficiency by increasing the dwell time and pollutant concentration against the kinetics enhancement by increasing the oxygen concentration.

Regarding the double negative effect of low ambient temperature, by increasing engine out emissions and decreasing DOC efficiency, is necessary to find new solutions for speeding up the engine warm-up. Two different thermal management strategies were proposed:

- The first approach was focussed on the engine and WCAC coolant temperature management for avoiding overcooling at low temperatures.
- The second layout was aimed to intake air heating for avoiding intake overcooling by recovering heat from the exhaust tailpipe by means of the EGHR system.

The intake air heating based on the EGHR system comes up as the best solution with notable reductions of HC, followed by slight reduction of CO and fuel consumption. The engine performance improvement by using the EGHR is significant for the first 600 s. On the other hand, both 0 flow, engine and WCAC, coolant shown similar enhancement in pollutant reduction and fuel savings.

7.3 Future work

While conducting this thesis some issues have been left because of lack of time or resources. The following suggestions could become the basis of future studies in the low ambient temperatures field for increasing the knowledge on pollutant formation and aftertreatment performance. As emissions regulation will become more stringent, the importance of low temperature influence on engines performance will play a major role. Future scenarios will boost the development of new technologies beyond the systems analysed in this work for reducing warming-up time and recovering engine waste heat not only form high temperature exhaust gases but from low temperature heat sources too. Main related research topics that could be addressed in the near term future comprises:

- Additional intake air heating systems such as electrical heaters may be interesting to compare with the proposed EGHR. Electrical heaters would allow to release higher thermal power to the intake air but by causing a possible penalty in fuel consumption.

- Direct EGHR by means of a gas-gas heat exchanger. As was depicted in Fig. 6.10 low global efficiency is observed when analysing the whole energy balance from the exhaust gas to the intake enthalpy. The reason behind this low efficiency is the high difference of the heat capacities between the exhaust gas and the coolant fluid. A 1^{o}C drop of exhaust gases along the EGHR heat exchange may increase the coolant temperature in 0.23 ^{o}C (calculation based on exhaust gas flow of 200 kg/h and coolant flow of 300 kg/h). By means of a gas-gas heat exchanger, in ideal conditions of heat transfer, the increase in the intake air may be as much as the exhaust gas drop. The gas-gas heat exchange shows the advantage of having high temperature differences between the exhaust and the intake flow, boosting the heat exchange between both streams. Nevertheless, the development of such heat exchanger may

entail significant constructive complexities as the exhaust and intake lines should be placed much closer one each other.

Bibliography

[1] C. R. Ferguson and A. T. Kirkpatrick. *Internal combustion engines: applied thermosciences*. John Wiley & Sons, 2015.

[2] A. Altshuler, M. Anderson, D. Roos, J. P. Womack, and D. Jones. *The future of the automobile: the report of MIT's international automobile program*. MIT press, 1986.

[3] F. Birol et al. "World energy outlook 2010". *International Energy Agency* 1.3 (2010).

[4] T. J. Crowley. "Causes of climate change over the past 1000 years". *Science* 289.5477 (2000), pp. 270–277.

[5] J. Cook, N. Oreskes, P. T. Doran, W. R. Anderegg, B. Verheggen, E. W. Maibach, J. S. Carlton, S. Lewandowsky, A. G. Skuce, S. A. Green, et al. "Consensus on consensus: a synthesis of consensus estimates on human-caused global warming". *Environmental Research Letters* 11.4 (2016), p. 048002.

[6] S. Manabe and R. T. Wetherald. "The effects of doubling the CO2 concentration on the climate of a general circulation model". *Journal of the Atmospheric Sciences* 32.1 (1975), pp. 3–15.

[7] S. H. Schneider. "The Greenhouse Effect: Science and Policy". *Science* 243.4892 (1989), pp. 771–781.

[8] R. Dickerson, S Kondragunta, G Stenchikov, K. Civerolo, B. Doddridge, and B. Holben. "The impact of aerosols on solar ultraviolet radiation and photochemical smog". *Science* 278.5339 (1997), pp. 827–830.

[9] R. Atkinson and A. C. Lloyd. "Evaluation of kinetic and mechanistic data for modeling of photochemical smog". *Journal of physical and chemical reference data* 13.2 (1984), pp. 315–444.

[10] C. B. Field, V. R. Barros, D. Dokken, K. Mach, M. Mastrandrea, T. Bilir, M Chatterjee, K. Ebi, Y. Estrada, R. Genova, et al. *IPCC, 2014: Climate Change 2014: Impacts, Adaptation, and Vulnerability. Part A: Global and Sectoral Aspects. Contribution of Working Group II to the Fifth Assessment Report of the Intergovernmental Panel on Climate Change*. 2014.

[11] E. W. Team et al. "ESRL Global Monitoring Division-Global Greenhouse Gas Reference Network" (2005).

[12] P. Tans and R. Keeling. *ESRL Global Monitoring Division-Global Greenhouse Gas Reference Network*. `www.esrl.noaa.gov/gmd/ccgg/trends/` and `scrippsco2.ucsd.edu/`. 2018.

[13] T. Laepple, S. Jewson, and K. Coughlin. "Interannual temperature predictions using the CMIP3 multi-model ensemble mean". *Geophysical Research Letters* 35.10 (2008).

[14] A. McEvoy, T. Markvart, L. Castañer, T Markvart, and L. Castaner. *Practical handbook of photovoltaics: fundamentals and applications*. Elsevier, 2003.

[15] J. Hansen, R. Ruedy, M. Sato, and K. Lo. "Global surface temperature change". *Reviews of Geophysics* 48.4 (2010).

[16] *GISS Surface Temperature Analysis (GISTEMP)*. 2018. URL: `https://data.giss.nasa.gov/gistemp/`.

[17] I. Union. *Communication from the Commission to the European Parliament, the Council, the European Economic and Social Committee and the Committee of the Regions*. Brussels, 2016.

[18] R. Hannappel. "The impact of global warming on the automotive industry". In: *AIP Conference Proceedings*. Vol. 1871. 1. AIP Publishing LLC, 2017, p. 060001.

[19] Council of European Union. *Proposal for a regulation of the european parlamient and of the council setting emission performance standards for new passenger cars and for new light commercial vehicles as part of the Union's integrated approach to reduce CO2 emissions from light-duty vehicles and amending Regulation (EC) No 715/2007*. 2017.

[20] H. Vikström, S. Davidsson, and M. Höök. "Lithium availability and future production outlooks". *Applied Energy* 110 (2013), pp. 252 –266.

[21] O. Egbue and S. Long. "Barriers to widespread adoption of electric vehicles: An analysis of consumer attitudes and perceptions". *Energy Policy* 48 (2012), pp. 717–729.

[22] D. Mage, G. Ozolins, P. Peterson, A. Webster, R. Orthofer, V. Vandeweerd, and M. Gwynne. "Urban air pollution in megacities of the world". *Atmospheric Environment* 30.5 (1996), pp. 681–686.

[23] H. Mayer. "Air pollution in cities". *Atmospheric Environment* 33.24-25 (1999), pp. 4029–4037.

[24] OECD. *The Economic Consequences of Outdoor Air Pollution*. OECD Publishing, Paris, 2016.

[25] M. J. Molina and L. T. Molina. "Journal of the Air and Waste Management Association Megacities and Atmospheric Pollution Megacities and Atmospheric Pollution". *Journal of the Air and Waste Management Association* 546 (2004), pp. 644–680.

[26] B. Gurjar, A. Jain, A. Sharma, A. Agarwal, P. Gupta, A. Nagpure, and J. Lelieveld. "Human health risks in megacities due to air pollution". *Atmospheric Environment* 44.36 (2010), pp. 4606–4613.

[27] WHO. *Health effects of transport related air pollution*. Ed. by B. K.-D. Michal Krzyzanowski and J. Schneider. WHO Regional Office for Europe, 2005.

[28] I. A. for Research on Cancer et al. "IARC: Diesel engine exhaust carcinogenic". *Press release* 213 (2012).

[29] J. G. Hemmingsen, P. Møller, K. Jantzen, B. A. Jönsson, M. Albin, A. Wierzbicka, A. Gudmundsson, S. Loft, and J. Rissler. "Controlled exposure to diesel exhaust and traffic noise–Effects on oxidative stress and activation in mononuclear blood cells". *Mutation Research/Fundamental and Molecular Mechanisms of Mutagenesis* 775 (2015), pp. 66–71.

[30] D. T. Silverman, C. M. Samanic, J. H. Lubin, A. E. Blair, P. A. Stewart, R. Vermeulen, J. B. Coble, N. Rothman, P. L. Schleiff, W. D. Travis, et al. "The diesel exhaust in miners study: a nested case–control study of lung cancer and diesel exhaust". *Journal of the National Cancer Institute* 104.11 (2012), pp. 855–868.

[31] S. Steiner, C. Bisig, A. Petri-Fink, and B. Rothen-Rutishauser. "Diesel exhaust: current knowledge of adverse effects and underlying cellular mechanisms." *Archives of toxicology* 90.7 (2016), pp. 1541–53.

[32] J. G. Hemmingsen, P. Møller, J. K. Nøjgaard, M. Roursgaard, and S. Loft. "Oxidative stress, genotoxicity, and vascular cell adhesion molecule expression in cells exposed to particulate matter from combustion of conventional diesel and methyl ester biodiesel blends". *Environmental science & technology* 45.19 (2011), pp. 8545–8551.

[33] T. R. Dallmann and R. A. Harley. "Evaluation of mobile source emission trends in the United States". *Journal of Geophysical Research: Atmospheres* 115.D14 (2010).

[34] K. M. Nichols, L. M. Thompson, and H. L. Empie Jr. "A review of NOx formation mechanisms in recovery furnaces" (1991).

[35] G. A. LAVOIE, J. B. HEYWOOD, and J. C. KECK. "Experimental and Theoretical Study of Nitric Oxide Formation in Internal Combustion Engines". *Combustion Science and Technology* 1.4 (1970), pp. 313–326.

[36] C. Fenimore. "Formation of nitric oxide in premixed hydrocarbon flames". In: *Symposium (International) on Combustion*. Vol. 13. 1. Elsevier. 1971, pp. 373–380.

[37] F. Payri and J. María. *Motores de combustión interna alternativos*. 2011.

[38] A. Abdel-Rahman. "On the emissions from internal-combustion engines: a review". *International Journal of Energy Research* 22.6 (1998), pp. 483–513.

[39] M. E. R. Perea. "Assessment of fuel consumption reduction strategies on a gasoline turbocharged direct injection engine with a cooled EGR system". PhD thesis. 2016.

[40] *Citizens to Preserve Overton Park, Inc. v. Volpe*. 1971.

[41] A. Faiz, C. S. Weaver, and M. P. Walsh. *Air pollution from motor vehicles: standards and technologies for controlling emissions*. World Bank Publications, 1996.

[42] T. J. BARLOW, S Latham, I. McCrae, and P. Boulter. "A reference book of driving cycles for use in the measurement of road vehicle emissions". *TRL Published Project Report* (2009).

[43] M Nesbit, M Fergusson, A Colsa, J Ohlendorf, C Hayes, K Paquel, and J. Schweitzer. "Comparative study on the differences between the EU and US legislation on emissions in the automotive sector". *Policy Department A: Economic and Scientific Policy, European Union* (2016).

[44] E. Directive. "90/C81/01,Emission Test Cycles for the Certification of light duty vehicles in Europe, EEC Emission Cycles". *EEC Emission Cycles, 1999* (1999).

[45] E. Regulation. "No 595/2009 of the European Parliament and of The Council of 18 June 2009 on type-approval of motor vehicles and engines with respect to emissions from heavy duty vehicles (Euro VI) and on access to vehicle repair and maintenance information and amending Regulation (EC) No 715/2007 and Directive 2007/46/EC and repealing Directives 80/1269". *EEC* 55 (2005).

[46] "Commission Delegated Regulation (EU) 2017/1502 of 2 June 2017 amending Annexes I and II to Regulation (EC) No 443/2009 of the European Parliament and of the Council for the purpose of adapting them to the change in the regulatory test procedure for the measurement of CO2 from light duty vehicles". *Official Journal of the European Union* L 221 (26 August 2017), pp. 4–10.

[47] P. Flynn. *Diesels-Promises & Issues.* Tech. rep. Cummins Engine Company (US), 2000.

[48] J. M. Luján, H. Climent, B. Pla, M. E. Rivas-Perea, N.-Y. François, J. Borges-Alejo, and Z. Soukeur. "Exhaust gas recirculation dispersion analysis using in-cylinder pressure measurements in automotive diesel engines". *Applied Thermal Engineering* 89 (2015), pp. 459–468.

[49] J. M. Luján, H. Climent, V. Dolz, A. Moratal, J. Borges-Alejo, and Z. Soukeur. "Potential of exhaust heat recovery for intake charge heating in a diesel engine transient operation at cold conditions". *Applied Thermal Engineering* 105 (2016), pp. 501–508.

[50] M. Adachi and H. Nakamura. *Engine Emissions Measurement Handbook: HORIBA Automotive Test Systems.* SAE International, 2014.

[51] A Maiboom, X Tauzia, and J.-F. Hétet. "Influence of high rates of supplemental cooled EGR on NOx and PM emissions of an automotive HSDI diesel engine using an LP EGR loop". *International Journal of Energy Research* 32.15 (2008), pp. 1383–1398.

[52] K. Narusawa, M. Odaka, N. Koike, Y. Tsukamoto, and K. Yoshida. "An EGR control method for heavy-duty diesel engines under transient operations". *SAE transactions* (1990), pp. 991–1004.

[53] D. W. Dickey, T. W. Ryan, and A. C. Matheaus. *NOx control in heavy-duty diesel engines-what is the limit?* Tech. rep. SAE Technical Paper, 1998.

[54] F. P. González and J. M. D. Fernández. *Motores de combustión interna alternativos.* Editorial Universitat Politècnica de València, 2011.

[55] B. N. Taylor and C. E. Kuyatt. *Guidelines for evaluating and expressing the uncertainty of NIST measurement results.* Citeseer, 1994.

[56] B. E. Flores. "A pragmatic view of accuracy measurement in forecasting". *Omega* 14.2 (1986), pp. 93–98.

[57] K. Robinson, S. Ye, Y. Yap, and S. T. Kolaczkowski. "Application of a methodology to assess the performance of a full-scale diesel oxidation catalyst during cold and hot start NEDC drive cycles". *Chemical Engineering Research and Design* 91.7 (2013), pp. 1292–1306.

[58] I. P. Kandylas, A. M. Stamatelos, and S. G. Dimitriadis. "Statistical uncertainty in automotive emissions testing". *Proceedings of the Institution of Mechanical Engineers Part D-Journal of Automobile Engineering* 213.D5 (1999), pp. 491–502.

[59] F. Soto, M. Alves, J. C. Valdés, O. Armas, P. Crnkovic, G. Rodrigues, A. Lacerda, and L. Melo. "The determination of the activation energy of diesel and biodiesel fuels and the analysis of engine performance and soot emissions". *Fuel Processing Technology* 174 (2018), pp. 69–77.

[60] *EPA regulation. 40 CFR Ch. I (7–1–12 Edition). 86.1828–01. Page 452.*

[61] *Commission Regulation (EC) No 692/2008 of 18 July 2008 implementing and amending Regulation (EC) No 715/2007 of the European Parliament and of the Council on type-approval of motor vehicles with respect to emissions from light passenger and commercial vehicles (Euro 5 and Euro 6) and on access to vehicle repair and maintenance information.* July 2008.

[62] A. J. Torregrosa, P. Olmeda, J. Martín, and B. Degraeuwe. "Experiments on the influence of inlet charge and coolant temperature on performance and emissions of a DI Diesel engine". *Experimental Thermal and Fluid Science* 30.7 (2006), pp. 633–641.

[63] A. J. Torregrosa, A. Broatch, P. Olmeda, and C. Romero. "Assessment of the influence of different cooling system configurations on engine warm-up, emissions and fuel consumption". *International Journal of Automotive Technology* 9.4 (2008), pp. 447–458.

[64] M. Weilenmann, J.-Y. Y. Favez, and R. Alvarez. "Cold-start emissions of modern passenger cars at different low ambient temperatures and their evolution over vehicle legislation categories". *Atmospheric Environment* 43.15 (2009), pp. 2419–2429.

[65] D. Ludykar, R. Westerholm, and J. Almén. "Cold start emissions at +22, -7 and -20°C ambient temperatures from a three-way catalyst (TWC) car: Regulated and unregulated exhaust components". *Science of the Total Environment* 235.1-3 (1999), pp. 65–69.

[66] M. Weilenmann, P. Soltic, C. Saxer, A.-M. M. Forss, and N. Heeb. "Regulated and nonregulated diesel and gasoline cold start emissions at different temperatures". *Atmospheric Environment* 39.13 (2005), pp. 2433–2441.

[67] C. Dardiotis, G. Martini, A. Marotta, and U. Manfredi. "Low-temperature cold-start gaseous emissions of late technology passenger cars". *Applied Energy* 111 (2013), pp. 468–478.

[68] O. Armas, R. García-Contreras, and Á. Ramos. "Pollutant emissions from engine starting with ethanol and butanol diesel blends". *Fuel Processing Technology* 100 (2012), pp. 63–72.

[69] E. Giakoumis and A. Zachiotis. "Investigation of a Diesel-Engined Vehicle's Performance and Emissions during the WLTC Driving Cycle—Comparison with the NEDC". *Energies* 10.2 (2017), p. 240.

[70] J. Ko, D. Jin, W. Jang, C.-L. Myung, S. Kwon, and S. Park. "Comparative investigation of NOx emission characteristics from a Euro 6-compliant diesel passenger car over the NEDC and WLTC at various ambient temperatures". *Applied Energy* 187 (2017), pp. 652–662.

[71] L. Sileghem, D. Bosteels, J. May, C. C. Favre, and S. Verhelst. "Analysis of Vehicle Emission Measurements on the New WLTC, the NEDC and the CADC". *Transportation Research: Part D: Transport and Environment* 32.0 (2014), pp. 70–85.

[72] J. Pavlovic, A. Marotta, and B. Ciuffo. "CO2 emissions and energy demands of vehicles tested under the NEDC and the new WLTP type approval test procedures". *Applied Energy* 177 (2016), pp. 661–670.

[73] D. Tsokolis, S. Tsiakmakis, A. Dimaratos, G. Fontaras, P. Pistikopoulos, B. Ciuffo, and Z. Samaras. "Fuel consumption and CO2 emissions of passenger cars over the New Worldwide Harmonized Test Protocol". *Applied Energy* 179 (2016), pp. 1152–1165.

[74] A.G.Stefnanopoulou, I.Kolmanovsky, and J. S. Freudenberg. "Control of Variable Geometry Turbocharged Diesel Engines for Reduced Emissions". *IEEE Transactions on Control Systems Technology* 8.4 (2000), pp. 733–745.

[75] M. Ammann, N. P. Fekete, L. Guzzella, and A. H. Glattfelder. "Model-based control of the VGT and EGR in a turbocharged common-rail diesel engine: Theory and passenger car implementation". *SAE transactions* 112.3 (2003), pp. 527–538.

[76] H. Peng, Y. Cui, L. Shi, and K. Deng. "Effects of exhaust gas recirculation (EGR) on combustion and emissions during cold start of direct injection (DI) diesel engine". *Energy* 33.3 (2008), pp. 471–479.

[77] A. S. Ramadhas and H. Xu. "Influence of Coolant Temperature on Cold Start Performance of Diesel Passenger Car in Cold Environment". In: *SAE Int. J. Engines*. 2016.

[78] Y. Zeldóvich. "The oxidation of nitrogen in combustion explosions". *Acta Pysichochimica USSR* 21 (1946), pp. 557–628.

[79] A. Maiboom, X. Tauzia, S. R. Shah, and J.-F. Hétet. "Experimental Study of an LP EGR System on an Automotive Diesel Engine, compared to HP EGR with respect to PM and NOx Emissions and Specific Fuel Consumption". *SAE International Journal of Engines* 2.2 (2009), pp. 2009–24–0138.

[80] Y. Park and C. Bae. "Experimental study on the effects of high/low pressure EGR proportion in a passenger car diesel engine". *Applied Energy* 133 (2014), pp. 308–316.

[81] D. Heuwetter, W. Glewen, C. Meyer, D. E. Foster, M. Andrie, and R. Krieger. "Effects of Low Pressure EGR on Transient Air System Performance and Emissions for Low Temperature Diesel Combustion". In: *SAE Int. J. Engines*. 2011.

[82] V. Bermúdez, J. M. Lujan, B. Pla, and W. G. Linares. "Effects of low pressure exhaust gas recirculation on regulated and unregulated gaseous emissions during NEDC in a light-duty diesel engine". *Energy* 36.9 (2011), pp. 5655–5665.

[83] B. Nitu, I. Singh, L. Zhong, K. Badreshany, N. A. Henein, and W. Bryzik. "Effect of EGR on Autoignition, Combustion, Regulated Emissions and Aldehydes in DI Diesel Engines". In: *SAE Int. J. Engines*. 2002.

[84] R. Schubiger, A. Bertola, and K. Boulouchos. "Influence of EGR on Combustion and Exhaust Emissions of Heavy Duty DI-Diesel Engines Equipped with Common-Rail Injection Systems". In: *SAE Int. J. Engines*. 2001.

[85] S. Wang, X. Zhu, L. Somers, and L. de Goey. "Effects of exhaust gas recirculation at various loads on diesel engine performance and exhaust particle size distribution using four blends with a research octane number of 70 and diesel". *Energy Conversion and Management* 149 (2017), pp. 918–927.

[86] X. Li, Z. Xu, C. Guan, and Z. Huang. "Impact of exhaust gas recirculation (EGR) on soot reactivity from a diesel engine operating at high load". *Applied Thermal Engineering* 68.1-2 (2014), pp. 100–106.

[87] H. Santos and M. Costa. "Evaluation of the conversion efficiency of ceramic and metallic three way catalytic converters". *Energy Conversion and Management* 49.2 (2008), pp. 291–300.

[88] J. M. Herreros, S. S. Gill, I. Lefort, A. Tsolakis, P. Millington, and E. Moss. "Enhancing the low temperature oxidation performance over a Pt and a Pt-Pd diesel oxidation catalyst". *Applied Catalysis B: Environmental* 147 (2014), pp. 835–841.

[89] S. Salomons, M. Votsmeier, R. E. Hayes, A. Drochner, H. Vogel, and J. Gieshof. "CO and H2 oxidation on a platinum monolith diesel oxidation catalyst". *Catalysis Today* 117.4 (2006), pp. 491–497.

[90] E. Zervas. "Parametric study of the main parameters influencing the catalytic efficiency of a diesel oxidation catalyst: Parameters influencing the efficiency of a diesel catalyst". *International Journal of Automotive Technology* 9.6 (2008), pp. 641–647.

[91] P. D. S. P. N. Botsaris. "Ambient temperature influence on catalytic outlet—inlet temperature difference". *Proceedings of the Institution of Mechanical Engineers, Part D: Journal of Automobile Engineering* 214.2000 (2000), pp. 95–100.

[92] K. Arnby, A. Törncrona, B. Andersson, and M. Skoglundh. "Investigation of Pt/γ-Al2O3 catalysts with locally high Pt concentrations for oxidation of CO at low temperatures". *Journal of Catalysis* 221.1 (2004), pp. 252–261.

[93] V. T. Morgan. "The Overall Convective Heat Transfer from Smooth Circular Cylinders". *Advances in Heat Transfer* 11.C (1975), pp. 199–264.

[94] J. Koop and O. Deutschmann. "Detailed surface reaction mechanism for Pt-catalyzed abatement of automotive exhaust gases". *Applied Catalysis B: Environmental* 91.1-2 (2009), pp. 47–58.

[95] F. Payri, V. R. Bermúdez, B. Tormos, and W. G. Linares. "Hydrocarbon emissions speciation in diesel and biodiesel exhausts". *Atmospheric Environment* 43.6 (2009), pp. 1273–1279.

[96] S. V. Bohac, M. Han, T. J. Jacobs, A. J. López, D. N. Assanis, and P. G. Szymkowicz. "Speciated Hydrocarbon Emissions from an Automotive Diesel Engine and DOC Utilizing Conventional and PCI Combustion". *SAE Technical Papers* 2006.2006-01-0201 (2006).

[97] I. Lefort, J. M. Herreros, and A. Tsolakis. "Reduction of low temperature engine pollutants by understanding the exhaust species interactions in a diesel oxidation catalyst". *Environmental Science and Technology* 48.4 (2014), pp. 2361–2367.

[98] M. J. Patterson, D. E. Angove, and N. W. Cant. "The effect of carbon monoxide on the oxidation of four C6 to C8 hydrocarbons over platinum, palladium and rhodium". *Applied Catalysis B: Environmental* 26.1 (2000), pp. 47–57.

[99] M. Kamijo, M. Kamikubo, H. Akama, and K. Matsushita. "Study of an oxidation catalyst system for diesel emission control utilizing HC adsorption". *JSAE Review* 22.3 (2001), pp. 277–280.

[100] Y. Hiramoto, M. Takaya, S. Yamamoto, and A. Okada. "Development of a New HC-Adsorption Three-Way Catalyst System for Partial-ZEV Performance". In: 2003.

[101] C. A. Romero, A. Torregrosa, P. Olmeda, and J. Martin. "Energy Balance During the Warm-Up of a Diesel Engine". *SAE Technical Paper* 2014-01-06 (2014), pp. 2–11.

[102] L. Jarrier, J. C. Champoussin, E. C. D. Lyon, R. Yu, and D. R. Renault. "Warm-Up of a D . I . Diesel Engine : Experiment and Modeling". *SAE Technical Paper* 2000-01-02 (2000).

[103] M. Gumus. "Reducing cold-start emission from internal combustion engines by means of thermal energy storage system". *Applied Thermal Engineering* 29.4 (2009), pp. 652–660.

[104] A. Broatch, J. M. Luján, J. R. Serrano, and B. Pla. "A procedure to reduce pollutant gases from Diesel combustion during European MVEG-A cycle by using electrical intake air-heaters". *Fuel* 87.12 (2008), pp. 2760–2778.

[105] P. Kauranen, T. Elonen, L. Wikström, J. Heikkinen, and J. Laurikko. "Temperature optimisation of a diesel engine using exhaust gas heat recovery and thermal energy storage (diesel engine with thermal energy storage)". *Applied Thermal Engineering* 30.6-7 (2010), pp. 631–638.

[106] P. Diehl, F. Haubner, S. Klopstein, and F. Koch. "Exhaust heat recovery system for modern cars". *Sae Transactions* 110.3 (2001), pp. 988–998.

[107] N. S. Ap and N. C. Golm. "Insulated Expansion Tank (IET) and Thermal Storage for Engine Cold Start". In: *SAE Technical Paper*. SAE Technical Paper., 1995.

[108] S. Arrhenius. "Über die Dissociationswärme und den Einfluss der Temperatur auf den Dissociationsgrad der Elektrolyte". *Zeitschrift für Physikalische Chemie* 4.1 (1889).

[109] G. De Nicolao, R. Scattolini, and C. Siviero. "Modelling the volumetric efficiency of ic engines: Parametric, non-parametric and neural techniques". *Control Engineering Practice* 4.10 (1996), pp. 1405–1415.

[110] B. Pla Moreno. "Análisis del proceso de la recirculación de los gases de escape de baja presión en motores Diesel sobrealimentados." PhD thesis. 2009.